Radboud Repository

Radboud University Nijmegen

PDF hosted at the Radboud Repository of the Radboud University Nijmegen

The following full text is a publisher's version.

For additional information about this publication click this link.
http://hdl.handle.net/2066/90937

Please be advised that this information was generated on 2017-12-06 and may be subject to change.

GaN on Diamond:
A Hot Combination?

GaN on Diamond: A Hot Combination?
Gerardus Wilhelmus Gerbe van Dreumel
Ph. D. Thesis Radboud University Nijmegen, October 2011
With summary in Dutch
ISBN: nummer
Printed by Ipskamp Drukkers, Nijmegen

GaN on Diamond: A Hot Combination?

Een wetenschappelijk proeve op het gebied van de
Natuurwetenschappen, Wiskunde en Informatica

Proefschrift

ter verkrijging van de graad van doctor
aan de Radboud Universiteit Nijmegen
op gezag van de rector magnificus, prof. mr. S. C. J. J. Kortmann,
volgens besluit van het college van decanen
in het openbaar te verdedigen op dinsdag 25 oktober 2011
om 15.30 uur precies

door

Gerardus Wilhelmus Gerbe van Dreumel

geboren op 14 februari 1981
te Wijchen

Promotoren:
Prof. Dr. E. Vlieg
Prof. Dr. J. J. ter Meulen

Copromotoren:
Dr. P. R. Hageman
Dr. J. G. Buijnsters

Manuscriptcommissie
Prof. Dr. S. E. Speller
Dr. W. J. P. van Enckevort
Dr. L. Macht (NXP Semiconductors)

Cover Design: Gerbe van Dreumel

Contents

Preface

Since its introduction at Bell Telephone Laboratories in 1947, solid state transistors are drastically improved. These electronic switching units are essential for many small devices, such as micro-processors and other logic circuits, found in numerous applications. The famous Moore's law predicts that every two years the number of transistors that are placed on an integrated circuit doubles. Besides this decrease in transistor size, ever increased power amplification is demanded from the transistors. To accomplish this, alternative semiconductor materials and new thermal management approaches need investigation.

With silicon reaching its physical limits, gallium nitride (GaN) is the ideal successor. It has a high breakdown voltage, thermal stability and is chemically inert. Therefore, since its reappearance in the early 1990s GaN has been regarded as a very interesting and highly promising material for both optical and microwave high-power electronic applications. Over the last twenty years researchers all around the world have made great efforts in order to redeem these promises. GaN based optical applications reached the stage of commercialisation as blu-ray disc players and game stations, while microwave high-power electronics are on the verge of their commercial breakthrough. Simultaneously, improved heat dissipation has been investigated through the application of high thermal conductive substrates like silicon carbide.

Anticipating on even smaller devices placed onto a smaller overall area, this research addresses the growth of GaN layers onto diamond substrates for the application of high power and high frequency device structures. By using diamond substrates, with the highest thermal conductance available, the power range in which GaN devices can be employed will be increased even further.

In the next chapter, the main properties of GaN and GaN-based devices will be introduced. Then, chapter 2 discusses the main properties of diamond and the origin of its high thermal conductive properties, while chapter 3 covers several other approaches to combine GaN with diamond, from the available literature. To conclude the introduction, part II describes all the techniques that are applied in this research, starting from growth techniques of GaN and synthetic diamond to the characterisation techniques of the samples involved. Part III handles the application of polycrystalline diamond substrates, especially for the optimisation of the growth process for the formation of (0001) oriented GaN layers. Finally, part IV describes the growth of GaN on nominal and vicinal single crystal diamond substrates and the first epitaxial layers produced with MOCVD.

Part I

Introduction

1

Gallium Nitride

1.1 Introduction

Gallium nitride (GaN) is the most important semiconductor material for electronic devices since silicon. It emits brilliant light and it is the key material for next generation high frequency, high power transistors capable of operating at high temperatures. The origin of these outstanding properties of GaN will be addressed in this chapter. Furthermore, there will be special focus on the differences, and particular advantages of GaN compared to other III-nitride semiconductors and on its applications.

Table 1.1: Structural and thermal properties of III-nitrides in wurtzite structure [1, 2]

		AlN	GaN	InN
Melting point (°C)		3487	2791	2146
Lattice constant (nm)	a_0	0.311	0.319	0.354
	c_0	0.498	0.519	0.57
Thermal expansion coeff. ($10^{-6}K^{-1}$)	$\parallel c$	5.3	3.2	3.7
	$\perp c$	4.2	6.2	5.7
Thermal conductivity at 300K ($W\ cm^{-1}K^{-1}$)		2.85	1.3	0.8

Periodic Table of the Elements

with relative atomic masses compared to Carbon (1993, according to IUPAC)

1 (I)	2 (II)	3	4	5	6	7	8	9	10	11	12	13 (III)	14 (IV)	15 (V)	16 (VI)	17 (VII)	18 (VIII)
1 H 1.01																	2 He 4.00
3 Li 6.94	4 Be 9.01					Atomic number / Symbol / Rel. atomic mass						5 B 10.81	6 C 12.01	7 N 14.01	8 O 16.00	9 F 19.00	10 Ne 20.18
11 Na 22.99	12 Mg 24.31											13 Al 26.98	14 Si 28.09	15 P 30.97	16 S 32.07	17 Cl 35.45	18 Ar 39.95
19 K 39.09	20 Ca 40.08	21 Sc 44.96	22 Ti 47.87	23 V 50.94	24 Cr 52.00	25 Mn 54.94	26 Fe 55.85	27 Co 58.93	28 Ni 58.69	29 Cu 63.55	30 Zn 65.39	31 Ga 69.72	32 Ge 72.61	33 As 74.92	34 Se 78.96	35 Br 79.90	36 Kr 83.80
37 Rb 85.47	38 Sr 87.62	39 Y 88.91	40 Zr 91.22	41 Nb 92.91	42 Mo 95.9	43 Tc (98)	44 Ru 101.1	45 Rh 102.9	46 Pd 106.4	47 Ag 107.9	48 Cd 112.4	49 In 114.8	50 Sn 118.7	51 Sb 121.8	52 Te 127.6	53 I 126.9	54 Xe 131.3
55 Cs 132.9	56 Ba 137.3	La-Lu	72 Hf 178.5	73 Ta 180.9	74 W 183.8	75 Re 186.2	76 Os 190.2	77 Ir 192.2	78 Pt 195.0	79 Au 197.0	80 Hg 200.6	81 Tl 204.4	82 Pb 207.2	83 Bi 209.0	84 Po (209)	85 At (210)	86 Rn (222)
87 Fr (223)	88 Ra (226)	Ac-Lr	104 Rf (261)	105 Db (262)	106 Sg (263)	107 Bh (262)	108 Hs (265)	109 Mt (266)									

57 La 138.9	58 Ce 140.1	59 Pr 140.9	60 Nd 144.2	61 Pm (145)	62 Sm 150.4	63 Eu 152.0	64 Gd 157.3	65 Tb 158.9	66 Dy 162.5	67 Ho 164.9	68 Er 167.3	69 Tm 168.9	70 Yb 173.0	71 Lu 175.0
89 Ac (227)	90 Th (232)	91 Pa (231)	92 U (238)	93 Np (237)	94 Pu (239)	95 Am (243)	96 Cm (247)	97 Bk (247)	98 Cf (251)	99 Es (252)	100 Fm (257)	101 Md (258)	102 No (259)	103 Lr (262)

Figure 1.1: The Periodic Table of Elements with gallium and nitrogen highlighted in columns III and V.

1.2 Properties

1.2.1 Structural and Thermal Properties

GaN consists of gallium and nitrogen atoms. They are positioned in columns III and V of the Periodic Table (Ga and N are highlighted in figure 1.1) and therefore GaN is called a III-V compound semiconductor. Among III-V semiconductors, nitrogen-based semiconductors are considered a special group, namely III-nitrides, because of the special properties the nitrogen atom exhibits. The large difference in electronegativity of nitrogen compared to the group-III atoms creates a strong, chemical bond within the solids (e.g. GaN has bonding energy of 9.12 eV atom pair^{-1} [3]). Group III-nitrides (AlN, GaN, InN) thus present hardness and high melting points, summarised in table 1.1. The main reason for this hardness is the difficulty in developing and displacing dislocations once the material is grown, thus removing one of the main mechanisms of degradation observed in other III-V compounds [4]. GaN has high chemical stability, even at elevated temperatures. Combined with its hardness, it makes GaN an attractive material for protective

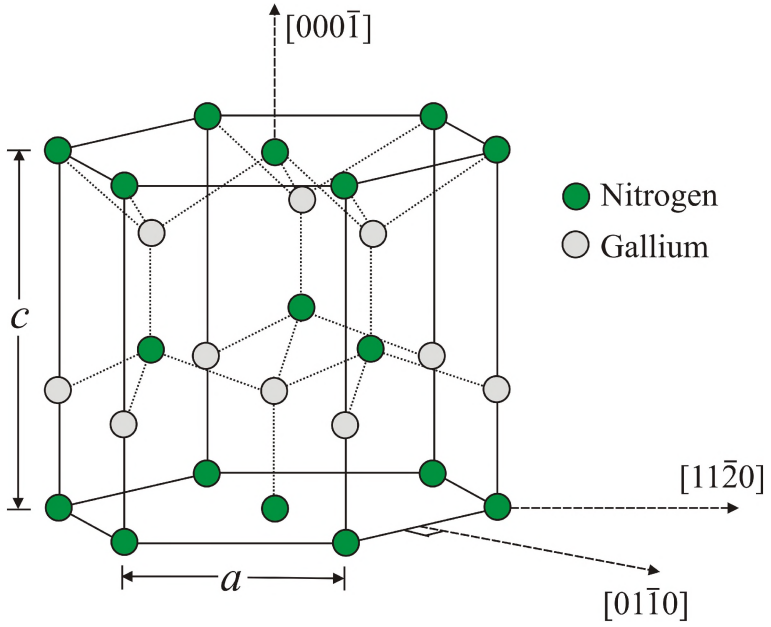

Figure 1.2: The GaN wurtzite crystal structure [7].

coatings. Because of its wide bandgap energy, discussed in section 1.2.2, it is also an excellent candidate for device operation in high temperature and harsh environments. As a matter of fact, the majority of GaN researchers are currently interested in semiconductor device applications. While the thermal stability of GaN allows freedom for high temperature processing, it presents a technological challenge as well. For instance, conventional wet chemical etching techniques used in semiconductor processing are not very successful for GaN device fabrication: In 1969 Maruska and Tietjen [5] already reported that GaN was insoluble in H_2O, acids, or bases at room temperature, but did dissolve in hot alkali solutions at a very slow rate [6]. This is also the reason why the crystallization of GaN from stoichiometric melts (industrial growth methods like Czochralski or Bridgman) are virtually impossible, and other techniques must be applied to produce GaN.

Most notable of the III-N semiconductor materials is GaN and it crystallises in three crystal structures shared by all group-III nitrides: the wurtzite, zincblende, and rocksalt structure. At ambient conditions, the thermodynamically stable structure for bulk GaN is the wurtzite form. It is characterised by two hexagonal lattice parameters, a and c, as depicted in figure 1.2. The wurtzite structure has a hexagonal symmetry, and each gallium atom is coordinated by four nitrogen atoms. Conversely, each nitrogen atom is coordinated by four gallium atoms.

There is no inversion symmetry in the lattice along the c-axis or [0001] direction, which by convention is the direction shown by a vector parallel to $<0001>$ pointing from the cation (Gallium) to the nearest neighbor anion (Nitrogen). As a result of this lack of inversion symmetry all atoms in a plane perpendicular to the c-axis are the same and alternating gallium and nitrogen. Hence, wurtzite GaN crystals have two distinct faces, commonly known as Ga-face and N-face, which correspond to the (0001) and (000$\bar{1}$) crystalline faces, respectively. Figure 1.3 shows the different faces of GaN.

In contrast to the wurtzite structure, the metastable zincblende and rocksalt polytypes are less common. They have cubic symmetry and are mainly synthesised by growing on

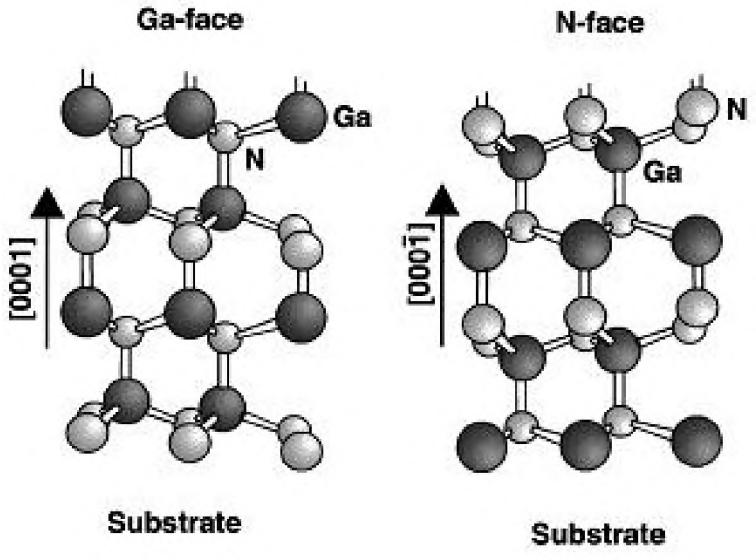

Figure 1.3: Different polarities (Ga- and N-faces) of wurtzite GaN [8].

specific crystal planes of cubic substrates such as Si, MgO, and GaAs. In these cases the intrinsic tendency to form the wurtzite structure is overcome by topological compatibility [6]. However, most applications can be realised using the more easily synthesised wurtzite crystal structure. Therefore, the characterization and discussion of the other crystallographic modifications of GaN are beyond the scope of this thesis and will not be considered.

Wurtzite and other low symmetry crystal structures can exhibit spontaneous polarization, as well as piezoelectric polarization arising from strain induced in the crystal structure. It is important to note that among all III-V materials only the group III-nitrides possess a spontaneously induced electrical field. Nitrogen is the smallest and the most electronegative group V element. The involvement of nitrogen, as mentioned above, makes the III-nitrides special among the other III-V compounds as this has a strong effect on their properties. Because of the $1s^2 2s^2 2p^3$ electronic configuration of the N atom, or rather the lack of electrons occupying the outer orbitals, the electrons involved in the gallium-nitride covalent bond will be strongly attracted by the Coulomb potential of the N atomic nucleus. This means that this bond will have much stronger ionicity compared to other III-V covalent bonds. The ionicity even results into macroscopic polarization if the crystal lacks inversion symmetry, which is the case for wurtzite III-nitrides. Since this polarization effect occurs when the lattice of the III-nitrides is in equilibrium, *i.e.* at zero strain, it is called spontaneous polarization. The direction of the spontaneous polarization in wurtzite III-V nitrides is the c-direction $\overrightarrow{c}$ = [0001] [4] which is beneficial for GaN high power transistor applications. More will be discussed in section 1.3.1.

Table 1.2: Optical properties of III-nitrides in wurtzite structure [1, 2]

	AlN	GaN	InN
Bandgap E_g (eV) 300K	6.2	3.44	0.7

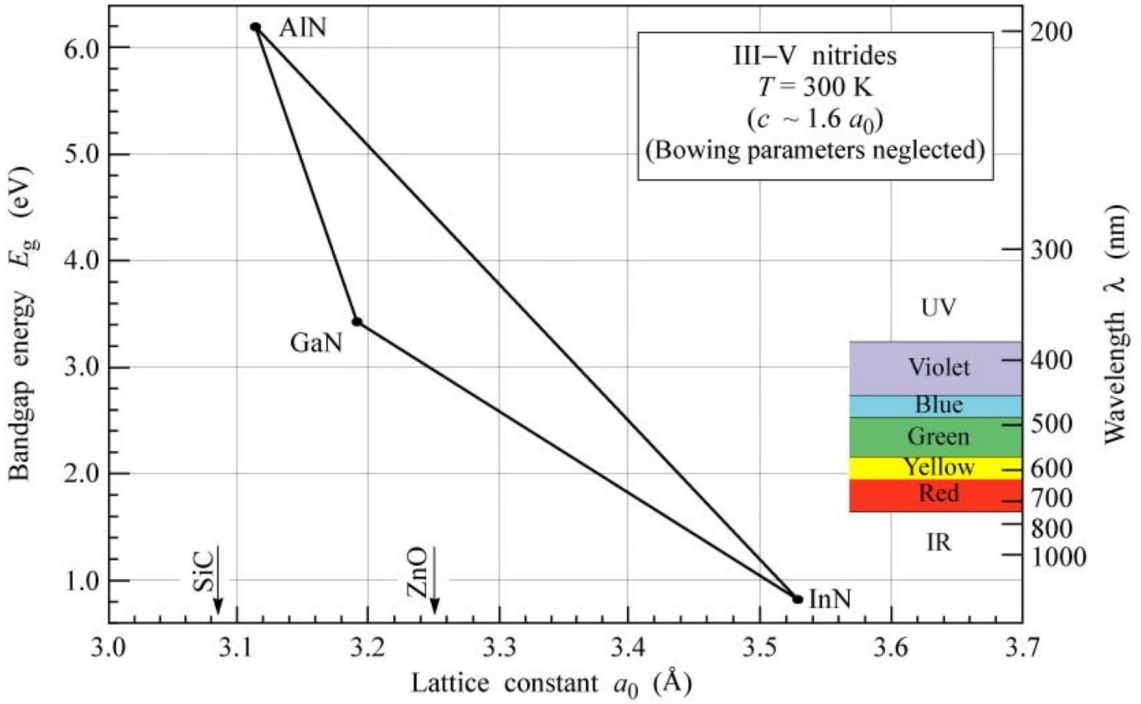

Figure 1.4: Bandgap energies versus the a_0 lattice constants of the III-nitride semiconductors [12].

1.2.2 Optical Properties

Besides the strong chemical bonding within the crystals, GaN has another main advantage compared to other semiconductors. The width of the energy band gap of the material also determines the ultimate stability of GaN based electronic devices under high ambient temperature or excessive power loads. The energy band gap, denotes the difference in energy between the highest valence electron energy states (valence band maximum) and the lowest conduction energy states (conduction band minimum). For GaN this band gap is wide compared to other III-V semiconductors, and is determined 3.44 eV (300K) [9].

The direct energy bandgaps of the III-nitrides are listed in table 1.2. In optoelectronic devices, the energy band gap dictates the wavelength of light that a semiconductor absorbs and emits. Therefore, the production of good lattice-matched ternary and quaternary alloys associated with the Al-Ga-In-N system opens up the opportunity to cover the entire visible spectrum for opto-electronic applications, as shown in figure 1.4 [11].

Table 1.3: Ratio of the lattice parameters (ideal wurtzite $c_0/a_0 = 1.6351$), spontaneous polarization P_{sp} and piezoelectric constants (e_{33}, e_{31}) for different III-V semiconductors [10]

	AlN	GaN	InN	GaAs	AlAs
c_0/a_0 [10]	1.6190	1.6336	1.6270	-	-
P_{sp} (C/m^2)	-0.081	-0.029	-0.032	-	-
e_{33} (C/m^2)	1.46	0.73	0.97	-0.12	-0.03
e_{31} (C/m^2)	-0.60	-0.49	-0.57	0.06	0.01

1.3 Applications

Group III-nitrides and their solid solutions are now being pursued for high-temperature, high-power electronics due to GaN's wide bandgap, high thermal conductivity, and the possibility of heterojunction-based devices [13]. The nitrides are also being widely developed for opto-electronic devices, including applications such as short-wavelength laser diodes and light emitters in emerging technologies like optical storage and full-color displays [14]. Some applications are discussed below.

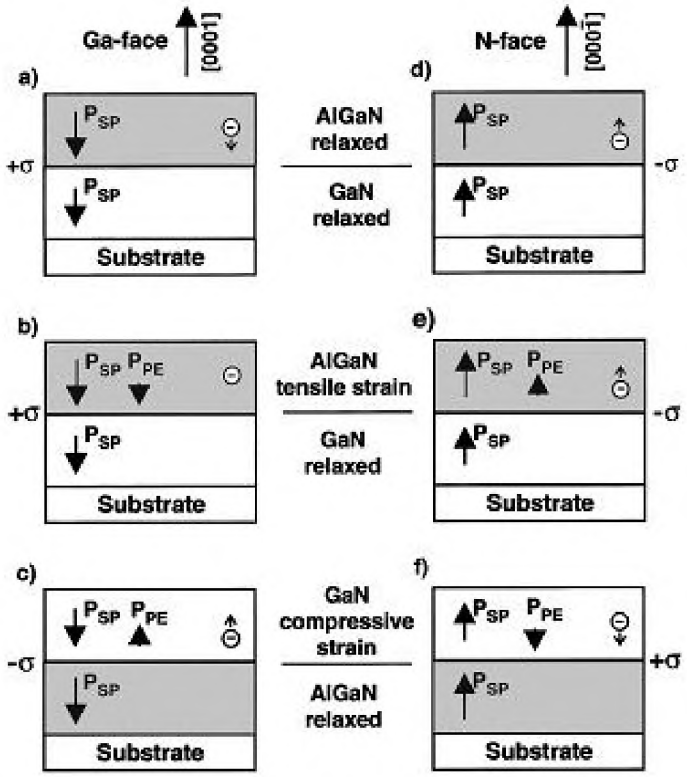

Figure 1.5: Spontaneous (P_{SP}) and piezoelectric (P_{PE}) polarization in Ga- and N-face for an AlGaN/GaN heterojunction structure [15].

1.3.1 Transistors

In section 1.2.1 the spontaneous polarization and piezoelectric properties of the III-N semiconductors were briefly addressed. These polarization-related properties are obviously important for devices because the electric fields influence the shape of the band edges and the carrier distribution inside nitride-based heterostructures. Therefore, spontaneous and piezoelectric polarization can influence the electrical properties of the transistor structures as well as the radiative recombination in light-emitting devices. In this section the electrical properties will be addressed.

Since polarization properties strongly depend on the structural parameters of the material and the deviation from the ideal wurtzite structure, there are some quantitative differences in spontaneous polarization of AlN, GaN, and InN (table 1.3). In the ideal wurtzite structure all Ga-N bonds have the same length and equal angles and it is thus stress free.

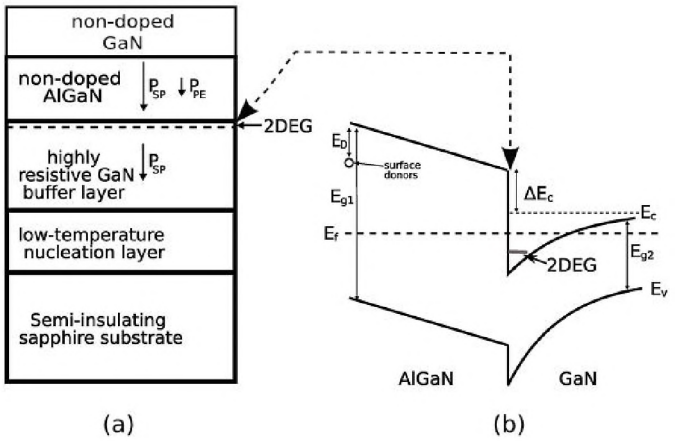

Figure 1.6: Schematic drawing of the standard HEMT structure (a) and corresponding band diagram (b). The vertical arrows on the left image show the direction of spontaneous and piezoelectric polarization in the structure. In the right image E_{g1} and E_{g2} represent the bandgaps of AlGaN and GaN respectively, while E_v, E_c, E_f, E_D and ΔE_c show the energies of the valence band, conduction band, fermi level, donor state, and the effective energy barrier height, respectively [1].

Deviation from this ideal structure leads to spontaneous polarization in the material. Because GaN has a c_0/a_0 ratio close to the ideal wurtzite structure (c_0/a_0 = 1.6351) it has the lowest amount of spontaneous polarization. Thus, going from GaN to either InN or AlN, leads to an increase in spontaneous polarization. In addition, the piezoelectric constants for AlN and InN were found to be larger than the corresponding value for GaN. Therefore, the built-in electric fields resulting from the polarization discontinuities at heterointerfaces have to be taken into account for proper calculations of band edges and carrier confinement in heterojunction structures [8].

The largest built-in electric fields are obtained when the difference in both spontaneous and piezoelectric polarization is maximised, thus when applying an AlN/GaN heterojunction structure (figure 1.5). Because of a low critical thickness of AlN on GaN and due to the lattice mismatch between AlN and GaN, in practice, mostly a strained $Al_xGa_{(1-x)}N$ alloy layer is used on top of a GaN layer (further called: AlGaN/GaN structure). In these structures the strong electric fields can enhance electron or hole accumulation at AlGaN/GaN interfaces: As shown in figure 1.5 it is possible to induce positive ($+\sigma$) or negative ($-\sigma$) charges at the AlGaN/GaN interface by changing the polarity of the stacked layers (figure 1.5). If the charge is positive ($+\sigma$), free electrons tend to compensate the polarization induced charge (figure 1.5a) and form a two-dimensional electron gas (2DEG) at the interface. This effect can be enhanced by growing a highly tensile-strained AlGaN layer (figure 1.5b) with a high Al content. For N-polar material the polarization induced charge is negative ($-\sigma$), so it will cause an accumulation of holes (figure 1.5c, d) at the heterojunction interface [16].

Devices based on this concept are called heterostructure field effect transistors, or high electron mobility transistors (HEMTs) in which the interface of an AlGaN/GaN structure is applied as fast moving channel for electrons. The precise location for the confinement of electrons (or holes) in the AlGaN/GaN heterostructure depends on the polarity of the material, as depicted in figure 1.5. The schematic diagram of figures 1.5(a, b, d and e), however, represents merely the basic model of the perfect HEMT structure based on

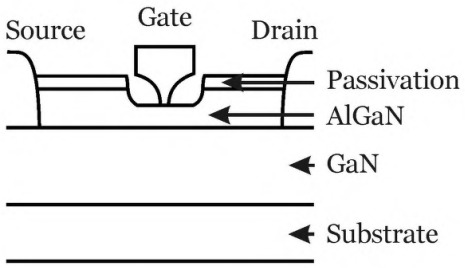

Figure 1.7: Schematic of a simple HEMT structure with contacts.

2DEG and two-dimensional hole gas (2DHG), respectively. The actual construction of the standard HEMT structure based on AlGaN/GaN layer with Ga-polarity grown on a sapphire substrate is presented in figure 1.6a.

As mentioned above, electric fields resulting from the polarization discontinuities at heterointerfaces alter the energy band levels in the material. The piezoelectric and spontaneous polarization lead to a positive induced charge ($+\sigma$ near the AlGaN/GaN interface (figure 1.5b) for a Ga-faced structure. To compensate for this positive charge electrons are attracted towards the interface. There they accumulate in the triangular energy pit under the Fermi level (E_f) near the interface (figure 1.6b) in the form of a 2DEG. Because of the low energy of this 2DEG, the high concentration of electrons and the sharp interface (low resistivity) a conducting channel is formed between the atoms at the interface, where the electrons can theoretically move without any resistance. A schematic of a basic HEMT structure is presented in figure 1.7. In this structure an electric field, originating from a voltage difference between the source and drain contacts, directs the carriers at the AlGaN/GaN interface from one side to another and thereby the carriers reach the extremely high electron (or hole) mobility that gives the transistor its name. Because the structure is based on polarization effects, there is in principle no need for the application of doped materials. More complicated HEMTs, however, are constructed with intensionally doped materials and well defined strains (like depicted in figure 1.5) to operate at even higher power levels and frequencies.

1.3.2 LEDs and Laser Diodes

Besides in structures for electronic purposes, GaN can also be used for light applications by addressing its wide bandgap. Efficient red, yellow, and somewhat less efficient green light emitting diodes (LEDs) existed for several years before GaN light emitters were developed. However, with these previous LEDs full color displays could not be realised because the blue and green emitting diodes were much too weak, and also did not cover the necessary color spectrum. Therefore, blue GaN-based LEDs are of dual importance: they are important as emitters where strong, energy efficient, and reliable green, blue, and ultraviolet light sources are needed, but in addition they enable, for the first time, the production of full color LED displays by complementing the color spectrum of available LEDs. Now short-wavelength LEDs are widely commercially available and are replacing the tungsten light bulb for their high energy savings.

The development of GaN based laser diodes has also progressed with tremendous speed in the last 15 years. Continuous wave, room temperature, solid state GaN-based lasers have already been demonstrated in 1996 [17], but the wavelength range, intensities,

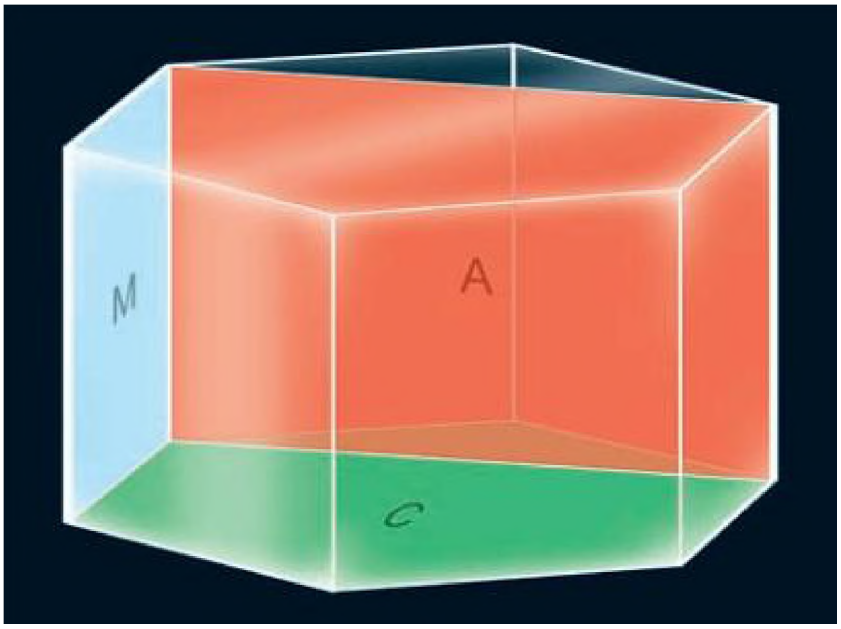

Figure 1.8: GaN has a hexagonal crystal structure. Internal electric fields plague devices grown on the c-plane ($\{0001\}$, green), but can be avoided by turning to GaNs m-plane ($\{10\bar{1}0\}$, blue) and a-plane ($\{11\bar{2}0\}$, red).

and lifetimes have been increased impressively since. The enormous amount of research in this area is justified. Blue, blue/green, and violet GaN lasers have big markets waiting: optical reading and writing of data in compact disk memories and opto-magnetic memories. The storage density in these memories is largely determined by the wavelength of the applied light, and violet lasers ($\lambda \approx 400$ nm) will increase the storage density by about a factor of four compared to the employment of red and infrared lasers (Commonly, $\lambda = 650$ and 780 nm). Although development is not fully optimised, this technique is already commercially applied in Blu-Ray Disk technology and in Sony's Playstation 3 game consoles.

An intrinsic advantage of III-nitride diodes is their improved temperature performance, high breakdown voltages (discussed in section 1.2.1), and high-carrier velocities (section 1.3.1) leading to higher conversion efficiencies in comparison to traditional diodes. To increase the conversion efficiency even further, polarization in the material needs to be as low as possible. While hole-electron seperation is an advantage in transistors, in diodes piezoelectric polarization effects in quantum wells can cause a spatial separation of electrons and holes, thereby decreasing the recombination efficiency (the Quantum-confined Stark Effect [18, 19]). To reduce this problem non-polar (m-plane and a-plane, figure 1.8) and the intermediate semi-polar GaN growth directions are currenlty investigated intensively.

A detailed description of the operation of GaN-based LEDs and laser diodes is beyond the scope of this thesis, but a thorough overview of available literature is given by Nakamura *et al.* [17].

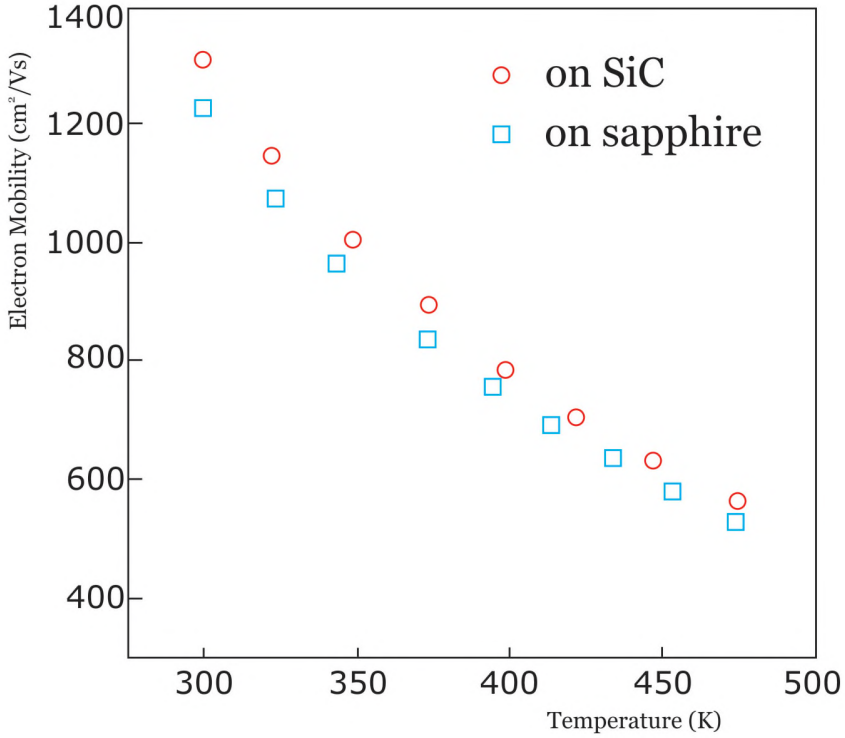

Figure 1.9: Decreased performance of AlGaN/GaN HEMTs at elevated temperatures [20].

1.4 More Power and Higher Temperatures

Since the beginning of the 1990s, new perspectives concerning high-power and high-temperature applications have been opened in GaN-based devices [13]. An ideal semiconductor material for power applications should posses excellent transport and thermal properties, a high breakdown voltage, chemical inertness, and mechanical stability. The III-nitride compounds successively fulfill most of these demands. The first GaN-based transistors were already demonstrated in 1993-1994 [21, 22], but recently developments led to many new achievements. The electron mobility in the 2DEG at the AlGaN/GaN interface exceeds 10000 cm^2/Vs at cryogenic temperatures and reaches 2000 cm^2/Vs at room temperature [23]. The maximum density of the 2DEG can exceed $6 \cdot 10^{13}$ cm^{-2}, which is more than one order of magnitude higher than for traditional AlGaAs/GaAs heterostructures [23]. Published output powers have reached densities of 32.2 W/mm [24] or 230W total output power [25] for continuous wave devices.

It is even possible to reach higher power outputs, however, currently GaN devices are hindered by self heating problems. Due to the high frequencies and powers at which the devices operate a lot of heat is produced within the structure. It is also the current tendency to produce smaller devices and place the electronics onto smaller overall areas, which also has a negative effect on the heat dissipation. For instance, the energy produced in the GaN HEMTs by operating at higher temperatures creates more lattice vibrations and defects in the structure. This leads to an increased resistivity in the 2DEG channel, which then results in lower electron mobilities for the 2DEG. Such an effect was measured by Shealy *et al.* for AlGaN/GaN devices grown on sapphire (Al_2O_3) and SiC substrates [20] as depicted in figure 1.9. It was also shown that the 'mean time to failure', an indication for the average life-time of electronic devices, is lowered exponentially with increasing

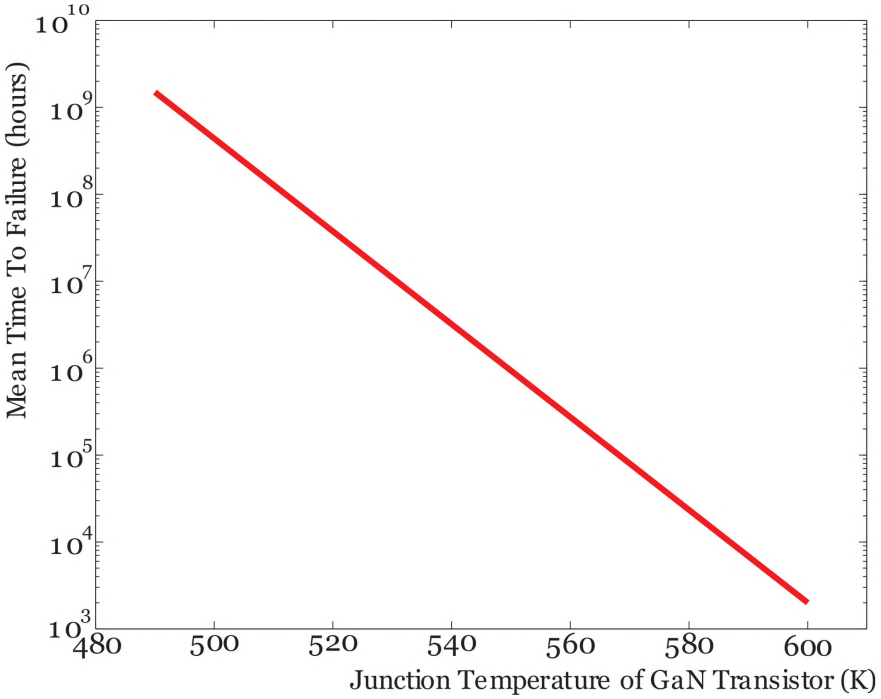

Figure 1.10: Reduced life-time of AlGaN/GaN HEMTs versus operating temperature [26].

interface temperature of the AlGaN/GaN device (figure 1.10).

To minimise these specific thermal problems it is vital to extract the heat from the active interface in AlGaN/GaN devices. This can be achieved by using alternative substrates that have higher thermal conductivity than the traditional sapphire and silicon substrates applied for GaN growth, which are currently used most often, because of their large availability and the large research experience available. Table 1.4 summarises the thermal conductivity of several suitable substrates. Diamond has, by far, the highest thermal conductivity that is available [27]. Therefore, in order to cool high power structures effectively, it is essential to spread the produced heat by placing a layer of high thermal conductivity diamond between the device and the cooling system. Thus, the attachment of GaN films onto diamond substrates, acting as heat sinks, would be a good solution to increase the power range in which GaN devices can be employed, as schematically shown in figure 1.11. For this reason, recently an increased interest has been observed in research targeting the integration of these two materials, which will be discussed in chapter 3. This research targets the direct growth of GaN layers onto diamond substrates

Table 1.4: Thermal conductivity and thermal expansion coefficients of several substrates for GaN epitaxy

		GaN	Al_2O_3	Si	4H-SiC	Diamond
Thermal conductivity at 300K (W $cm^{-1}K^{-1}$)		1.3	0.35	1.5	4.0-4.5	15-20
Thermal expansion coeff. at 300K ($10^{-6}K^{-1}$)	$\|c$	3.2	9.0	2.62	3.6	1.0
	$\perp c$	6.2	5.0		3.7	

by using MOCVD, for the application of high power and high frequency device structures to enhance the temperature range for which GaN can be employed.

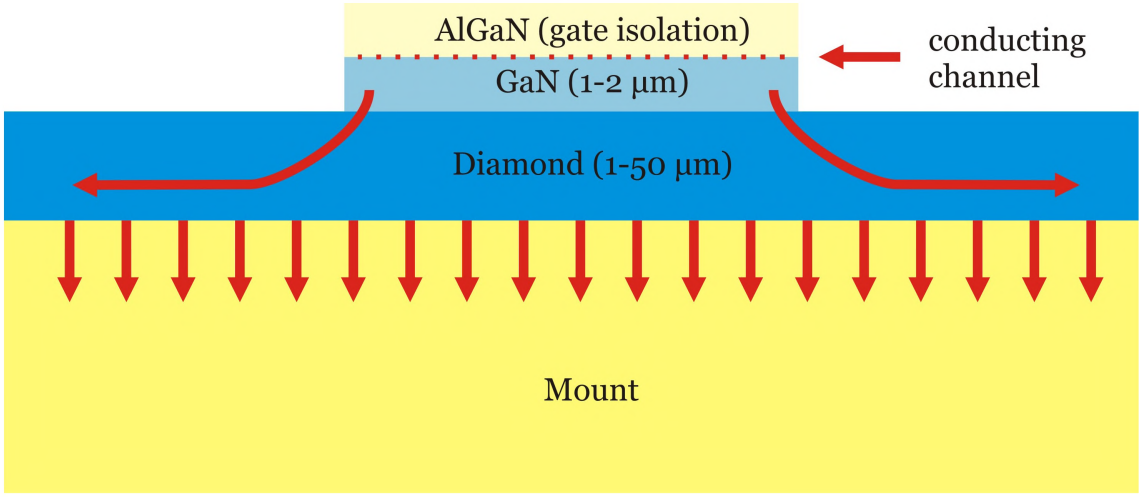

Figure 1.11: Schematic representation of the dissipation of heat from an AlGaN/GaN structure by the addition of a diamond layer.

2

Diamond

2.1 Introduction

Diamond appeals to everyone's imagination. Especially as a gem, it is fascinating, rare, and everlasting. Some of the larger natural diamonds have been known for ages and are surrounded by many anecdotes associated with royalty, richness, misfortune, war, and theft. Although the use of diamonds in jewelry may be the most intriguing, due to its unique properties diamond has found a wide range of applications in industry as well. Depending on the type of application, diamond can be found in a large variety of shapes and forms. It can be used as a powder, a single crystal, a polycrystalline film, or as electronic device material [28]. Especially, the use in electronics is gaining increased interest for the last two decades. In this area the application of diamond is two-fold.

First of all, when doped with boron, diamond is a semiconductor material with a wide bandgap (5.4 eV) and with extreme high hole mobilities ($\mu_p \sim 3800$ cm^2 V^{-1} [29]). This is even higher than, for instance, the 2DEG in GaN ($\mu_n \sim 2000$ cm^2 V^{-1} [30]), despite that holes are heavier than electrons, and thus normally have lower mobilities.

Secondly, as mentioned in section 1.4, diamond is the optimal heat spreader due to its high thermal conductivity, which allows for the generation of extremely high power densities in electronic devices.

Thus, diamond allows a device structure capable to generate an extremely high power density using it as an ideal heat sink that can operate at extremely high temperatures due to its high thermal stability. Then, the high diamond thermal conductivity means that power devices are built on an integrated heat spreader. This may in turn allow to reach the intrinsic device limits, whereas all traditional wide bandgap semiconductor electronic devices are thermally limited in their output power density [31].

So, single crystal diamond seems to be a very attractive material for electronic applications due to its unique combination of extreme breakdown properties, high carrier

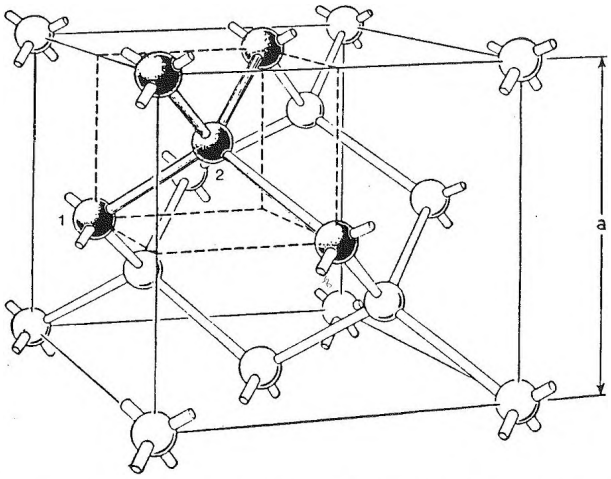

Figure 2.1: The diamant structure, showing the tetrahedral coordination and the short interatomic distance (1-2) of 1.54 Å. The cubic unit cell with lattice parameter a is also depicted [32].

mobility and drift carrier velocity. But, the use of diamond for active semiconductor devices has been restricted up to now by several limiting factors. One limitation has been the small size of single crystal substrates (below 5 mm). Another limit is associated with the deep boron acceptor and the absence of any reliable $n-$doping technology with shallow donors. This, for now, restricts active diamond devices to $p-$type unipolar carrier transport [31]. Therefore, most research in diamond electronics still concentrates on adding diamond layers to established structures to enhance the output power of devices.

2.2 The Diamond Structure

Diamond is an extraordinary material because carbon is the smallest element that forms a true, three-dimensional network of covalent bonds. In diamond, natural as well as synthetic, the carbon atoms make up a three-dimensional lattice in which each of their outer four electrons is shared with an electron of the four neighboring carbon atoms [28]. So each carbon has four covalent bonds to four other carbon atoms forming a tetrahedral network, as depicted in figure 2.1. The resulting lattice is very compact with a density of 3.52 g/cm^3, and is named after its most illustrious example, the diamond crystal structure [33, 34]. Because of this high density, only few impurity atoms can fit into the lattice structure of diamond of which nitrogen, hydrogen, and boron are the most common impurities.

Due to the limited size of carbon, the interatomic distance in the network is very small (1.54 Å), resulting in an exceptionally high density of very strong bonds. Consequently, diamond also exhibits unequalled physical properties with respect to mechanical hardness, spectral transparency, and chemical inertness (see table 2.1).

Accoustic and thermal waves, can propagate very fast and over long distances in diamond (tight bonding network) because they are not much hindered by the light carbon atoms. This is for instance reflected by the high thermal conductivity and velocity of sound in diamond (1833 m s^{-1} [35]). Usually, it is the combination of several of these properties which enables diamond, at least theoretically, to outperform any other material in a large number of applications ([33] and references therein).

Table 2.1: A selection of the unique properties of diamond (RT = room temperature) [36, 37]

Mechanical	
Extreme mechanical hardness (Vickers hardness 50-100 GPa)	
Strongest known material:	Highest bulk modulus ($\sim$ 1200 GPa)
	Lowest compressibility ($\sim$ 8.3 x 10^{-13} m^2 N^{-1})
High wear resistance and low coefficient of friction in many tribological systems	
Thermal	
Highest thermal conductivity at RT ($\sim$ 2000 W $m^{-1}K^{-1}$)	
Low thermal expansion coefficient at RT ($\sim$ 1 x $10^{-6}K^{-1}$)	
Optical	
Optical transparency in the electromagnetic spectrum from deep UV to far IR	
High refractive index and large colour dispersion	
Wide bandgap of 5.4 eV	
Electrical	
Semiconductor when n- or p-doped	
Good electrical insulator (resistivity of 10^{12}-10^{16} Ωcm at RT)	
Low or negative electron affinity	
Chemical	
Chemically inert and corrosion resistant	
Biocompatible	

Diamond is available in different forms. In principle, all diamonds can be categorised in just 2 classes (with 5 subclasses) by their infrared (IR) spectrum [38]. Type I diamond exhibits a large amount of incorporated nitrogen, while type II diamond is virtually free of nitrogen. A diamond can be formed naturally or synthetically (discussed in chapter 5), but it is only classified by its purity. Almost all natural diamonds are of type I, subclass a [39], and synthetic diamond is mostly classified in type Ib or IIc [34]. More on this classification of diamonds can be found in Davies' article from 1977 [38].

2.3 Thermal Conductivity

When the temperature of a material is raised, the heat tends to spread over the complete volume of the material. This heat transport is found to be governed by particle-involved mechanisms which try to restore thermodynamic equilibrium in the system subjected to a temperature gradient [40]. One can generally partition this thermal conductivity of a material into

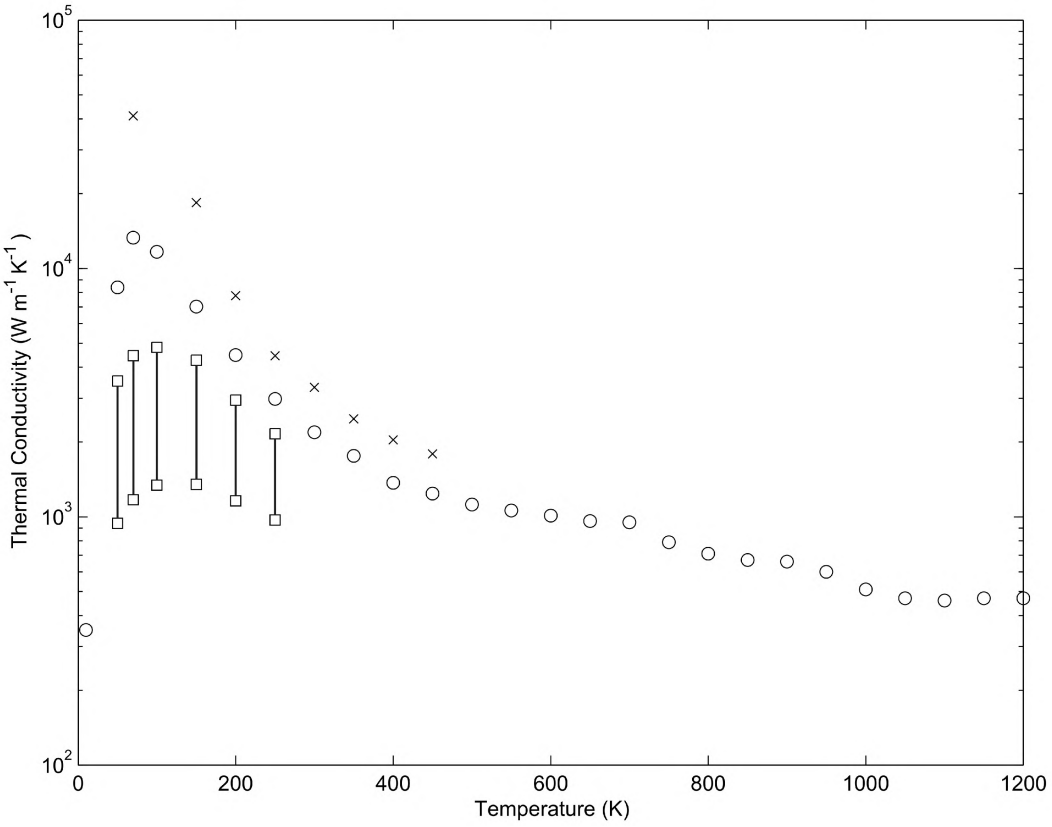

Figure 2.2: Averaged values for the thermal conductivity for natural (O) and isotopically purified (X) type IIa and type Ia (□) diamond as a function of temperature from available literature. For type Ia material the conductivity depends on the specific impurity level and a range of values is plotted ([32] and references therein).

- the electronic thermal conductivity, which depends on the electronic band structure, electron scattering, and electron-phonon interaction, and
- the lattice conductivity, which depends mainly on the phonons, nuclear vibrations, and phonon scattering [41].

These two (quasi) particles, electrons and phonons, are the main heat carrying entities. In metals, the electrical carriers transport the majority of the heat. But in (non-doped) diamond, being an electric insulator, the lattice waves are the dominant heat conductor. Therefore, the electronic thermal conductivity will not be considered below. Furthermore, there are other possible excitations in materials such as electromagnetic waves and spin waves, that may, under certain circumstances, contribute a small additional term to the thermal conductivity in, for instance, metals. For the most part, these small and often conjectured contributions can generally be ignored as well [40, 42].

In lattice thermal conductivity, when a temperature gradient is present in diamond, the thermal energy is considered as extra vibrations of the bonds between the carbon atoms, propagating in the form of lattice waves. These waves can then be viewed as a lineair combination of various normal modes, called phonons. The crystal lattice of diamond consists of relatively low mass atoms and strong bonds. The strong bonds pass the phonons on easily and because the carbon atoms are so light, they do not interfere

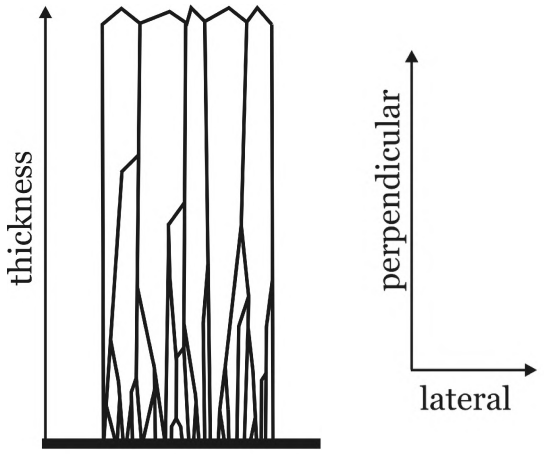

Figure 2.3: Schematic view of the structure of a polycrystalline diamond film. The directions of perpendicular and lateral heat flow are shown on the right. De diamond film is nucleated at the bottom and grows upward (after [32, 43]).

much with the thermal waves as well. The phonons thus travel in short time over relatively long distances in diamond in comparison to other materials, i.e., they have a long mean free path in diamond.

Lowering the mean free path of such a phonon in the material, and thus the resistance to heat flow, arises mostly from scattering of the phonons by defects in the crystal structure (lattice defects, grain boundaries, isotopes, impurities, etc.) and from collisions of phonons with each other, resulting in an alteration of phonon frequencies and momenta. Impurities predominantly shorten the phonon mean free path by adding additional scattering centers. In the next sections these considerations will be used to evaluate the thermal conductivity in single crystal and polycrystalline diamond.

2.3.1 Single Crystal Diamond

When comparing single crystal diamonds, the thermal conductivity is mostly determined by the purity of the crystal. The purest type IIa diamond has the highest thermal conductivity, while in type Ia and Ib material, containing more nitrogen impurities, the thermal conductivity is significantly lower. The most important impurities that lower thermal conductivity are nitrogen, hydrogen and the ^{13}C isotope of carbon [32]. Figure 2.2 shows the results available in literature. Especially for type Ia diamond the data are scattered, caused by different amounts of impurity in the investigated samples. In this case, a range of data points is given. The impact of the heavier ^{13}C isotope of carbon is clearly visible in the graph. Due to the low mass of the carbon atoms, changes in the isotopical content of diamond significantly affect its thermal conductivity, as the phonons are scattered due to the difference in mass of the different isotopes of carbon [32]. Therefore, isotopically purified diamond (99.999% ^{12}C) has been investigated intensively and measured to have a thermal conductivity of about 4000 W $m^{-1}K^{-1}$ at room temperature, increasing to 41,000 W $m^{-1}K^{-1}$ at T = 100 K [40, 44].

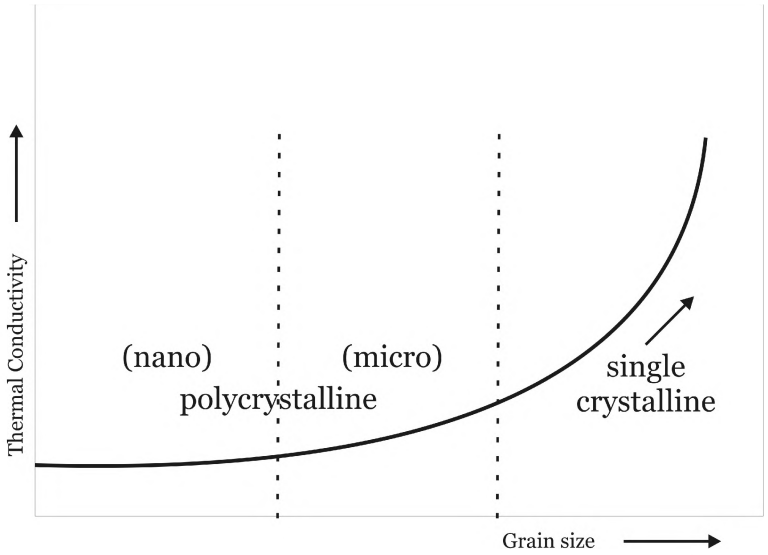

Figure 2.4: Thermal conductivity versus average grain size in a diamond film.

2.3.2 Polycrystalline Diamond

In polycrystalline films, diamond is grown from a large amount of nuclei on the surface of a substrate (see chapter 5). Therefore, the thermal conductivity may be highly anisotropic. Figure 2.3 depicts a schematic cross-section of a polycrystalline diamond film, with many small crystallites at the nucleation surface, of which only a small proportion grows as elongated crystals towards the surface of the film [45]. The thermal conductivity measured through the thickness of the film, along the single crystals (perpendicular direction), may be significantly higher than in the lateral direction, where the heat flow is hindered by grain boundaries [43]. Therefore, the thermal conductivity is also strongly affected by the diamond grain size, mainly because of the increased amount of grain boundaries with decreasing grain size (figure 2.4). It was shown that grain boundaries consist of hydrocarbon materials, like transpolyacetylene, diamond-like carbon, graphite and amorphous carbon with high contents of hydrogen [46]. Obviously, such a grain boundary is a source of highly localised thermal resistance [47] lowering the thermal conductivity dramatically. In the perpendicular direction, due to the columnar structure in the film, thermal conductivity is similar to values obtained from single crystal diamond [48, 49]. For the lateral dimension no well-defined value can be given for the thermal conductivity, because of the large distribution in crystallite sizes, grain boundary material, layer thickness and growth circumstances changing with each sample. However in general, when the quality of the produced material is good, polycrystalline diamond still outperforms copper in terms of thermal conductivity.

3

GaN/Diamond Heterostructures

3.1 Introduction

As was clarified in section 1.4, the preparation of GaN with a diamond layer appears to be a good solution to increase the temperature range for which GaN devices can be employed. To produce such heterostructures, several strategies have been explored to deposit both GaN and diamond with the other material as a substrate. The following sections will provide more information from literature on the achievements and main problems encountered with these combinations so far.

3.2 Deposition of CVD Diamond onto GaN

Adding a diamond layer on an existing GaN structure is the most direct approach to enhance the thermal stability of that structure. This, however, has been hindered much by the specific conditions of diamond growth. One of the major issues limiting diamond CVD onto GaN is the lack of high temperature stability of GaN under the typical diamond CVD process conditions. Although its normal melting point is almost 2800 °C (table 1.1), GaN reacts with hydrogen already at temperatures around 800 °C, decomposing into volatile products via the following reactions:

$$2N_{(surface)} + 3H_2(g) \rightleftharpoons 2NH_3(g); \tag{3.1}$$

$$2Ga_{(surface)} + H_2(g) \rightleftharpoons 2GaH(g). \tag{3.2}$$

Thus, the usual deposition conditions for diamond CVD including a substrate temperature in the range 600 - 800 °C can result in etching of the GaN. Alternatively, GaN can decompose according to:

$$2GaN(s) \rightleftharpoons 2Ga(l) + N_2(g), \tag{3.3}$$

although this requires temperatures $> 800\,°C$ due to the high barrier for the formation of liquid Ga droplets [50].

In literature several approaches to protect the GaN substrate from the volatile conditions have been reported, and these will discussed in short next.

3.2.1 Addition of an Annealing Step

May *et al.* [50] suggested that annealing of the GaN might be a suitable approach to reduce GaN decomposition. Therefore, they proposed an alternation between a growth and a healing step in a hot filament CVD setup. First, the most suitable filament distance was determined as this distance affects the substrate temperature and thus the GaN decomposition rate, but also influences the growth rate for diamond. Then, alteration of the CH_4-concentration and addition of N_2 were tested. Finally, a 2-step process was developed in which a cycle of 20 minutes of 1% CH_4/H_2 gas composition and 20 minutes of 2% N_2/H_2 was repeated for 8 hours. The idea is that during the 'nitrogen-free' steps, the diamond growth continues normally, although the GaN substrate begins to decompose. During the subsequent 'methane-free' step the nitrogen reacts with the GaN surface and 'heals' any fissures before they have a chance to grow too large and disrupt the integrity of the surface. The application of this technique resulted in a continuous, but porous layer of diamond of relatively poor quality and with a bad adherence to the surface. However, the decomposition of GaN was reduced substantially in comparison to earlier experiments [50].

3.2.2 Carburisation of GaN

Oba *et al.* [51, 52] introduced another multistep microwave plasma-assisted chemical vapour deposition technique (MPCVD) based on Bias-Enhanced Nucleation (BEN, [53]). First, the substrate, 1 μm (0001)-oriented hexagonal GaN grown on AlN/Al_2O_3, is hardened by introducing carbon into this layer. This process is called carburisation and the treatment time was 30 minutes. Then, the substrate is negatively biased at -100 V, to stimulate diamond nucleation [54] and the actual deposition is performed in 420 minutes [51]. Although CN_x is introduced into and probably ónto the substrate, XRD and Raman spectroscopy indicate the growth of (111) face of diamond grains, as predicted by comparison of atomic arrangement of GaN and diamond [52]. Results on the remaining quality of the GaN layer were not reported.

3.2.3 Protection by a SiN_x Layer

Finally, the application of a SiN_x [55, 56] or 'silicon-based' [57] protective layer was studied by several groups. Seelmann-Eggebert *et al.* [55] and Dipalo *et al.* [57] applied a GaN-based FET structure as a substrate, while Zou *et al.* used epitaxial GaN layers on sapphire [56].

Seelmann-Eggebert *et al.* reported delamination of their SiN_x layer in the plasma used for diamond growth [55] in contrast to Dipalo *et al.* who described a complete FET structure in which the diamond layer is integrated as an electrode. This structure is experimental and its operation leaves room for improvement [57]. None of the groups

reported surface investigation of the GaN layers after deposition, nor is the performance tested at high temperature.

On epitaxial GaN layers the best results were obtained in an argon-based plasma. The protective layer of 120 nm thickness is deposited with CVD, and subsequently seeded by fine diamond particles from an agitated emulsion to prepare diamond nucleation. The growth of diamond was conformal to the patterned substrate and no cracks were observed [56].

3.3 GaN Layers on Diamond

Another interesting possibility to avoid the decomposition of GaN is the alternative construction of the GaN-diamond heterostructures: the deposition of GaN on a diamond substrate. The application of MOCVD (section 4.3) for this purpose has been attempted first by Hageman *et al.* [58] followed by MBE (section 4.5.1) growth of GaN only very recently.

3.3.1 MOCVD Growth

On a (110) single crystal diamond, a low temperature AlN is deposited as nucleation layer for the MOCVD experiments. The resulting MOCVD GaN layer is polycrystalline and hexagonal with, as a result of carbon incorporation originating from the substrate, a very poor optical quality as determined by photoluminescence. Additional enlargement of the thickness of the GaN film using HVPE preserved the hexagonal structure and resulted in a layer of good optical quality. X-Ray diffraction analysis revealed that the dominant orientation of the GaN crystallites parallel to the substrate changed from (0001) for the thin MOCVD film to $(11\bar{2}2)$ for the HVPE layer [58].

Furthermore, Zhang *et al.* also prepared fine-grained polycrystalline GaN films with preferred (0001) orientation on the nucleation surfaces of freestanding diamond films for surface acoustic wave filters. Although no epitaxial film was grown, the rms surface roughness of the GaN layer was found to be only 5.3 nm. However no further information is given on the optical and structural properties [59].

3.3.2 Molecular Beam Epitaxy

In contrast to the above mentioned MOCVD growth of GaN on (110) single crystal diamond, recent studies applying ammonia-based MBE used the less available, but geometrically more similar in lattice structure [60], single crystal diamond substrates with (111) orientation and an AlN buffer layer [61, 62]. This resulted in smooth (0001) oriented GaN films of good optical quality. However, for thicknesses over 250 nm cracks were observed on the surface ascribed to the large thermal expansion coefficient mismatch between GaN and diamond [61].

With these results the first GaN/AlGaN HEMT with a monolithically integrated heat spreader could be realised by direct growth on (111) single crystal diamond and subsequent processing. Its characteristics are approaching the values for these devices grown on Si, but thermal aspects have not been investigated yet [62].

3.4 Other Approaches for Making GaN/Diamond Heterostructures

Next to direct growth of GaN or diamond, other techniques targeting the integration of diamond heat spreaders with GaN structures should be mentioned here too. The next sections cover the basics of two alternatives already available commercially: The application of diamond in silicon-on-insulator substrates and the so-called atomically attaching of diamond layers on GaN films.

3.4.1 Silicon-on-Diamond Substrates

Silicon-on-diamond (SOD) substrates are the thermally enhanced equivalent of silicon-on-insulator (SOI) wafers commonly used in the silicon semiconductor industry [63]. These SOI wafers, fabricated by numereous different processes [64, 65], often consist of a film of single crystalline Si separated by a layer of insulating SiO_2 from the bulk Si substrate, preventing parasitic current leakage to the bulk substrate. Clearly, the substitution of SiO_2 with electrically insulating, but also high thermally conductive diamond upgrades SOI substrates to handle increased thermal loads [66], which was also confirmed by simulations on the subject [63]. In 1992, Annamalai *et al.* were the first to succesfully fabricate this SOD concept [67], and it was shown that devices on SOD sustain more than 10 times the power of an equal device on SOI [68].

Since SOD is basically Si with a buried diamond insulator under the surface, the substrate can also be used for developing GaN structures similar to GaN on 'normal' bulk Si. This has been demonstrated by Zimmer and Chandler who prepared GaN layers and devices on SOD and made GaN on SOD up to 100 mm commercially available at sp^3 Diamond Technologies Inc., Santa Clara, CA, USA [63, 69, 70].

3.4.2 Atomically Attaching of Diamond Layers

Following the same motives, Group4 Labs (Fremont, CA, USA) developed their own technique to combine GaN with diamond. Their process starts with GaN epilayers grown on a sacrificial Si substrate. Then this layer is transferred to a mechanical carrier, after which the original substrate is removed by etching [71]. The exposed buffer is treated with a proprietary dielectric coating [72] and a 50 nm adhesion layer [73], followed by 'atomically attaching' of a polished CVD diamond wafer. The mechanical carrier is then removed, leaving the GaN layer ready for further processing [74].

Subsequently, a GaN/AlGaN HEMT grown on this structure is reported to operate well [75]. Currently, only Group4 Labs offers GaN/Diamond substrates with diameters up to 100 mm and in 2 different diamond thermal conductivity grades (800 and 1500 W $m^{-1}K^{-1}$) on their website with prices starting from $ 450 for 10x10 mm^2 substrates.

3.5 Concluding Remarks

In contradiction to the many different techniques that have been explored, no method for the deposition of diamond on GaN has been developed in which the GaN remains unaffected and a flawless polycrystalline diamond layer has been obtained. This is caused

by the high deposition temperatures necessary for diamond growth, which results in thermal decomposition of the GaN substrate. The techniques mentioned in section 3.2 are all in some way effective in protecting the GaN substrate (although the growth details of the protective layer and the precise state of the GaN after diamond growth are not mentioned in all reports) but the quality of the diamond layer should be improved in most cases. Maybe subtle changes in growth conditions or the exploration of lower growth-temperature techniques, like the application of microwave plasma-activated CO_2/CH_4 gas mixtures [76], provide better growth conditions. The addition of chlorinated gases to the growth mixture can also allow lower temperature diamond deposition [77, 78], however this approach probably would not be viable in the presence of GaN, which is known to be rapidly etched by Cl_2 [79].

The research of commercially available alternatives mentioned in section 3.4 has demonstrated that the application of diamond for thermal management purposes is very effective, eventhough a barrier remains between the active device structure and the diamond heat sink. Therefore, direct MOCVD growth of GaN on diamond still is a good alternative that should be investigated thoroughly.

Part II

Techniques

4

Gallium Nitride Growth

4.1 Introduction

In section 1.3 various applications for GaN are listed. They all need mass-produced devices, which performance is equally linked to growth methods and processing technologies. Bulk growth methods are used for the production of GaN substrates. Due to the low availability of these GaN substrates most GaN layers for devices are commenced on foreign substrates by a variety of methods. Their benefits and disadvantages will be discussed in the upcoming sections. First, common substrates for GaN epitaxy are described and compared. As this research mostly concentrates on the growth of GaN by MOCVD, this technique will be described then, after which the other methods for GaN epitaxy and techniques applied for bulk growth are briefly discussed.

4.2 Substrates for Epitaxy

Because bulk GaN crystals have low commercial availability, most researchers have relied on heteroepitaxy, which is crystal growth on substrates of another material, for device fabrication. Most often, the lattice constant mismatch has been the primary criterion for determining the suitability of a material as a substrate for GaN epitaxy. A wide variety of materials have been studied for GaN epitaxy including insulating metal oxides, metals, metal nitrides, and other semiconductors. The properties and (dis)advantages of diamond have been discussed already in chapters 2 and 3, as well as SOD substrates (chapter 3). Other important supporting materials for the epitaxial growth of wurtzite GaN that are of interest to this research are discussed below. An extensive summary of all attempted substrates is given by Liu and Edgar [80].

In practice, properties other than the lattice constants such as the materials crystal structure, surface finish, composition, reactivity, chemical, thermal, and electrical properties and thermal conductivity, are important in determining the suitability of a substrate,

as these greatly influence the resulting properties of the epitaxial layer. The substrate employed determines the crystal orientation, polarity, polytype, surface morphology, strain, and the defect concentration of the GaN film. Thus, the substrate properties may ultimately determine whether the device achieves its optimal performance [80].

4.2.1 Sapphire

Sapphire, (Al_2O_3), was the first substrate used in the study of GaN epitaxy by HVPE in 1969 [5], and it is still the most commonly used substrate for GaN growth. The large lattice constant (30% larger than GaN perpendicular to the c-axis) leads to a 16% lattice mismatch with GaN in combination with a 30 ° rotation of the GaN lattice with respect to the sapphire lattice [81]. Such a large mismatch leads to a high dislocation density (commonly $\sim 5 \cdot 10^9$ cm^{-2}) in the GaN epitaxial films, which reduces the charge carrier mobility, and the minority carrier lifetime, which both degrade device performance. Additionally, sapphire's thermal expansion coefficient is greater than GaN, thus biaxial compressive stress in the layer is produced during cooling down from deposition to room temperature. For thick films, such as can be grown by HVPE, the stress can cause both the film and the substrate to crack [82]. The thermal conductivity of sapphire is low (about 0.35 W cm^{-1}K^{-1} at 100 °C), thus, it is relatively poor in removing heat as compared to other substrate materials. The cleavage planes of the epitaxial GaN layer are not parallel to those of sapphire (because of the forementioned rotation [83]), making laser facet formation as well as cleaving very difficult. Sapphire is electrically insulating, thus, all electrical contacts must be applied to the front side of the device, reducing the area available for devices and significantly complicating device fabrication. In addition, there is evidence that oxygen from the sapphire causes unintentional doping of the GaN layer, raising its background electron concentration [80]. However, with a proper nitridation process and an optimised low temperature buffer layer of either AlN or GaN, very smooth GaN films can be obtained (see section 4.4).

4.2.2 Silicon Carbide

Silicon carbide (SiC) has several advantages over sapphire for GaN epitaxy, including a smaller lattice constant mismatch ($\sim$3.8%) for c-plane oriented films, and a much higher thermal conductivity ($\sim$4.0 W cm^{-1}K^{-1}), which is important for high power applications [2].

The crystal planes in epitaxial GaN are parallel to those of the SiC substrate, making facet formation by cleaving easier. However, it also comes at a high cost, in limited availability and size, and has relatively poor crystal quality and surface finish compared with conventional silicon and sapphire substrates. This roughness and also subsurface polishing damage are sources of defects for the GaN epitaxial layer. SiC's thermal expansion coefficient is less than that of GaN, thus, the films are typically under biaxial tension at room temperature [80]. Moreover, GaN epitaxy directly on SiC is problematic, due to poor wetting of SiC by GaN. Even though the lattice constant mismatch for SiC is smaller than that for sapphire, it is still sufficiently large to cause a large density of defects in the GaN layers ($1 \cdot 10^9$ cm^{-2}) [65].

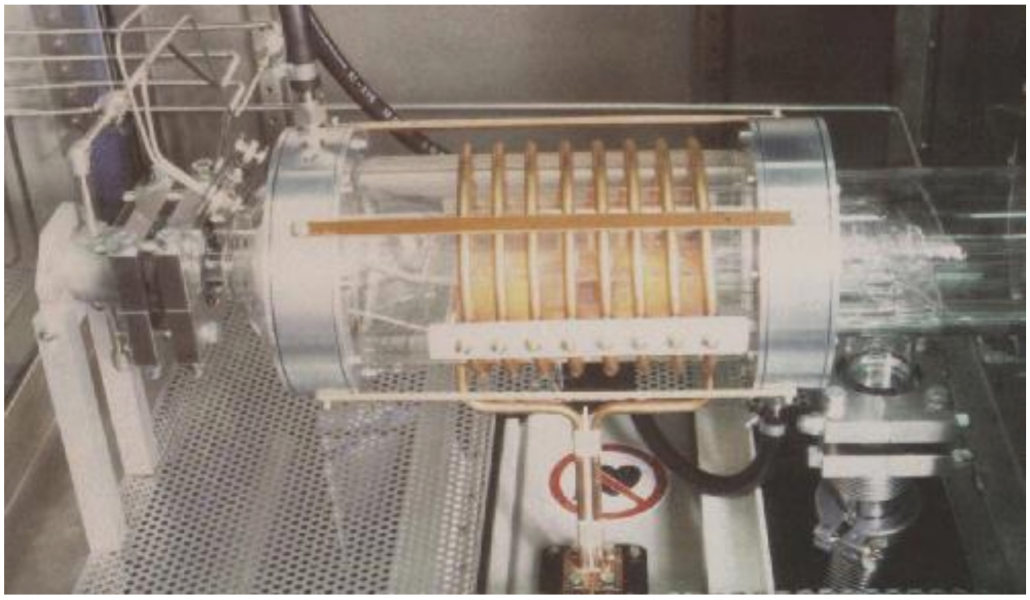

Figure 4.1: The MOCVD reactor [7].

4.3 Metalorganic Chemical Vapour Deposition

Metalorganic chemical vapour deposition (MOCVD) is by far the most common technique for growing GaN and other III-V layers. It is often referred to as organometallic vapour-phase epitaxy (OMVPE) and other permutations of these same letters (OMCVD and MOVPE). Although the terminology organometallic, to describe the precursor molecules, agrees with the general chemical nomenclature, MOCVD and MOVPE are most commonly used. CVD is the general term describing the growth process, since it implies nothing about whether the resultant layer is single crystalline, polycrystalline, or amorphous [7, 84].

4.3.1 The MOCVD Reactor

For the growth of GaN described in this thesis an Aixtron 200 RF reactor is used (figure 4.1), however the gas system necessary for this MOCVD system is home-built (figure 4.2). The reactor (figure 4.1) has a horizontal design and is made of quartz. It is heated with a RF coil and the reactor walls are actively cooled with water. The reactor walls are substantially colder than the heated susceptor to minimise deposition on the walls. The susceptor is placed parallel to the gas flow direction and is equipped with a rotating disc, on which the substrate is placed, to obtain uniform growth. Rotation is realised by a small gas flow. The temperature is regulated by a thermocouple placed below the centre of the susceptor disc, all the growth temperatures in this thesis are the values acquired by this thermocouple [7].

The gas handling system takes care of the transport and dosimetry of the gasses into the reactor. Ammonia (Group V) is stored in a cylinder (figure 4.2, top center). The group III species are all metalorganic compounds, which are stored in stainless steel bubblers (figure 4.2, bottom left). The gas handling system (figure 4.2, center) is equipped with valves, flowmeters (FC) and pressure controllers (PC) to make it possible to transport the

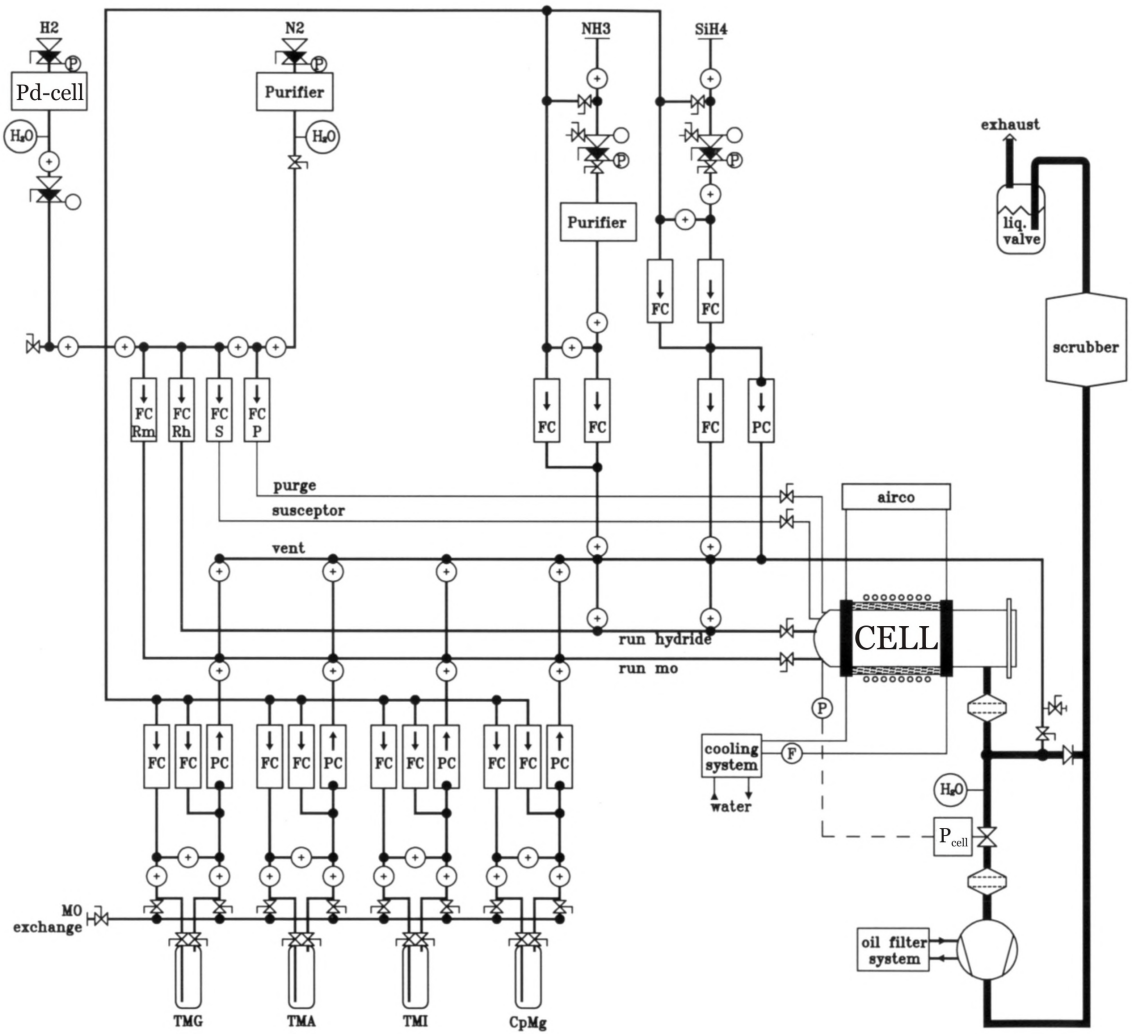

Figure 4.2: Schematic diagram of the MOCVD system.

correct amounts of growth and doping species into the reactor cell. A vent-run system is incorporated to allow for fast switching of the gasses between run lines (growth) or vent lines (exhaust). The complete system is fully computerised, so that the automatic handling of valves, flow and pressure controllers, as well as the temperature and pressure in the reactor cell, is possible. This automisation increases the controllability and safety of the process [85].

The exhaust of the reactor cell is connected to a vacuum pump with a pressure regulating system. A scrubber then cleans the waste gasses for proper emission to the air (figure 4.2, far right).

4.4 Principles of MOCVD

MOCVD is a non-equilibrium growth technique, which depends on the transport of gas phase organometallic precursors, hydrides (like ammonia, NH_3, as a nitrogen source), and carrier gasses to a heated substrate on which the precursors are pyrolysed and the film is deposited [86]. The underlying chemical mechanisms are complex, involving a

combination of gas phase and surface reactions. Composition and growth rate are regulated by precisely controlling mass flow rate and dilution of various components in the gas stream. The organometallic precursors are either liquids, such as trimethylgallium (TMG) and trimethylaluminum (TMA), or solids like trimethylindium (TMI). The organometallic sources are stored in bubblers through which a carrier gas (typically hydrogen) flows. The bubbler temperature determines the vapour pressure over the source material. Carrier gas will saturate with vapour from the source and transport the precursor to the heated substrate. NH_3 is used as nitrogen source in nitride growth. The high thermal stability of NH_3 is one of the main reasons for the high substrate temperatures, typically more than 1000 °C. Dopant materials can be organometallic precursors, like bis(cyclopentadienyl)magnesium or ferrocene for p-type doping, or hydrides (like silane and disilane) for n-type doping.

Regardless of the choice of substrate, many of its shortcomings such as its crystal quality or poor bonding characteristics with GaN can be ameliorated through an appropriate surface preparation such as nitridation, deposition of a low-temperature AlN or GaN nucleation layer, multiple buffer layers [87] and other techniques. However, the growth parameters are also largely restricted by the choice of the substrate. Therefore, a typical MOCVD growth run consists of several consecutive stages, depicted in figure 4.3. Often the growth process starts with an in situ cleaning step (for example: 5 minutes at 1170 °C in H_2 atmosphere) followed by nitridation of the substrate (section 4.4.1). Then a special nucleation layer is deposited (4.4.2), which after annealing is suitable for the growth of the main layer of GaN and AlGaN (4.4.3). Each step has its own purpose and optimal settings, but it is the combination of settings in all stages that finally results in excellent quality GaN layers and devices.

For example, the high interfacial energy between a GaN layer and the sapphire substrate leads to 3D island growth, so the growth and annealing of GaN, AlN or $Al_xGa_{(1-x)}N$ nucleation layers are inevitable processes for the step flow growth. The thermal annealing process transforms the as-deposited nucleation layer into isolated islands with (0001) facets. Subsequently, enhanced lateral growth suppresses threading dislocations caused by coalescence of GaN islands in the initial stage of low-pressure MOCVD [88].

In the next sections, the theoretical background of each stage will be discussed.

4.4.1 Nitridation

In 1988, Kawakami *et al.* were the first to employ nitridation of sapphire (Al_2O_3) to overcome the lattice mismatch between this substrate and epitaxial AlN. A nitridation layer was formed by chemical conversion of the Al_2O_3 surface in NH_3 gas at 1200 °C and low pressure and it was found to improve the quality of subsequently grown GaN enormously [89]. However, Keller *et al.* concluded that too long nitridation increased the dislocation density, while decreasing the electron mobility and photoluminescence signal of the GaN films [90].

As sapphire is the most common substrate for epitaxial GaN growth the nitridation stage is of great importance. However, it is only applicable for sapphire, because for other substrates (with the exception of GaAs [80]) no chemical conversion of the substrate is obtained after treatment with nitrogen [91].

When analyzing the surface composition, several groups found that the top layer of the sapphire after nitridation consists of amorphous $AlN_xO_{(1-x)}$ [89, 92–94], while oth-

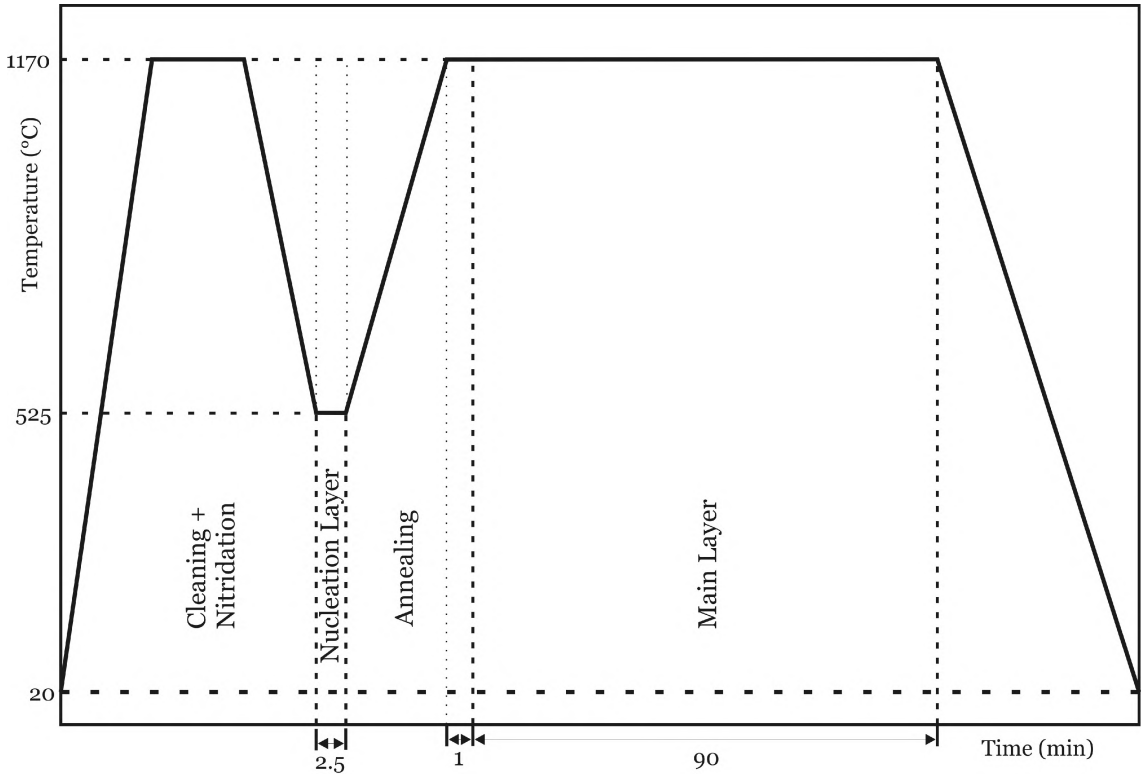

Figure 4.3: Temperature profile of a typical growth run of GaN on a sapphire substrate using MOCVD. The different stages of the growth process are indicated in the corresponding segments.

ers observed that the oxygen content was decreasing over time and crystalline AlN was formed [91, 95]. At the temperatures used in MOCVD growth $AlN_xO_{(1-x)}$ should be unstable and nitridation of sapphire should only form AlN [96]. However, some intermediate form, where nitrogen is built into the Al_2O_3 lattice resulting in a thin top layer of $AlN_xO_{(1-x)}$, is also possible [97, 98].

4.4.2 Nucleation Layer and Annealing

In addition to nitridation, the addition of a low temperature GaN or AlN nucleation layer (usually about 500-600 °C) dramatically improves the surface morphology and crystalline quality of GaN deposited next at high temperature (usually about 1100-1200 °C) on sapphire. For other substrates, like SiC, $Al_xGa_{(1-x)}N$ nucleation layers have also been considered as they have a smaller lattice mismatch to GaN and can be electrically conductive. The influence of variations in process conditions in the growth of the nucleation layer on the quality of subsequent GaN layers have been explored, such as growth temperature [99, 100] and nucleation layer thickness [100–102]. Although it is established that nucleation layers improve the quality of subsequently grown GaN films, there is no significant difference between using GaN or AlN as the nucleation material for growth on sapphire [103]. For other substrates, the use of AlN as nucleation material is often preferred, because it has improved wetting on many substrates and thus facilitates a better nucleation of the GaN main layer [97].

The effect of the nucleation layer is closely related to the thermal annealing stage that follows, because the low temperature deposited material is more or less amorphous [104]

and needs to recrystallise to well oriented nuclei in order to produce good quality GaN [105]. This recrystallisation of the nucleation layer is normally combined with the necessary ramping of the temperature from its deposition temperature to the growth temperature of the main GaN layer [106]. Also, this thermal treatment is found to be an essential process in the reduction of stacking faults in the main GaN layer [100, 106].

As the temperature is increased, the amorphous nucleation layer decomposes uniformly from about 850 °C. Decomposition of the original nucleation layer material drives the formation of nuclei on top of the nucleation layer, via an evaporation and recondensation mechanism [105]. These well oriented small nuclei, having a relatively small misorientation, begin to appear on the nucleation layer near 1000 °C, increasing the layer's roughness. The nuclei are formed by gas-phase transport of gallium or aluminum atoms generated during nucleation layer decomposition that recombine with ambient NH_3. Once the original nucleation layer material is fully decomposed, the nuclei stop growing in size and begin to decompose again. Under optimum conditions, thus when the nucleation layer is completely recrystallised, approximately 1/3 of the nucleation layer material is reincorporated into the nuclei from the vapour. The remaining nucleation layer material is evaporated [105]. In principle, for thicker nucleation layers the thermal annealing time should be longer and in this way, nucleation layers with different thicknesses can be annealed to similar morphology, as was discovered by Ito *et al.* [100].

4.4.3 Main Growth

While the nucleation layer is designed to create 3D nuclei on the substrate, for the main GaN layer the circumstances are altered towards (quasi-)2D growth to obtain an, as flat as possible, surface. Therefore, in the first minutes of main layer growth, the nucleation islands need to coalesce to form an epitaxial layer. During this coalescence, spatial differences between adjacent islands cause tension on the coalescence interface and this leads to the generation of threading dislocations on that interface. This appears to be the main source for dislocations in the following GaN layer, but also, when the islands are slightly rotated in the plane of growth, low angle tilt boundaries, composed of edge dislocations, will develop during coalescence [107]. A lower density of larger islands thus results in a lower dislocation density [88].

To stimulate the lateral growth, often the reactor pressure and growth temperature are altered in comparison to previous growth stages. Enlargement of the ratio between NH_3 and TMG is also shown to improve the 2D growth mode [108]. Then, a high quality layer with sharp interface or surface can be grown, finally leading to well operating devices.

4.5 Other Techniques for GaN Epitaxy

4.5.1 Molecular Beam Epitaxy

Molecular beam epitaxy (MBE) is an Ultra-High-Vacuum (UHV)-based technique for producing high quality epitaxial structures with very good thickness control. Since its introduction in the 1970s as a tool for growing high-purity semiconductor films, MBE has evolved into one of the most widely used techniques for producing epitaxial layers of metals, insulators and superconductors in research. The principle underlying MBE

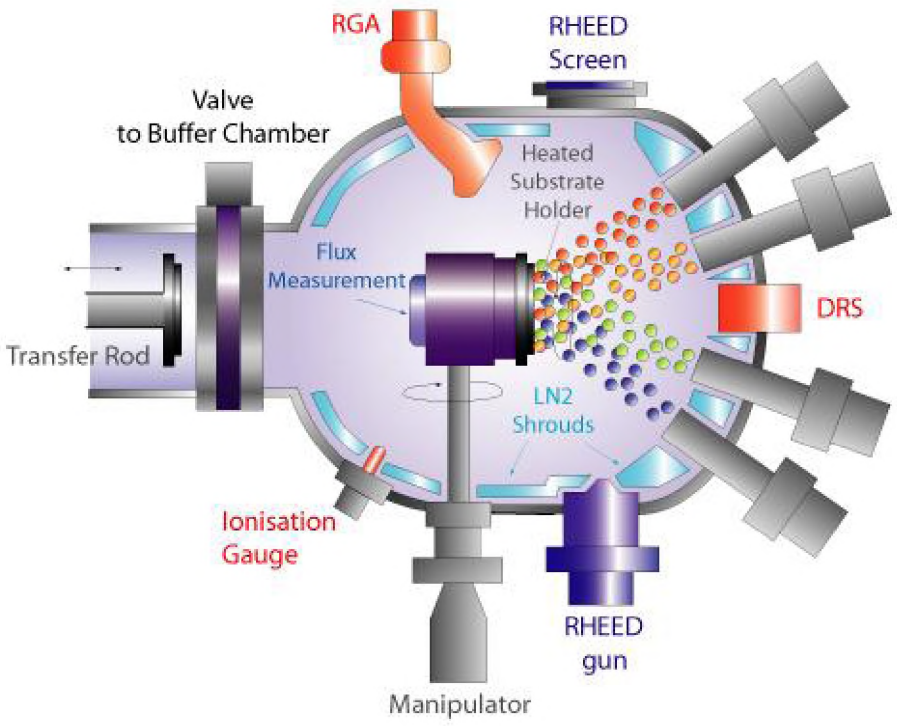

Figure 4.4: Schematics of an MBE system. The RGA is used for residual gas analysation, while DRS (diffuse reflectance spectroscopy) is applied for additional substrate temperature measurements. LN2 shrouds denotes the area cooled with liquid nitrogen.

growth is relatively simple: it consists essentially of atoms or clusters of atoms, which are produced by heating up an elemental or molecular source (figure 4.4). They then migrate in an UHV environment and impinge onto a hot substrate surface, where they can diffuse and eventually incorporate into the growing film. The rate of growth depends on the flux of material in the molecular beams, which can be controlled by the temperature and switched on and off with shutters. Typical growth rates are 1 monolayer per second or 1 micron per hour, which is equivalent to a partial pressure of $1 \cdot 10^{-6}$ mbar in the flux arriving at the substrate in the molecular beams. Great care is taken to ensure that only negligible quantities of impurity atoms are introduced into the material: substrates are carefully prepared and cleaned; ultra pure sources are used; the base pressure of the reaction chamber is kept in the low 10^{-10} mbar range and the walls of the chamber are cooled with liquid nitrogen [65].

Despite the conceptual simplicity, a great technological effort is required to produce systems that yield the desired quality in terms of material purity, uniformity and interface control. The choice of MBE and other growth techniques depends on the desired structure and needs. For example, for devices such as quantum wells or distributed Bragg reflectors, or even novel designs of transistors, where quality of interface and tight thickness control is required, MBE is the growth tool of choice. However, in the case of mass production MBE suffers from a lower yield, compared to MOCVD systems. Not only is the growth rate smaller, but also reactor and sample preparation is much more time consuming [65].

4.5.2 Hydride Vapour Phase Epitaxy

Hydride Vapour Phase Epitaxy (HVPE) is used to grow various types of semiconductors such as InP, GaAs, GaN, and related compounds. In each case, the reactants are delivered to the substrate in the gas phase, in which HCl reacts with the group three component, and the group five component is delivered as a hydride (figure 4.5). Growth of GaN is done by bubbling HCl gas with a hydrogen carrier gas through a gallium boat in the source zone at 800 °C forming $GaCl_3$; ammonia, with hydrogen carrier gas, is transported to the substrate through a separate quartz tube. All of this takes place in a heated quartz chamber and the substrate, mostly sapphire, is placed on a quartz susceptor, which is heated to ∼1100 °C. HVPE is characterised by very high growth rates of > 100 μm/h, compared to ∼1-2 μm/hour for the aforementioned methods. It does not allow growth of heterostructures as good as the other methods due to largely inaccurate thickness control. In addition, the impurity concentration is not as low as in deposition systems with lower growth rates such as MOCVD and MBE. However, thanks to its high growth rate and therefore sheer thickness potential for GaN layers, it might be a method of creation of free standing GaN substrates. In fact, such substrates have been available for some time already, but the available volume is nowhere near the industrial demand. Some manufacturers also use the HVPE technology to produce LEDs, since the amount of ammonia used is estimated to be at least one order of magnitude lower compared to MOCVD. Also, HVPE uses pure metals as starting materials rather than metalorganic precursors, which are a factor of 10 more expensive per gram of metal. With improved deposition control, HVPE might become the best solution for growth of low complexity optoelectronic devices [109].

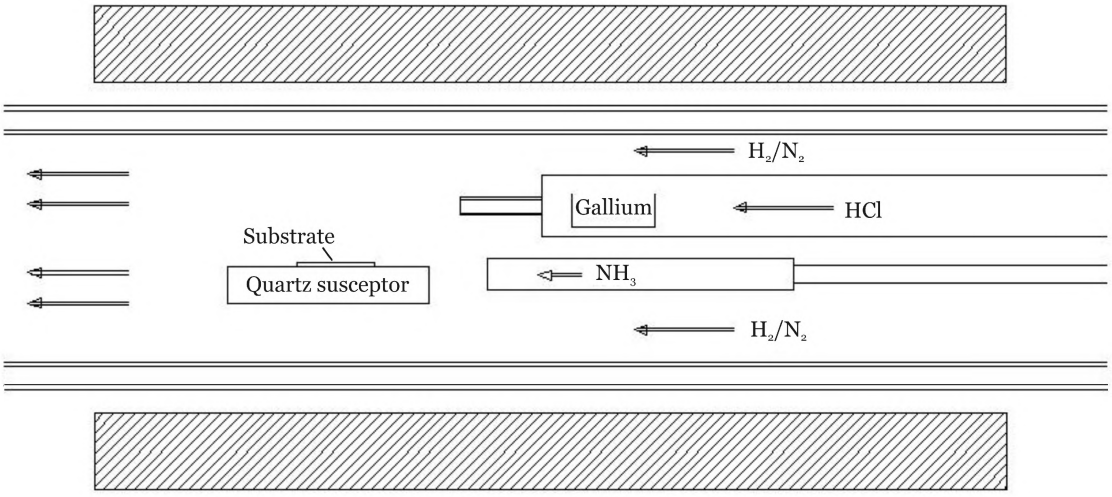

Figure 4.5: Lay-out of the HVPE system operational at the Radboud University Nijmegen.

4.6 GaN Bulk Growth

The three techniques mentioned above concentrate on growth of GaN layers upon various substrates, due to a lack of commercially available GaN single crystal substrates. Therefore, new techniques were developed that concentrate on the production of free standing

GaN platelets, for instance the ammonothermal method (section 4.6.1) and high nitrogen pressure solution method (section 4.6.2).

4.6.1 Ammonothermal Method

The idea of the ammonothermal technique was inspired from the field of hydrothermal technology, used commercially in quartz mass production (tens of tons per year are produced), where supercritical aqueous solutions are used for the recrystallisation of silicon oxides. The ammonothermal method is regarded as an analogue of the hydrothermal one, where ammonia instead of water is used as a solvent and thus nitrides can be grown instead of oxides. The typical temperatures and pressures applied are 400-600 °C and 0.1-0.3 GPa, respectively. The scheme of the crystal growth process is the following: GaN containing feedstock is dissolved in one zone of the high-pressure autoclave, then transported by convection induced by the temperature gradient toward the second zone, where GaN crystallises on native seeds due to the supersaturation of the solution (figure 4.6). In addition, the use of mineralisers is necessary in order to enhance the solubility of GaN in ammonia. In the case of ammonobasic environment of ammonothermal growth, NH_2^- ions are introduced into the solution, while NH_4^+ ions are added in case of an acidic environment. Neither of them are supplied in a neutral environment [110].

It was reported that the ammonothermal method works both in the ammonobasic [111] and the ammonoacidic [112] regime. Growth takes place on both the Ga and the N-face of the GaN seed crystals with a growth rate up to 150 μm/day. However, some important details of these two approaches are different. The main difference is that in ammonobasic growth the GaN feedstock dissolves in the low-temperature zone and crystallises in the high-temperature zone located in the lower part of the autoclave (figure 4.6), while in ammonoacidic growth this situation is reversed. The latter also requires special equipment that does not dissolve in this strong acidic environment.

The growth of III-nitride bulk crystals from solution in an autoclave has several advantages over other growth techniques: (1) simple equipment, (2) process scalability, (3) simultaneous growth on multiple seeds, (4) high-quality bulk crystals, and (5) lower process temperatures compared with other growth techniques. The slow growth rate is one of the disadvantages of this method, especially in lateral growth; enlarging crystals in surface size is therefore complicated. Moreover the availability of high quality seed crystals is limited. However, if available, hundreds of templates or seeds can be loaded at the same time and grown simultaneously [65].

4.6.2 High Nitrogen Pressure Solution Method

The High Pressure Research Center in Warsaw has developed a technique to grow bulk GaN platelets, namely the so called 'high nitrogen pressure solution' method [3]. GaN is crystallised in gas pressurised chambers with volumes up to 1500 cm^3, allowing crucibles with a working volume of 50-100 cm^3. The high pressure, high temperature reactor consists of a pressure chamber and a multizone furnace. Additionally, it is equipped with systems for in-situ annealing in vacuum, electronic stabilisation and programming of pressure and temperature and cooling of the pressure chamber. Bulk crystals are produced from gallium melts saturated with 1 at.% nitrogen at temperatures up to 1700 °C and nitrogen pressures of 20 kbar. The structural properties of the bulk crystals are excellent

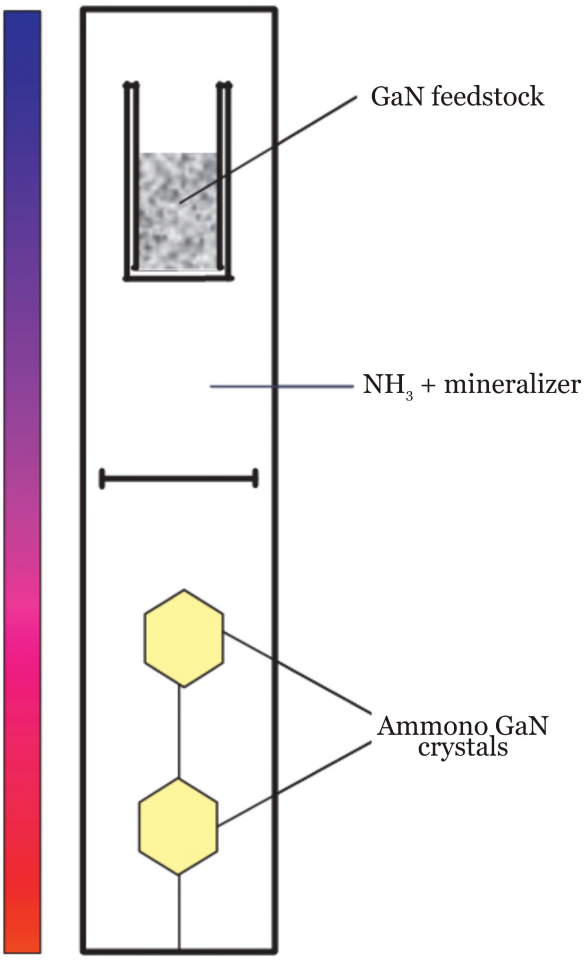

Figure 4.6: Schematic of the Ammonothermal-bulk growth method from ammonobasic solutions. The colored bar in the left represents the temperature gradient: Red - highest temperature, Blue - lowest temperature [111].

with very narrow X-ray rocking curve widths for all crystals planes, low dislocation densities, and negligible strain. The optical and electrical properties of the bulk crystals are, however, poor compared to heteroepitaxial GaN layers deposited on sapphire and other substrates, a consequence of high concentrations of residual impurities (oxygen, carbon) and point defect concentrations (believed to be primarily Ga vacancies) [3].

Such substrates could be used for production of real state-of-the-art devices because of their extremely low density of dislocations (∼5-8 orders of magnitude less than heteroepitaxially grown GaN layers) and perfect matching of thermal expansion coefficients. However, at present the volume of production as well as the size of such GaN single crystals hinder their use for other than research purposes [65].

5

Diamond Deposition

5.1 Introduction

Natural diamonds are created through a process which takes millions of years. Conditions for diamond formation are found deep below the Earth's surface, in the upper mantle region, where temperatures are very high and pressure can get quite intense. There, carbon is crystallised from magma solution into diamond.

The scarcity and consequently the high cost of natural diamonds drove people to find ways to synthesize diamond artificially. Since the 1940s, intensive research led to several techniques that make it possible to produce several grades of diamond on demand. First, the high-pressure high-temperature (HPHT, section 5.4) diamond synthesis process was developed, mimicking the way in which natural diamonds are formed by geophysical processes deep in the earth [113, 114]. The diamond crystals produced by the HPHT technique are used for a wide range of industrial processes, such as cutting and machining mechanical components, and polishing and grinding of optics. In these applications, the extreme hardness and wear resistance of the crystals are utilised. However, the drawback of the HPHT method is that it still produces diamond in the form of single crystals ranging in size from micrometres to millimeters, and this limits the amount of applications for which it can be used. Therefore, in the 1980s a method was developed in which diamond is deposited in the form of a thin film, allowing more of the diamonds properties to be exploited.

Rather than trying to duplicate nature's method (as in the HPHT technique), diamond can also be produced by adding carbon atoms one-at-a-time to an initial template, in such a way that a tetrahedrally bonded carbon network is formed. If this is accomplished from the gas phase using much lower pressure and temperature than in HPHT, it will give an obvious advantage in terms of equipment and energy costs. These ideas led to the development of an alternative method called Chemical Vapour Deposition (CVD) of

diamond [115, 116]. Like the MOCVD growth of GaN (section 4.3), this method involves a gas phase chemical reaction occuring above and on top of a solid surface, leading to deposition of a thin layer onto that surface [117]. In this chapter, CVD diamond deposition is discussed in detail, after which some words are spent on other methods for synthetic diamond growth.

5.2 Chemical Vapour Deposition of Diamond

5.2.1 Introduction

Today, a wide variety of methods of forming diamond at low pressures and moderate temperatures (listed and reviewed in [118]) exist, all requiring a means of activating gas phase carbon-containing precursor molecules. This activation can involve thermal methods (e.g. a hot filament), electric discharge (e.g. DC, RF or microwave plasma), laser activation or a combustion flame (such as an oxyacetylene torch). Figure 5.1 illustrates some of these experimental methods schematically. While each method differs in detail in addition to gas phase activation, they also share a number of other features in common. For example, the temperature of the substrate is usually higher than 700 °C to ensure the formation of diamond rather than amorphous carbon. Also, growth of diamond (rather than graphite) normally requires that the precursor gas (usually CH_4) is diluted in excess of hydrogen, in a typical mixing ratio of 1 vol.% CH_4.

These gases first mix at the inlet of the reactor chamber before diffusing toward the substrate surface. En route, they pass through an activation region (e.g. a hot filament or electric discharge), which provides energy to the gaseous species. This activation causes molecules to fragment into reactive radicals and atoms, creates ions, and heats the gas up to temperatures approaching a few thousand degrees Celsius. Beyond the activation region, these reactive fragments continue to mix and undergo a complex set of chemical reactions until they strike the substrate surface. At this point the species can either adsorb and react with the surface, desorb back into the gas phase, or diffuse around close to the surface until an appropriate reaction site is found. If a surface reaction occurs, one possible outcome, if all the conditions are fulfilled, is diamond [117].

In 1994, Bachmann *et al.* already found that diamond growth is independent of the nature of the gas phase precursors, and that the gas phase chemistry is so rapid that it simply and effectively breaks down the constituent gases to smaller, reactive components [120]. Based on more than 70 deposition experiments in different reactors and using different process gases, they developed the 'Bachmann triangle diagram' (figure 5.2), which is a C-H-O composition diagram. Bachmann *et al.* found that independent of deposition system or gas mixture, diamond will only grow if the gas composition is close to and just above the CO tie-line, as depicted in the triangle. The size of the domain, which shape was confirmed by thermodynamic calculations [121], changes with the deposition temperature and pressure of the gas phase, but is neither dependent on the deposition technique nor on the specific input gases used [33]. Note that most experiments, involving just a few percent CH_4 in H_2, are constrained to a small region in the lower left-hand corner of figure 5.2. Gas mixtures that have a composition more rich in oxygen (towards the lower right corner in the triangle) produce no deposited material at all, only CO or CO_2 is formed. On the carbon-rich side, deposition of non-diamond carbon dominates [118].

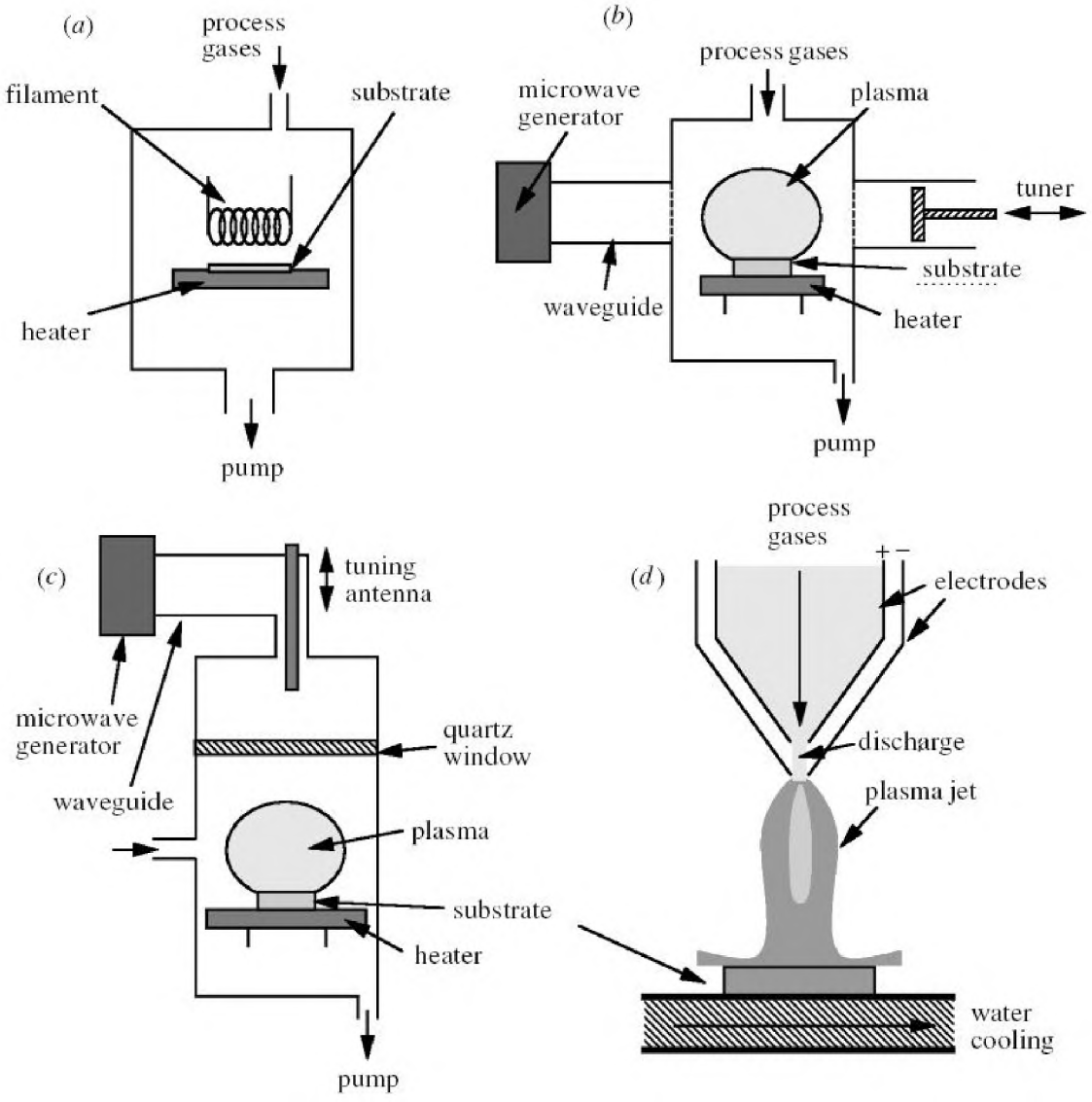

Figure 5.1: Examples of the more common types of low pressure CVD reactor. (a) Hot filament, (b) NIRIM-type microwave plasma reactor, (c) ASTEX-type microwave plasma reactor, and (d) DC arc jet (plasma torch), from [117].

These films thus contain a mixture of graphite, diamond-like carbon, and amorphous carbon. If diamond is formed (the central region of figure 5.2) non-diamond carbon is formed as a side product in nearly all cases. It was found that atomic hydrogen, produced by activation of H_2, plays an important role here. In fact, it is now believed that atomic hydrogen is the most critical component in the gas phase mixture and drives the whole chemical system. In a hot filament system, atomic hydrogen is produced heterogeneously by thermal decomposition of H_2 on the filament surface. In a plasma system atomic hydrogen is created by electron impact dissociation of H_2. A high concentration of atomic hydrogen is crucial for a number of main processes in diamond growth [117].

First of all, atomic hydrogen is known to etch graphitic sp^2 carbon many times faster than sp^3 carbon. Thus, the hydrogen atoms remove any graphitic clusters that may form on the surface, while leaving the diamond clusters behind, resulting in a (slow) build-up

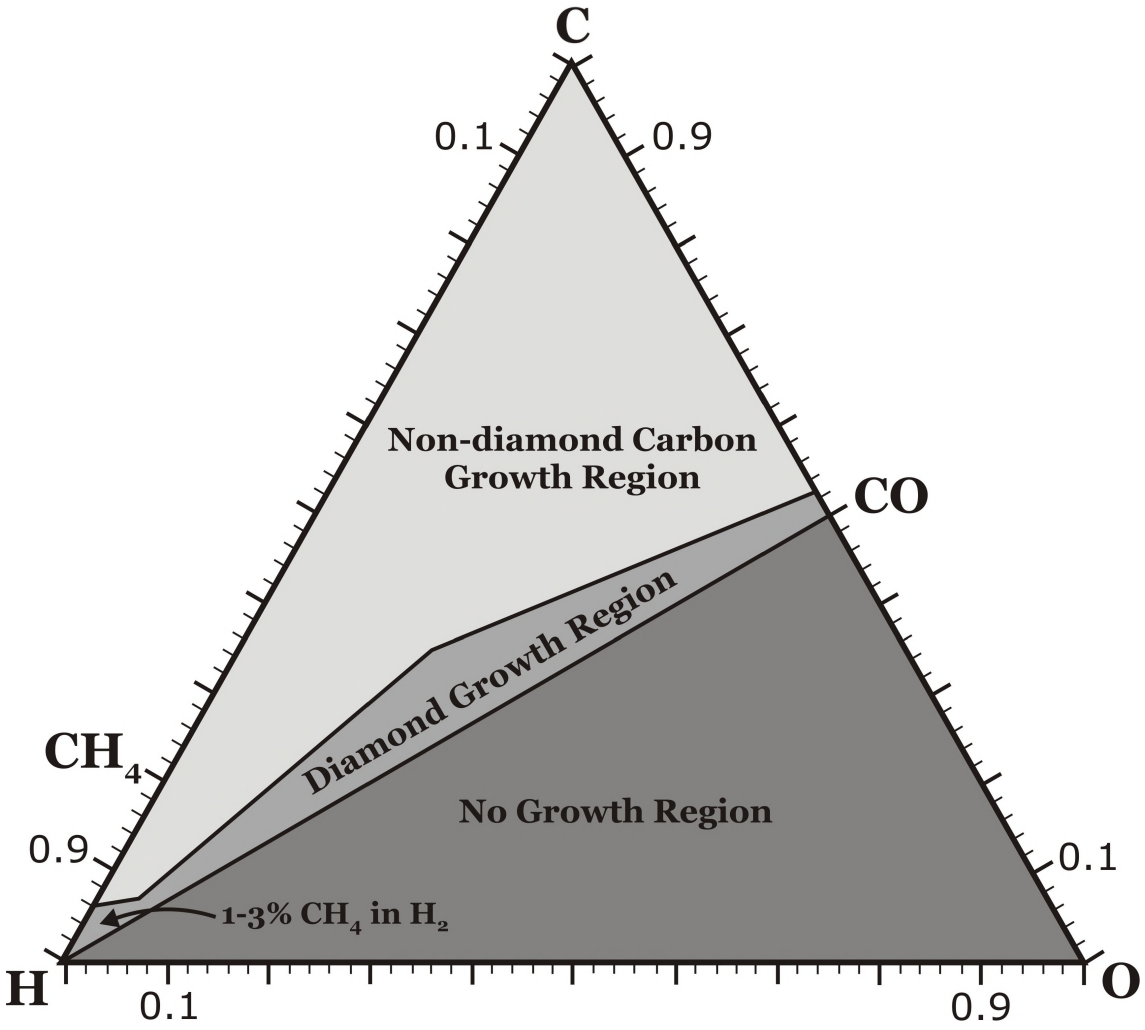

Figure 5.2: A simplified form of the Bachmann triangle C-H-O composition diagram. Below the CO tie-line, no film growth is achieved. Above the CO tie-line, non-diamond carbon is generally deposited, except in a narrow window close to the tie-line, which produces polycrystalline diamond films, adapted from [119].

of diamond [117].

Moreover, although the bulk of diamond is fully sp^3 bonded, at the surface there is effectively a 'dangling bond', which needs to be terminated in order to prevent rearrangement of the surface to graphite. This surface termination is performed by hydrogen (or sometimes OH), which keeps the sp^3 diamond lattice stable. During diamond growth, some of these hydrogen atoms need to be removed and replaced by carbon-containing species [117]. This removal of surface bonded hydrogen atoms can take place by thermal desorption or by abstraction involving atomic hydrogen following the reaction

$$C - H(\text{surface}) \; + \; H\cdot \; \longrightarrow \; C\cdot \; + H_2 \uparrow . \tag{5.1}$$

Finally, hydrogen atoms react with neutral species such as CH_4 to create reactive radicals, such as $\cdot CH_3$, which can then attach to suitable surface sites [117].

The basic picture which emerges for CVD diamond growth is believed to be as follows. During growth, the diamond surface is nearly fully saturated with hydrogen. This coverage limits the number of sites where hydrocarbon species (like $\cdot CH_3$) may adsorb,

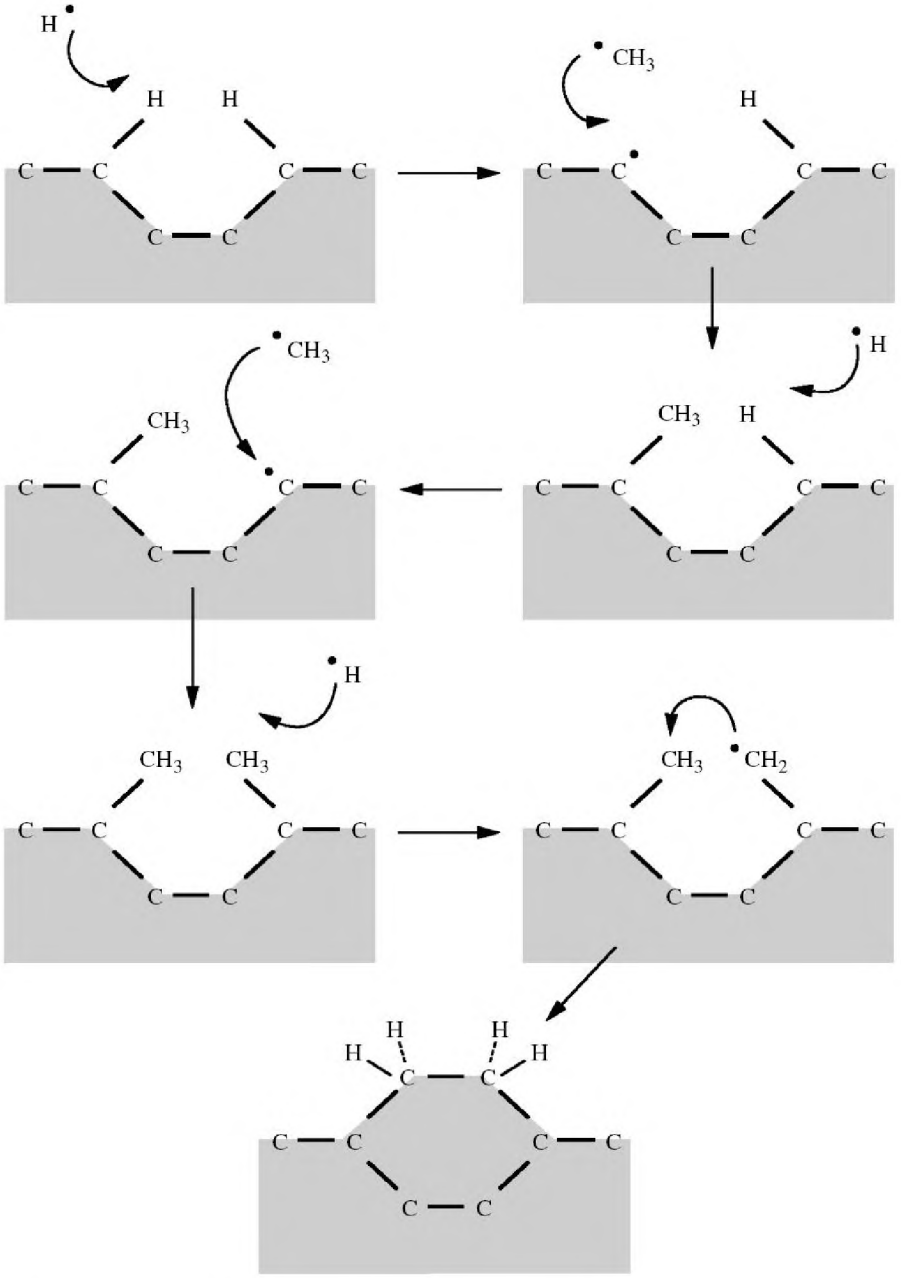

Figure 5.3: A schematic of the reaction process occuring at the diamond surface leading to stepwise addition of CH_3 species and diamond growth, from [117].

and also block migration sites once they are adsorbed. A schematic of the resulting processes is shown in figure 5.3. Atomic hydrogen abstracts a surface hydrogen to form H_2, leaving behind a reactive surface site. Most likely, this surface site reacts with another hydrogen atom from the gas phase, returning the surface to its previous stable situation. However, occasionally a gas phase $\cdot CH_3$ radical collides and reacts with the reactive surface site, effectively adding a carbon to the lattice. This process of hydrogen abstraction and methyl addition may then occur on a site adjacent to the attached methyl. A further hydrogen abstraction process on one of the absorbed groups creates a radical, which attacks the other nearby carbon group to complete the ring structure, locking the two car-

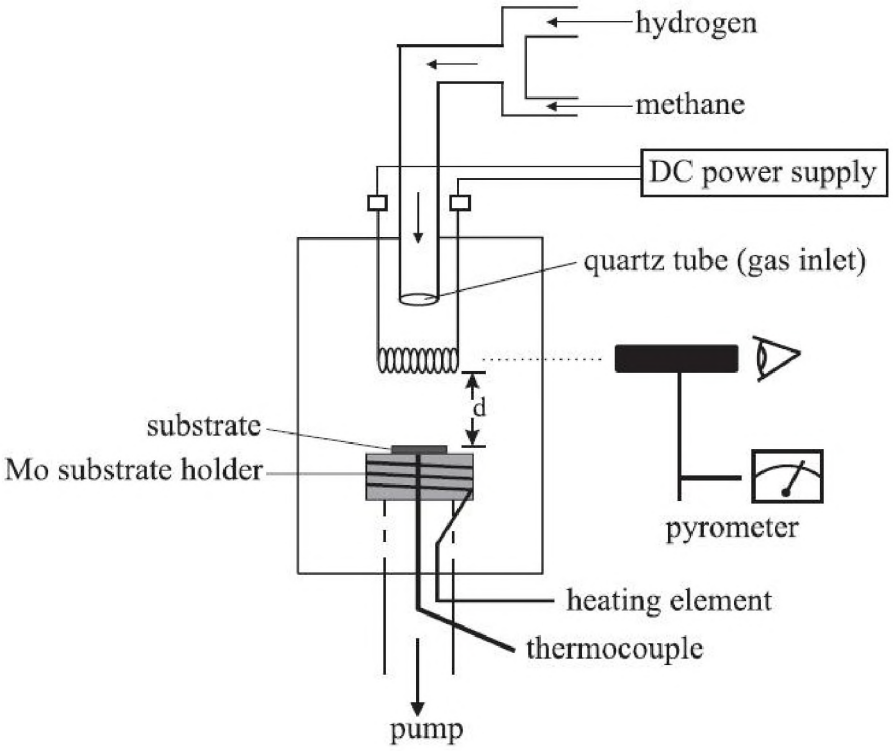

Figure 5.4: Schematic representation of the hot filament-assisted CVD reactor, from [28].

bons into the diamond lattice. Thus, diamond growth can be considered to be a stepwise addition of carbon atoms to the existing diamond lattice, catalysed by the presence of excess atomic hydrogen. In oxygen-containing systems, it is believed that the OH radical plays a similar role as atomic hydrogen, except that it is more effective in removing graphitic carbon, leading to higher growth rates and better quality films. It should be emphasized that the picture outlined above and in figure 5.3 is a very simplified description of diamond CVD growth. The exact mechanism is also dependent on the gas phase chemistry, the reactor and activation method applied, and even on the nature of the substrate surface used.

The oldest diamond CVD technique is based on the thermal activation of the hydrogen and hydrocarbon gases by means of a hot filament, *i.e.* the hot filament chemical vapour deposition (HFCVD) process. As this method is also applied for the work described in this thesis, a detailed description of its principles will be given next.

5.2.2 Hot Filament CVD

The oldest and still widely studied method to produce, mostly polycrystalline, diamond films is the hot filament CVD technique. The reactor applied in this research [28, 34] is very similar to the original design of Matsumoto [123] and depicted schematically in figure 5.4. The reaction chamber consists of a quartz tube (75 mm in diameter) with metal end-flanges. A gas mixture, comprising a few percent of methane in hydrogen, with flow rates of a few hundred standard cubic centimeters per minute (sccm) is fed into this chamber. The central part is the metal filament, here handmade from 0.5-mm thick tantalum (99.95%) wire. The filament is heated to about 2200 °C at which the power

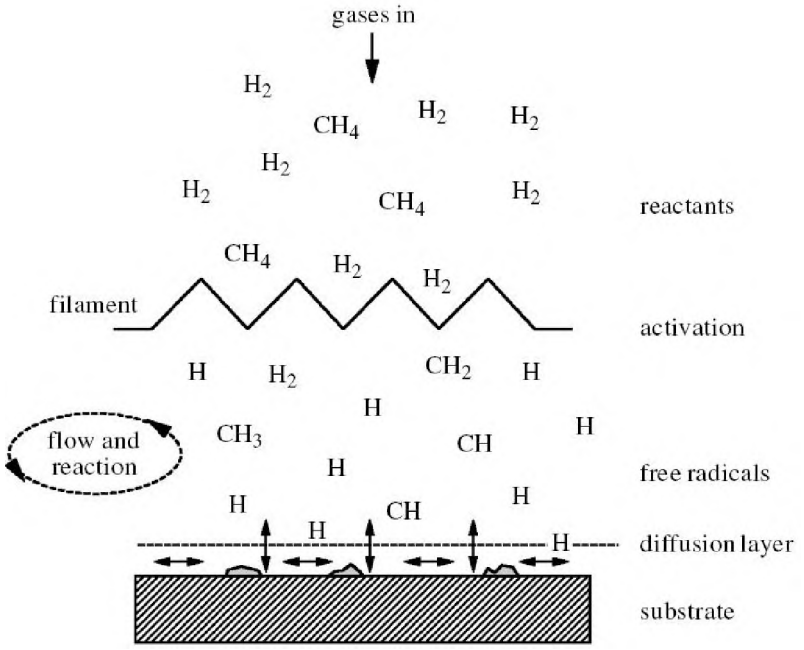

Figure 5.5: Schematic of the physical and chemical processes occuring during HFCVD [122].

consumption is in the order of 250 W. This hot filament is used to activate the gas mixture. The deposition is performed at reduced pressures (50 to 100 mbar) and the substrate is placed within a small distance from the filament (d $\sim$ 10 mm). Under optimal conditions and using a single filament, homogeneous deposition areas of about 15x25 mm^2 can be established. In the early design, the complete reaction vessel was heated by an external furnace [123]. The HFCVD setup used in the present work, does not have an external furnace, but instead the substrate is heated to about 800 °C using a resistance-heating element mounted in the molybdenum substrate holder [28, 124].

Prior to a series of deposition runs, a carburization treatment of the filament is necessary in order to minimize contamination of the growing diamond film caused by evaporation of metal from the filament. The pure tantalum filament is carburized by heating it to 2200-2400 °C, while passing a methane/hydrogen mixture over it. In about 4 hours the methane concentration is increased stepwise from 0.5% to 1.0% leading to the formation of Ta_2C and TaC phases, due to the in-diffusion of atomic carbon in the filament. This results in a stable filament composition, which leads to a more constant and reproducible gas phase activation [28].

As mentioned already in section 5.2.1, in HFCVD the filament produces the necessary thermal energy to dissociate the source gases. So, close to the filament surface, the reactant gases methane (CH_4) and hydrogen (H_2) are activated. Here, dissociation and formation reactions take place, leading to reactive, free radicals, such as $\cdot H$, $\cdot CH_2$, $\cdot CH_3$, $\cdot C_2$, etc. Due to the gas flow and the diffusion within the reactor, the reactive radicals are transported towards the substrate surface (figure 5.5). Close to this surface, a thin diffusion layer is formed. Within this diffusion layer, radicals, such as $\cdot CH$ and $\cdot CH_3$, will reach the substrate surface and ultimately chemisorption of these active radicals will take place. By hydrogen abstraction from these adsorbed radicals, carbon is incorporated into the growing surface, as was already depicted in figure 5.3. When the surface carbon concentration reaches a critical value for diamond nucleation, or when a surface carbon

cluster reaches a critical size, the nucleation and growth of diamond crystallites can take place. As nucleation of diamond is difficult, seeding, by scratching with diamond powder prior to growth, is often applied.

In comparison to other diamond deposition techniques, HFCVD produces diamond at a relatively low growth rate (typically around 1.0 μm h^{-1}), which is caused by the relatively low activation of the precursor molecules produced by the filament and the application of small gas flows in the reactor. Another major drawback of the HFCVD technique is the use of the filament itself. Because of the deformation during the carburisation process and the high brittleness of the tantalum carbide phases as compared to pure tantalum, the filament demands careful handling. The lifetime of the filament is relatively short ($\sim$ 25 hours). Besides, the filament heats up the substrate nonuniformely and the filament material slowly evaporates causing contamination of the grown diamond film. Nevertheless, HFCVD provides some advantages over other diamond CVD techniques. In the HFCVD process, the power consumption is only proportional to the deposition area, while for other diamond CVD techniques it is proportional to the volume of the gas activation. Moreover, by the use of arrays of multiple filaments the method can be scaled up to areas in the order of square meters for industrial applications, and can it be applied for the conformal deposition on more complex surfaces.

Table 5.1: Methods for gas phase activation and frequently used abbreviations for the different chemical vapour deposition (CVD) techniques [33]

Technique	Abbreviation
Hot Filament	HFCVD
Plasma Assisted	PACVD
- Micro-Wave discharge	MWCVD
- Direct Current discharge	DCCVD
- Radio Frequency discharge	RFCVD
- Electron Cyclotron Resonance	ECRCVD
Thermal Plasma torch	TPCVD
- DC Electric Arc jet	DCEACVD
- RF plasma jet	RFCVD
Combustion torch	flame-CVD
Laser Excitation	LECVD

5.2.3 Other CVD Techniques

As stated earlier (section 5.2.1), there are several other possibilities to activate the source gases in diamond CVD. These are summarised in table 5.1. From all these methods,

microwave plasma CVD (MWCVD) is currently the most widely applied technique for diamond growth, despite requiring significantly more investment in equipment. The fact that no filament is involved makes MWCVD systems inherently cleaner than HFCVD systems, and so they have become the system of choice for electronic applications. MWCVD reactors use very similar growth parameters as in HF reactors, but in MWCVD, microwave power is coupled into the chamber via a dielectric window (usually quartz) in order to create a discharge. The microwaves couple energy into gas phase electrons, which in turn transfer their energy into the gas through collisions. This leads to heating and dissociation of the gas molecules, the formation of active species, and finally diamond deposition onto a substrate, which is immersed in the plasma. Apart from high powers and hence higher growth rates, another advantage of microwave systems over other types of reactors is that they can use a wide variety of gas mixtures. These include mixtures with high oxygen content, or containing chlorinated or fluorinated gases or argon. The two most commonly used types of MWCVD reactor are the NIRIM-type (figure 5.1b) and the ASTEX-type reactor (figure 5.1c) [117].

In the NIRIM-type reactor [125], a quartz discharge tube is placed between the opposite sides of a fundamental mode rectangular waveguide, appropriate for the propagation of 2.45 GHz microwaves (figure 5.1b). The arrangement is such that the electric field maximum is centred at the middle of the discharge tube, creating a stable plasma at that position. The exact position of the plasma can be altered by tuning the waveguide, using a sliding short tuner. The substrate is introduced from the bottom of the discharge tube using a dielectric rod to prevent microwave leakage [117].

The other common type of microwave reactor (figure 5.1c) was designed in the late 1980s, and was then commercialised by Applied Science and Technology, Inc. (ASTEX, [126]). In this reactor, microwaves are coupled into a water-cooled metal cavity through a quartz window, using an antenna. The ASTEX-type reactors overcome a lot of the limitations of the NIRIM-type reactors. Because the plasma has no contact with the reactor walls, the incorporation of impurities is greatly reduced. If operated under well-defined deposition conditions, it is possible to deposit diamond continuously and unattended for several days or even weeks [126]. The use of higher microwave power allows the production of diamond discs of 50 mm in diameter and 1 mm thickness in approximately one week [117, 127].

Plasma jet, arc jet or plasma torch methods are a promising alternative to the conventional low-pressure HF and MW systems. These techniques were introduced in the mid- to late-1980s. In a plasma jet, gas at relatively high flow rates (slm compared to sccm used for HF and MWCVD) passes through a high-power electrical discharge and forms a jet of ionised particles, atoms and radicals, which then expand into a secondary chamber to strike a substrate at high velocity. The most commonly used plasma jet is the DC arc jet (see figure 5.1d), which uses a dc-voltage to drive high, relatively stable currents to ionise the process gases. Other technologies include discharges without electrodes, such as the RF inductively coupled and microwave plasma jet sources. The main feature of all these plasma jet techniques is the high growth rates that can be achieved, typically greater than 100 μm h^{-1}. However, the main drawback of such high power, high rate systems is that the deposition area is limited to the small area struck by the jet (usually ca. 100 mm^2). Substrate cooling is another major problem, since maintaining uniform substrate temperatures in such a rapidly varying high power system is difficult [117].

A variant on the plasma jet is the simple oxyacetylene welding torch, also called the

combustion flame method [128]. Since this system is very cheap, and can be operated in air at atmospheric pressure without the need for complex vacuum equipment, it proved a popular technique for growing diamond. In these systems, the torch is operated in a regime where the acetylene flow is slightly higher than the oxygen flow, and this creates a region within the flame (called the acetylene feather) which is high in carbon-containing radical species. The large flows of the source gases from the burner nozzle shields the deposition area from the ambient air, so that no reactor vessel is required. By this method, the gas phase is very effectively activated, which offers the possibility to reach deposition rates in excess of 150 μm h^{-1}. However, the main drawbacks of the combustion flame method are similar to those of the plasma jet. The radial non-uniformity of the deposited material limits the area which can be coated, and cooling the substrate in a reliable and uniform manner is also problematic, leading to the presence of a significant amount of non-diamond carbon [33, 117].

Some other CVD deposition methods have been employed to grow diamond thin films, including laser-assisted CVD, pulsed laser deposition, and hydrothermal growth. However, these techniques are exploited only in relatively small number of cases, with varying degrees of success and are thus not discussed here. More detailed descriptions on these methods can be found elsewhere [117].

5.3 Substrates for CVD Diamond Growth

Most of the CVD diamond films reported to date have been grown on single crystal silicon wafers, but this is by no means the only possible substrate material. All materials that have a sufficiently high melting point and neither react excessively nor have a large mutual solubility with carbon are suitable substrates for the diamond CVD process [33].

The first demand eliminates the use of important materials such as plastics and aluminum, because these have a melting point (at the process pressure) lower than the temperature window (700-1100 °C) required for diamond growth. The latter demand indicates that Fe substrates are incompatible with diamond growth, because carbon diffuses into the bulk of this material, while it is desperately needed at the surface to form nucleation centres [33]. For these materials, diamond growth often only begins after the substrate is saturated with carbon, and this can dramatically affect the physical properties of the resulting composite.

The suited substrates can be divided into two categories: carbides or carbide formers like SiC, WC, Si, B, Mo, W, Ta, and Cr and non-carbide formers like Cu, Ag, and Al_2O_3 (sapphire). As a result of the formation of a thin interfacial carbide layer, well-adhering diamond films can be formed on the first group of materials [117]. The carbide layer promotes the growth of CVD diamond, and aids its adhesion by (partial) relief of stresses at the interface. Of course, substrates composed of carbide, such as SiC, WC, and TiC are particularly amenable to diamond deposition as well [33].

Substrates of the second category (Cu, Sn, Pb, Ag, Au, Ge, and Al_2O_3) do not form a carbide layer, and so any diamond layer will not adhere well to the surface. This can be used as a method to obtain free-standing diamond films, as the films will often readily delaminate after deposition. It appears, as discussed in chapter 3, that GaN can be placed in this category, because no carbide layer seems to be formed, although this is difficult to determine due to the decomposition of GaN under diamond growth conditions.

The difficulties with growth on alternative materials have ensured the continuing popularity of silicon as a substrate material. It has a sufficiently high melting point (1410 °C), it forms a thin carbide layer and it has a comparatively low thermal expansion coefficient. Tungsten and molybdenum display similar virtues and are also widely used as substrate materials [117]. In this research, however, Si and SiC are mainly used as the substrate for HFCVD growth. Because it is difficult to obtain high nucleation densities on Si and SiC, nucleation pretreatments are necessary, like for instance the application of ultrasonic abrasion with micro-sized diamond powder [129].

5.4 Other Methods to Produce Synthetic Diamond

High Pressure-High Temperature (HPHT) synthesis of diamond became a commercial reality during the 1950s and remains the major manufacturing method for synthetic diamond products, of which the main application is in tooling solutions for industry [113].

In essence, HPHT emulates the way in which natural diamonds are created deep in the earth, where the enormous pressure causes carbon crystals with the dense structure of diamond to be thermodynamically more stable than those of other carbon allotropes, such as graphite. The exact design and reaction volume sizes of the equipment are closely guarded company secrets. Graphite, often the carbon source, is dissolved in a melt of transition metals like iron, nickel, cobalt or their alloys. The melt acts as a solvent-catalyst by lowering the activation energy, so that the graphite-to-diamond conversion proceeds at much lower temperatures and pressures (typically 1400 °C and 5 GPa, respectively) than would be required for direct conversion. The diamond crystals that are produced by this method are typically a few mm in size, but in most cases the amounts of defects are too high for use as gemstones. They are, however, extremely useful as hard-wearing edges on cutting tools and drill-bits, and are being widely applied in the machine tool industry, oil and gas drilling, mining, quarrying, and construction [33].

Next to CVD and HPHT synthesis, the use of shock waves to produce diamond is investigated thoroughly as well. This resulted in the invention of the ultrasonic cavitation procedure [130] and the formation of diamonds via detonation synthesis [131]. In the first technique, intense sound waves are used to produce bubbles in a suspension of graphite in organic liquid and dissolved carbon-containing gas. When the bubbles collapse under the effect of positive pressure and surface tension forces, the gas mixture in the bubble experiences a rapid, strong adiabatic compression. This implosion produces the necessary combination of pressure and temperature to allow graphite-to-diamond transformation in the liquid [132]. In detonation synthesis, the shockwave generated by an explosion of carbon-containing material, usually a mixture of trinitrotoluene (TNT) and hexogen (RDX), is applied to enforce the formation of diamond [131]. In contrast to the ultrasonic cavitation procedure, detonation synthesis is well commercialised and diamond powder, achieved via this technique, is nowadays produced in considerable quantities in China, Russia and Belarus [133].

6

Characterisation Techniques

To determine the properties of the deposited materials a wide range of different techniques is available. In order to obtain a clear picture of the structural, electronic, and optical properties of the material under investigation, often one is forced to apply multiple characterisation techniques. The most commonly used characterisation methods in this thesis are briefly discussed here.

6.1 Scanning Electron Microscopy

In Scanning Electron Microscopy (SEM), a beam of electrons is focused onto the sample and scanned over the surface by means of a deflection coil (figure 6.1). Inside the sample the electrons undergo several interactions, upon which electrons and photons are emitted from the sample. A fraction of the emitted electrons is collected by the appropriate detectors from which an image can be generated.

Most SEM images are generated from either secondary electrons, backscattered electrons, or elemental X-rays. The latter are used in energy-dispersive X-ray spectroscopy (EDX) to determine the specimen's chemical composition, but this technique will not be discussed in detail here. Secondary and backscattered electrons can be separated by energy. The secondary electrons posses lower energies than the backscattered ones. The higher energy backscattered electrons have not undergone any energy loss as they underwent only elastic collisions with atoms in the material. In contrast, as secondary electrons posses little kinetic energy, they are likely to become trapped when traveling from any deeper in the sample. Therefore, they are usually emitted from within the first few nanometers below the sample's surface, which leads to a resolution up to 10 times better than for backscattered electrons. However, artifacts are sometimes seen due to abnormalities in the materials' spatial and electronic structures [134].

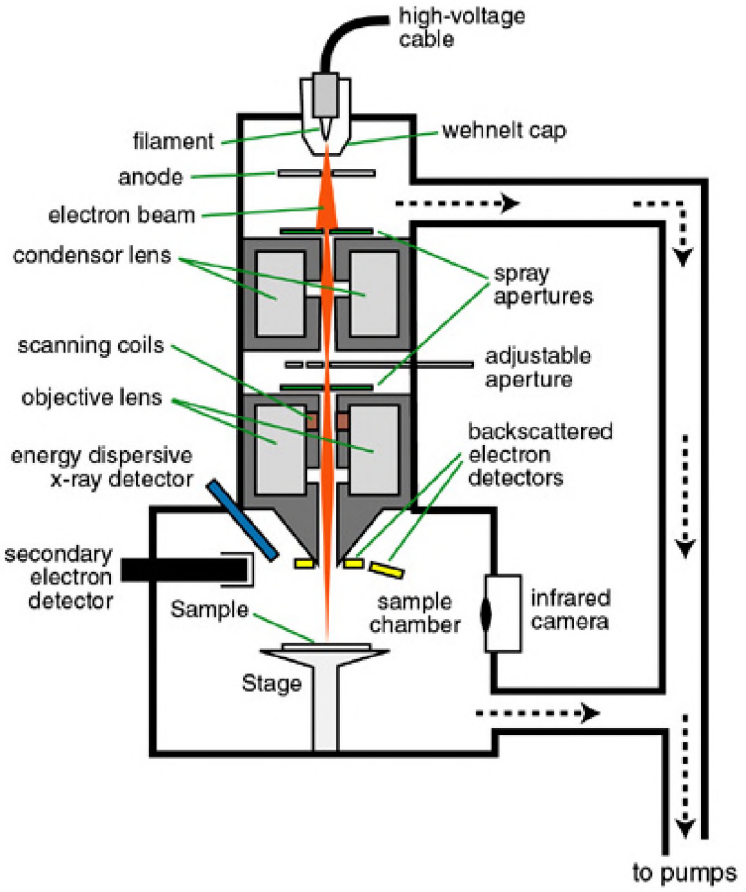

Figure 6.1: Schematic of a Scanning Electron Microscope.

The SEM setup used mostly in this research is a Jobin Yvon 6330F Field Emission SEM, imaging with secondary electrons. The resolution of the SEM extends into the nm-scale and the magnification can be adjusted between 25 and 100000×. The costs are reasonable, operation is fairly simple, and the measurement time is short.

6.2 X-Ray Diffraction

For the studies described in this thesis the X-ray diffraction equipment (Bruker D8 Discovery) at the Applied Materials Science department was used to measure the orientation and to evaluate the quality of the grown films. The wavelength used for the measurements was Cu K_α, $\lambda = 1.5418$Å, mostly for measuring rocking curves and $\theta/2\theta$ (or $\omega/2\theta$ or Bragg Brentano) patterns.

In XRD measurements, the sample is probed with a collimated beam of X-rays (figure 6.2a). The periodicity in the crystal structure of the material under investigation determines the diffraction pattern coming from the sample. The diffraction peaks follow Bragg's law:

$$\lambda = 2d_{hkl}sin(\theta), \tag{6.1}$$

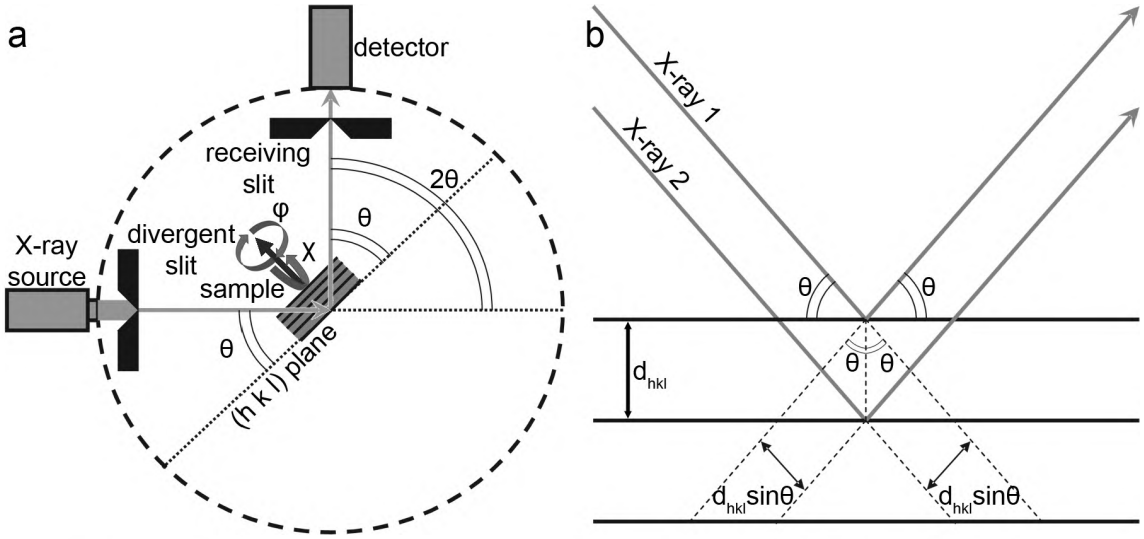

Figure 6.2: Schematic of XRD setup (a) and the principle of Bragg reflection (b).

with d_{hkl} the lattice spacing between (hkl) and θ the diffraction angle, as depicted in figure 6.2b. Thus, only if there is constructive interference between the parallel X-rays a signal is produced on the detector and the stacking of the planes (hkl) in the crystal can be determined. This is done by rotating the sample over an angle θ, while keeping the detector at an angle 2θ, thus obeying Bragg's law. A peak is recorded solely, when θ reaches a value that, according to that law, corresponds to the actual crystal plane stacking spacing d_{hkl} of the sample. Matching the values of d_{hkl} to known or calculated values, the orientation of the crystal lattice can be derived. A $\theta/2\theta$ scan reveals the plane stacking, and consequently the out-of-plane orientations, of the layer under investigation. The above applies solely to the so-called symmetric peaks, which are detected regardless of the rotation ϕ of the sample along an axis perpendicular to the (hkl) plane. For such symmetric peaks the stacking in figure 6.2b does not change when rotating the sample by an angle ϕ around the vertical axis. Its peak position and width are a measure for the quality of the material [134].

Moreover, additional information on, for instance, defects can be acquired when probing a different plane stacking (hkl) which reflection intensity *does* change when rotating the sample around the ϕ axis. However, this imposes an additional restriction on the Bragg condition: a signal is detected solely with the correct settings for θ, 2θ, and now also ϕ. For other values of ϕ the intensity goes to zero. Peaks with this additional requirement for the ϕ angle are referred to as asymmetric.

When the detector is fixed at a 2θ angle obeying Bragg's law for the material under investigation and the source is moved slightly back and forth around the θ angle, the broadening of the recorded curve is amongst others related to the dislocation density of the material. This is called a 'rocking curve'. In principle, assuming other factors like stress and thickness are constant, the dislocations broaden the distribution of the lattice constants, which in turn can be probed by XRD. The orientation of the dislocation and its Burgers' vector have to correspond to the orientation of the crystalline direction under investigation. E.g., in the case of GaN the broadening of the symmetric (0002) peak is caused by screw dislocations, while a rocking curve of the asymmetric $(10\bar{1}5)$ direction is

broadened by edge and mixed type dislocations [134].

In thin film growth, the orientation of the substrate is generally known. The out-of-plane orientations of the film can be determined by the above described $\theta/2\theta$ scan. So, the crystal plane whose normal vector points upwards, normal to the substrate surface is known. For GaN on (0001) sapphire, this is usually the (0001) GaN plane. However, the in-plane orientation of the GaN layer with respect to the substrate, *i.e.* the angle ϕ between $(10\bar{1}0)$ GaN and $(10\bar{1}0)$ sapphire, is unknown. This orientation can be resolved by locating one asymmetric peak, which belongs to the thin film under investigation. Rotating the sample by an angle ϕ or tilting by χ will cause this peak to appear at specific angles in correspondence with the symmetry of the lattice. For example, rotating the sample 360° will yield six different peaks for a material with hexagonal symmetry. Additionally, if the sample is tilted during the measurement to include an asymmetric substrate peak in the same scan, the in-plane orientation of the film with respect to the substrate can be determined. Such a scan is called a pole figure. Pole figures can also be used to study the texture of the sample. Sharp individual peaks indicate good crystallinity. For polycrystalline films with no preferred orientation, the asymmetric peaks are broadened out and one measures a continuous ring rather than individual peaks [134].

Another common XRD technique is the reciprocal space map. Basically, a Bragg peak of particular interest is selected and then a 2D high resolution scan of this peak is recorded. The scan is performed along two preselected crystalline directions. A reciprocal space map reveals the distribution of the lattice parameter, associated with this peak, along these directions. It can be used to visualise strain distributions in thin films [134].

6.3 Raman Spectroscopy

Raman spectroscopy is a powerful, nondestructive, light scattering technique used to diagnose the vibrational and rotational structure of materials. The sample is probed with monochromatic laser light of a known frequency and polarisation, by which bonds in the material are excited. The majority of the scattered light is of the same frequency as the excitation source; this is known as Rayleigh or elastic scattering (figure 6.3, top). A very small amount of the scattered light (about $10^{-5}\%$ of the incident light intensity) is shifted in energy from the laser frequency due to interactions between the incident photonic waves and the vibrational energy levels of the molecules in the sample. If the final vibrational state of the molecule is more energetic than the initial state, then the emitted photon will be shifted to a lower frequency in order for the total energy of the system to remain balanced. This interaction is called Stokes or inelastic scattering (figure 6.3, center). However, when the incident light interacts with a crystalline lattice which is already in an excited vibrational state and the final vibrational state is less energetic than the initial state, then the emitted photon will be shifted to a higher frequency. This process is called Anti-Stokes scattering, because the energy difference between the incident and emitted light is equal to the Stokes scattering but opposite in direction (figure 6.3, bottom).

The frequency of the scattered light can be measured accurately. Considering that the scattered light changes in frequency compared to the laser frequency, the rule of conservation of energy dictates that some energy is deposited in the sample. So, the Raman shift corresponds to the energy difference between two vibrational (or rotational) energy levels of the molecule, and in this way much information about the vibrational (and rotational)

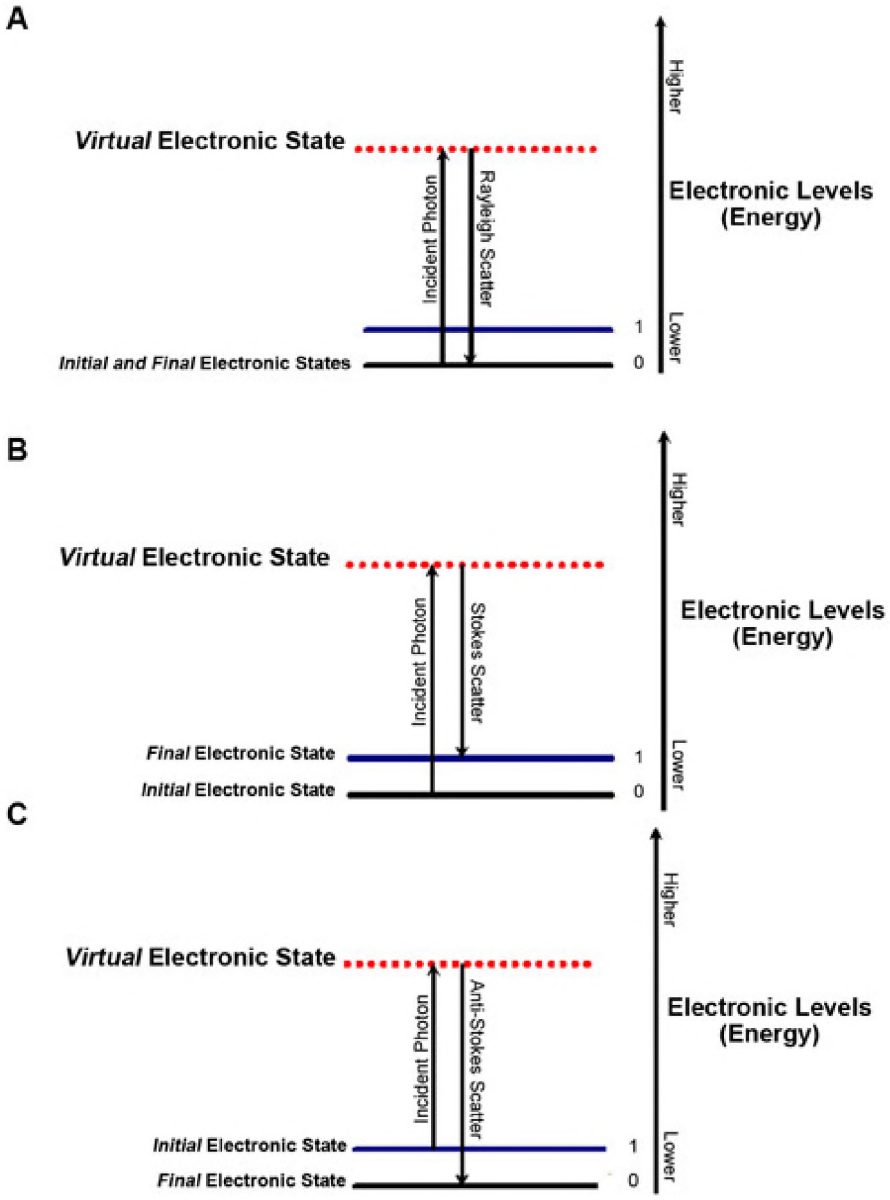

Figure 6.3: Energy level diagram showing the principles of Raman scattering: (A) Rayleigh scattering; (B) Stokes Raman scattering; and (C) anti-Stokes Raman scattering [135].

energy states of the material can be obtained. Although the scattered light is frequency shifted with respect to the excitation frequency, the magnitude of the shift, $\Delta h\nu$, in principle, is independent of the excitation frequency or intensity. This shift is thus an intrinsic property of the sample.

In general, only a part of the possible excitations of a given material are Raman active, depending on the polarisation of the incident light and the orientation and polarisation of the probed molecular bond. Additionally, altering the direction of the incident laser beam with respect to the sample and measurements on the geometric dependence of the scattering, provide information on the equilibrium structure of the material through the rules of group theory. In this way, complete structural information of the material can be

derived with Raman spectroscopy.

As strain in a material alters the molecular bonds and thus their vibrational and rotational frequencies, Raman spectroscopy can be applied to estimate the stress in a sample. Certain molecular bonds are more suitable for strain determination as their geometry overlaps more with the direction of the strain. Moreover, a shift in the position of other Raman peaks from their bulk value can also be used to derive the free carrier concentration in the material, as this has the same effect on energy levels as strain. In this way, several structural properties can be measured accurately.

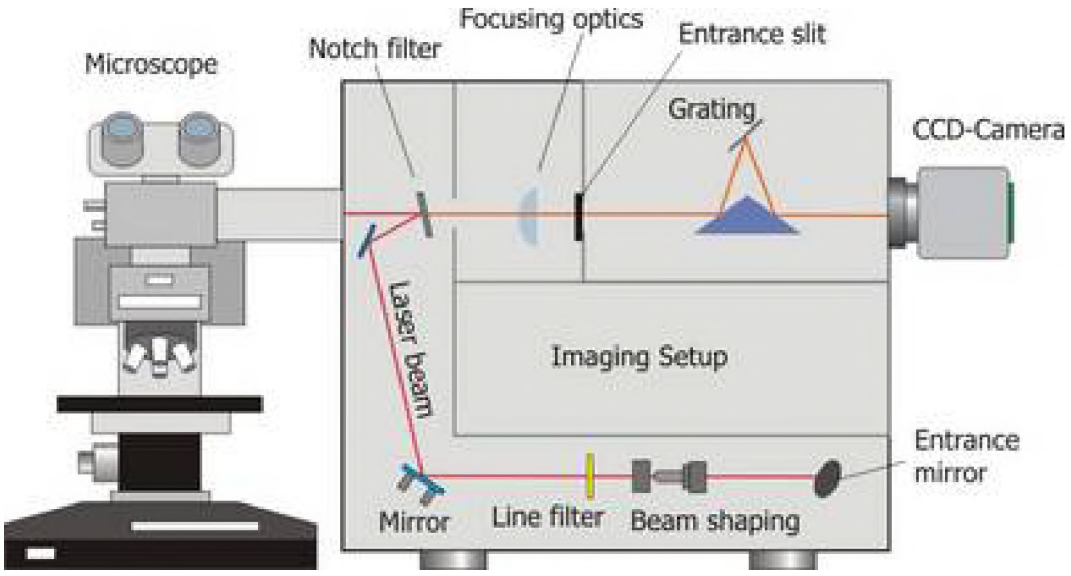

Figure 6.4: Schematic of the Renishaw Raman 1000 setup used in these studies.

Another advantage of Raman spectroscopy is its complementarity to other techniques. For instance, infrared (IR) and Raman spectroscopy both measure the vibrational energies of molecules, but these methods rely on different selection rules. While the dipole moment of the molecule must change during vibration for the molecule to be IR active in that particular vibration state, in Raman spectroscopy the polarisation must change with the vibration to make it Raman sensitive. Thus, Raman spectroscopy complements IR spectroscopy.

In this thesis, a Renishaw 1000 μ-Raman spectrometer (figure 6.4) with an Ar ion laser at wavelength $\lambda = 514.8$ nm and 10 or 20 mW power was used to investigate the samples in backscattering geometry at room temperature.

6.4 Photo- and Cathodoluminescence

Luminescence is defined as the emission of light by materials, after being excited by some external means. A possible way is to excite the luminescence by using a focused high energy electron or ion beam. This is called cathodoluminescence (CL). Another commonly used method is absorption of photons of energy higher than the band gap of the material: photoluminescence (PL). The resulting process, in which photons of energy lower than the excitation photons are radiated, is known as the photoluminescence process, and is

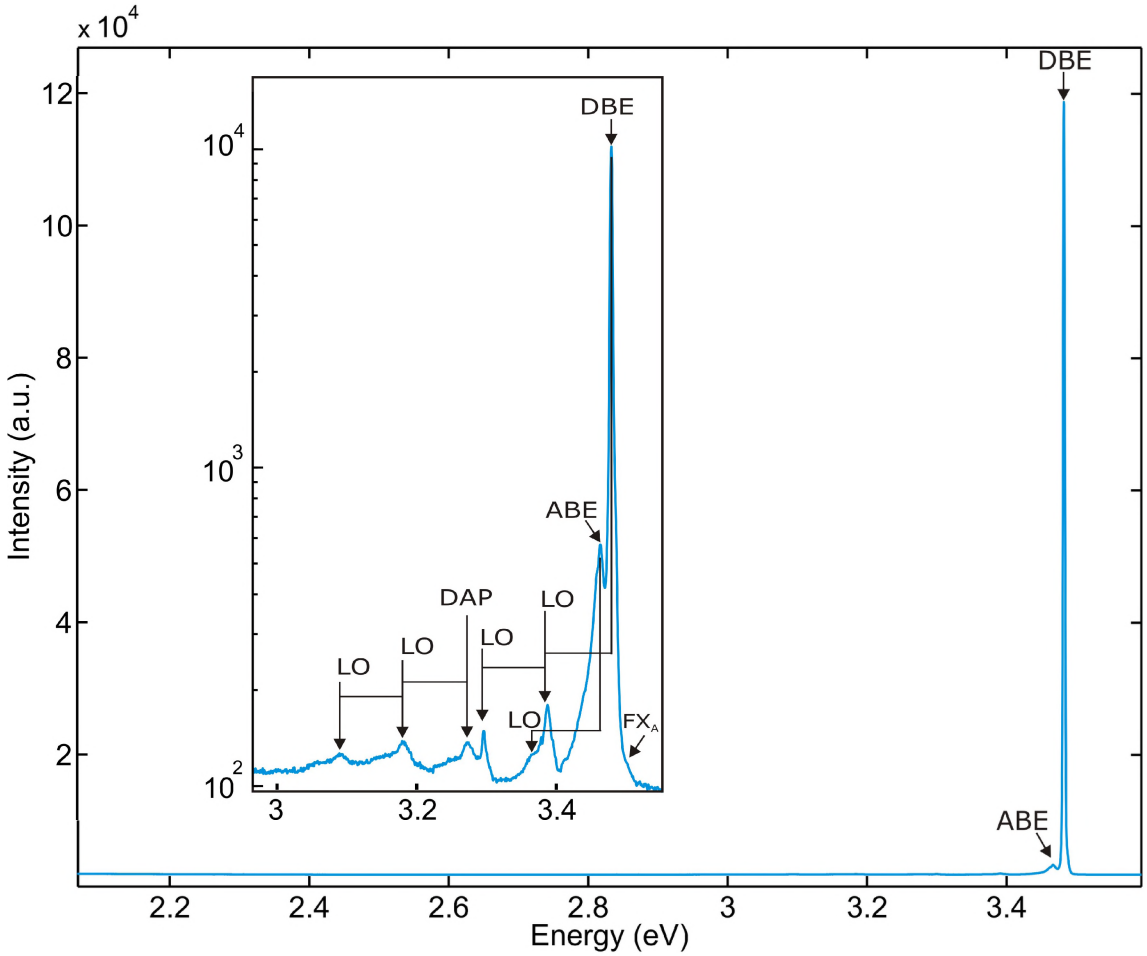

Figure 6.5: Typical spectrum of a good GaN film on sapphire at 4.5 K. The inset shows a detailed fragment of the downright area of the large spectrum. Note the logarithmic scale of the inset. The labels are explained in the text.

caused by radiative recombination of thermalised electron-hole pairs. Numerous characteristics can be extracted from the position and the line-shape of the observed PL peaks. Not only the efficiency of the luminescence can be evaluated, but also very essential electronic properties can be studied in detail: band gap parameters, the presence and amount of impurity and defect levels, estimates of strain and free carrier concentration, binding energies of excitons, as well as the homogeneity of the optical properties [4, 134]. A typical PL spectrum of a high optical quality GaN film is shown in figure 6.5, in which the prominent features are labeled. DBE is the peak caused by recombination of donor-bound excitons, while ABE originates from the transition of acceptor-bound excitons. The recombination of donor-acceptor pairs results in the weaker DAP peak. In addition to that, there is a very effective coupling of DBE, ABE and DAP to longitudinal optical phonons (LO). Finally, the spectrum also shows the position of free excitons from the A-band (FX_A, a state in the crystal-field splitted valence-band in wurtzite GaN). More details can be found in [4].

The large band gap of GaN requires excitation radiation in the ultraviolet part of the spectrum. In our case this is obtained from the 325 nm (3.815 eV) line of a continous-

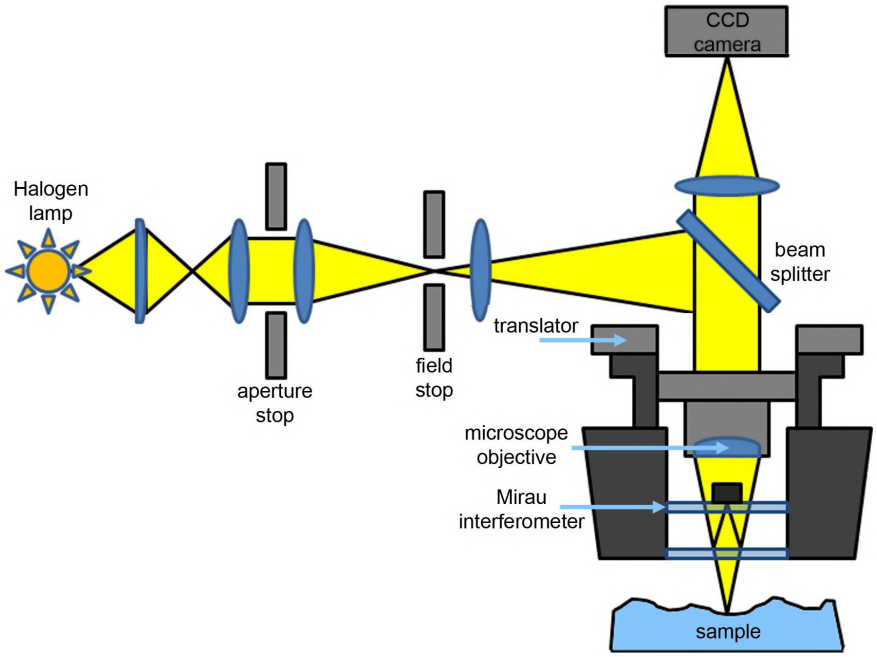

Figure 6.6: Schematic of the microscopic white light interferometer used in the present studies (adapted from the Veeco manual). In the figure it is equipped with a Mirau-type interferometric objective, typically employed for magnifications of up to 50×.

wave HeCd laser for the PL setup. Excitation powers are usually in the range of 10 μW to 10 mW, controlled by neutral density filters, while the excitation spot is typically 50-200 μm in diameter. Samples are mounted on the cold finger of a continous flow helium cryostat, allowing samples temperatures to be varied in the range 4.5-300 K.

In addition, CL spectra are recorded using an 8200 MKII cold-cathode luminescence system. During examination, at room temperature, the acceleration voltage is maintained at 15 keV, while the current density at the samples is kept constant around 10 μA mm^{-2} at a pressure of 0.1 Torr.

6.5 Profilometry

Optical profilers (figure 6.6) are specialised interference microscopes that utilise the interference of two beams of light for characterizing surface topographies. The two beams are commonly made by splitting a light beam coming from a single source, which emits at a single wavelength λ. One beam is then directed towards the sample's surface, while the other is reflected back from a reference mirror. As the beam reflected from the sample's surface is superimposed on the reference beam, interference patterns appear. Small differences in height $h(x, y)$ on the sample's surface introduce small differences in the path lengths of the two beams. The relative phase difference $\epsilon(x, y)$ between the beams is then equal to $2 \cdot (2\pi/\lambda) \cdot h(x, y)$. Constructive interference occurs when the phase difference equals $2n \cdot \pi$, where n is an integer. The recorded intensity for this site on the surface is

then high. Should the phase difference $\epsilon(x, y)$ be equal to $(2n+1)\cdot\pi$, the two waves cancel one another and no light reaches the detector. This is called destructive interference.

Imaging the sample in this manner, one obtains an interferogram. The height differences on the sample surface are then translated into a pattern of bright and dark contrast fringes. The fringes are the result of repeated constructive and destructive interference. Two adjacent dark fringes, for example, indicate a height difference of $\lambda/2$. Using interferometric phase-mapping programs, a height profile of the sample surface can be derived from this interferogram.

By making three or five interferograms, each with the reference mirror shifted over $\pi/8$, a height profile can be calculated. This approach is commonly referred to as Phase Shifting Interferometry (PSI). However, this technique is only applicable to smooth surfaces, where the height difference between adjacent pixels on the detector does not exceed $\lambda/4$. PSI relies on the height differences between adjacent fringes being equal to $\lambda/2$. A single $\lambda/2$ height difference or n + $\lambda/2$ height difference between adjacent pixels cannot be distinguished, as both will result in similar contrast fringes.

This problem can be resolved by utilizing additional light sources with different wavelengths. Ultimately, one can use white light. This method is called Vertical Scanning Interferometry (VSI). While PSI examines the shape of the fringes, VSI seeks the ultimate focus position by moving the detector perpendicular to the sample's surface. The interferometer is aligned so that the interference intensity distribution along the vertical scanning direction has its minimum (darkest contrast fringes) at the best focus position. Though VSI can be applied across a wider range of surface heights, PSI has the higher resolution [134].

Most interferometric investigations in this thesis are obtained by applying VSI.

Part III

Polycrystalline Diamond Substrates

7

Growth of GaN on Nano-Crystalline Diamond Substrates

* In this study GaN has been grown on nano-crystalline diamond substrates utilising metal-organic chemical vapour deposition (MOCVD). It is shown that the growth of closed GaN films onto synthetic diamond substrates is feasible, when applying the correct buffer layer and growth parameters. XRD measurements showed that the GaN formed is of wurtzite structure and polycrystalline, but the high intensity of the (0002) diffraction peak indicates a preferential crystallite orientation. This preferred [0001] orientation was confirmed by SEM and Raman analysis. The optical quality of the deposited GaN layer was investigated using cathodoluminescence and showed a large yellow luminescence peak. This work comprises a first step in preparing heterogeneous layers and GaN devices with a diamond heat sink as a substrate, facilitating the thermal management of these devices.

7.1 Introduction

Gallium nitride (GaN) has shown to be a very suitable material for use in high-power semiconductor devices. However, modern (opto-)electronics still encounter severe cooling problems, due to the production of large amounts of heat in a small area. In order to cool these devices effectively, it is essential to spread the narrow heat flux by placing a layer of high thermal conductivity between the device and the cooling system.

Nano-crystalline Chemical Vapour Deposited (CVD) diamond has a high thermal conductivity that is similar to copper [27]. Therefore direct attachment of the diamond layer to the device, leaving out any intermediate substrate, should lead to an optimal spread

*Published in: G.W.G. van Dreumel, J.G. Buijnsters, T. Bohnen, J.J. ter Meulen, P.R. Hageman, W.J.P. van Enckevort, and E. Vlieg, Diamond Relat. Mater. 18 (2009), 1043.

of heat. Thus the direct growth of GaN films onto diamond substrates, acting as heat sinks, would be a good solution to increase the power range in which GaN devices can be employed. In this way, the smooth surface of a nano-crystalline diamond substrate can provide the necessary high nucleation density for epitaxial GaN growth.

For this purpose, nano-crystalline diamond is deposited on a silicon wafer, which in turn is used as a template for the MOCVD growth of GaN layers. The latter growth is based on previous results with single-crystal diamond substrates [58]. This time, a GaN low-temperature buffer layer is used to accommodate the difference in lattice constants between GaN and diamond.

7.2 Experimental

Silicon (100) was ultrasonically abraded for 1 h with micro-sized diamond powder for homogeneous and fast diamond nucleation as described by Buijnsters *et al.* [129]. This procedure results in a slight increase in the silicon substrate roughness (*i.e.* 0.7 nm) due to surface defects and to the formation of nanoscale residual diamond powder fragments at the surface. Nano-crystalline diamond films were deposited on the thus prepared substrate in a home-built, hot-filament CVD reactor. During growth the substrate temperature was kept constant at 800 °C in a mixture of 2% CH_4/H_2 (total flow 300 sccm) at 15 mbar applying a filament temperature of about 2200 °C. After 4 hours a nano-crystalline diamond layer of 4.5 μm thickness was obtained. After the deposition the samples were cleaned with isopropanol in an ultrasonic bath and dried overnight at 120 °C.

Then GaN was deposited in an Aixtron AIX-200 RF MOCVD reactor. To minimize graphitization of the diamond layer at high temperatures, a nucleation GaN layer was deposited following the principle of growth on sapphire [105]. This layer (~50 nm) should also accomodate for the lattice mismatch between the diamond and GaN. It was deposited in 7.5 minutes at 525 °C and annealed for 1.0 minute at 1170 °C. Immediately after annealing the main growth was started under normal GaN growth conditions, *i.e.* 35 mbar at 1170 °C, using H_2 carrier gas [136]. The precursor flows were set at $5.25 \cdot 10^{-5}$ mol/min for TMG and $1.0 \cdot 10^{-1}$ mol/min for NH_3, giving a V/III ratio of about 1870, for the growth period of 90 minutes.

The morphology of the as-grown surfaces was studied by applying SEM (Jeol JSM 6330F) and the roughness was measured using a Wijco NT-1100 optical profiler in PSI-mode. A $\theta/2\theta$ XRD pattern of the layer has been recorded with the help of a Bruker D8 diffractometer using Cu K_α and Cu K_β radiation, while a Renishaw 1000 micro-Raman spectrometer with an Ar ion laser at wavelength $\lambda = 514.8$ nm and 10 mW power was used to investigate the samples in backscattering geometry at room temperature. Luminescence spectra were recorded using a 8200 MKII cold-cathode luminescence system fitted with an OceanOptics USB4000 Spectrometer. During examination, at room temperature, the acceleration voltage was maintained at 15 keV, while the current density at the samples was kept constant around 10 $\mu A/mm^2$ at a pressure of 0.1 Torr.

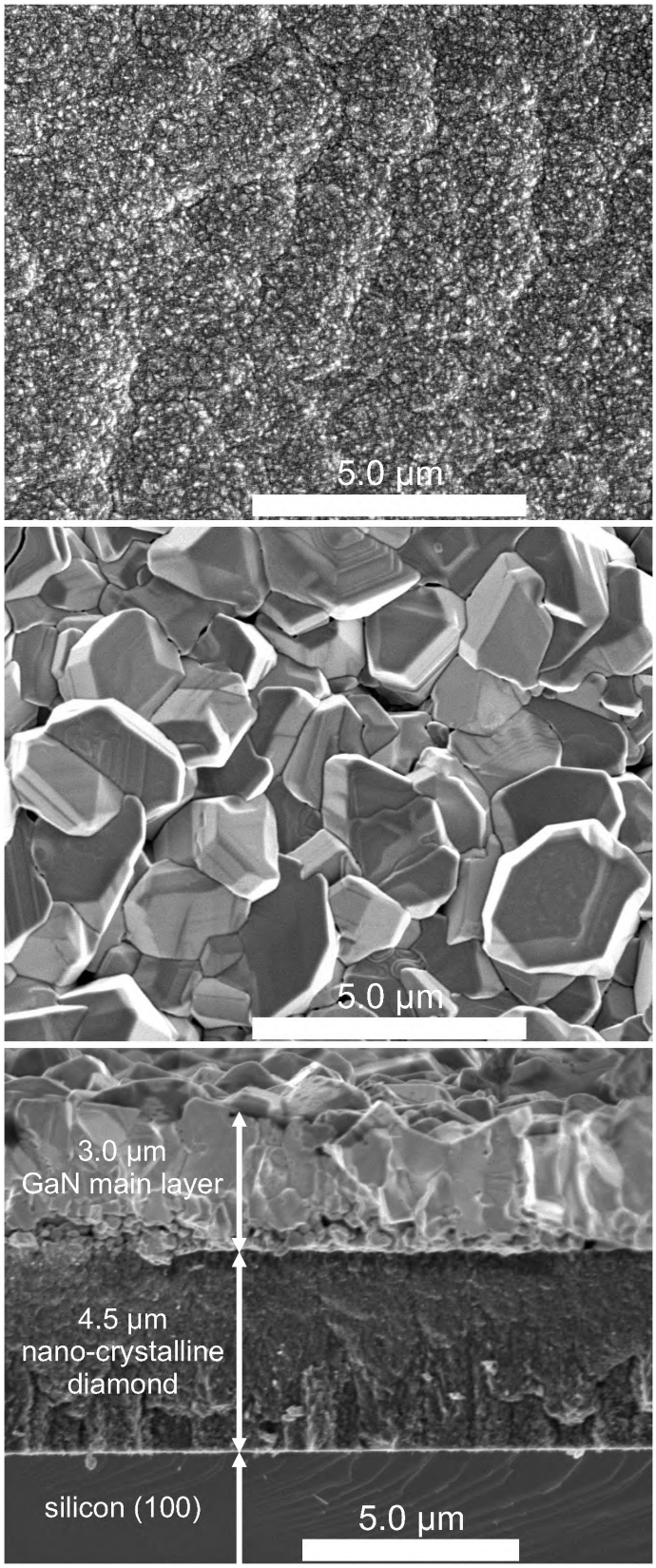

Figure 7.1: SEM images of the nano-crystalline diamond substrate (top), as-grown GaN layer (middle) and cross-section, showing the interfaces (bottom).

7.3 Results and Discussion

7.3.1 Scanning Electron Microscopy

Compared to the nano-crystalline features of the diamond substrate (figure 7.1, top), the size of the GaN crystals is large: about 1 μm in diameter (figure 7.1, middle). The GaN layer consists of differently oriented closely packed GaN grains. The hexagonal form of the majority of the crystals shows that the [0001] face is of high morphological importance. Some cracks and delamination were observed on the surface, which indicate that large tensional stresses were formed during the cooling down to room temperature. The origin of these stresses lies in the difference in thermal expansion coefficient between GaN and diamond, $\beta = 6.2 \cdot 10^{-6}$ K^{-1} and $\beta = 1 \cdot 10^{-6}$ K^{-1} respectively [137–139]. Furthermore, the SEM micrographs showed numerous secondary nucleated crystals.

The cross-section (figure 7.1, bottom) gives a detailed view of the composition of the heterostructure. On top of the Si (100) substrate small clusters of nano-crystalline diamond were formed. They grew further and coalesced to form a closed layer of 4.5 μm thickness. The main GaN layer has a thickness of about 3.0 μm and its roughness is striking compared to the flat and abrupt silicon-diamond and diamond-GaN interfaces.

7.3.2 Profilometry

For the nano-crystalline diamond template an average roughness of 11 nm was found (RMS = 14 nm), whereas for the GaN layer this increased to 833 nm (RMS = 1.3 μm). The cross-section SEM image (figure 7.1, bottom) confirms the results of these measurements.

7.3.3 X-Ray Diffraction

In figure 7.2, the as-grown layer (middle) is compared to the substrate's diffraction pattern (top) and the data of h-GaN powder (bottom) synthesized by Senthil Kumar *et al.* [140]. All reflections in the spectrum can be attributed to the substrate or to orientations of hexagonal GaN powder. Therefore it is clear that the as-grown layer consists of wurtzite structured GaN, which is thermodynamically the most stable structure. The peak intensities in the powder spectrum (figure 7.2, bottom) are in agreement with calculated data for the wurtzite structure [141]. However, the high relative intensities for the (0002), (10$\bar{1}$2) and (10$\bar{1}$3) orientations of the GaN grown in this study indicate preferred growth with the c-axis perpendicular to the substrate. This is consistent with the observations from the SEM studies.

7.3.4 Raman Microscopy

Wurtzite GaN has the symmetry of point group C_{6v}. Group theory predicts six allowed Raman active optical phonon modes: A_1 (TO), E_1 (TO), A_1 (LO), E_1 (LO) and 2 E_2 modes [142]. Normally in the applied backscattering geometry only the A_1(LO) and the E_2 modes are observed if the c-axis of GaN is parallel to the incident laser beam direction, thus when crystals with growth direction [0001] are investigated.

Figure 7.3 depicts a typical Raman spectrum taken from the GaN layer. Next to the modes mentioned above, it also shows a sharp feature at 535 cm^{-1}, which is attributed

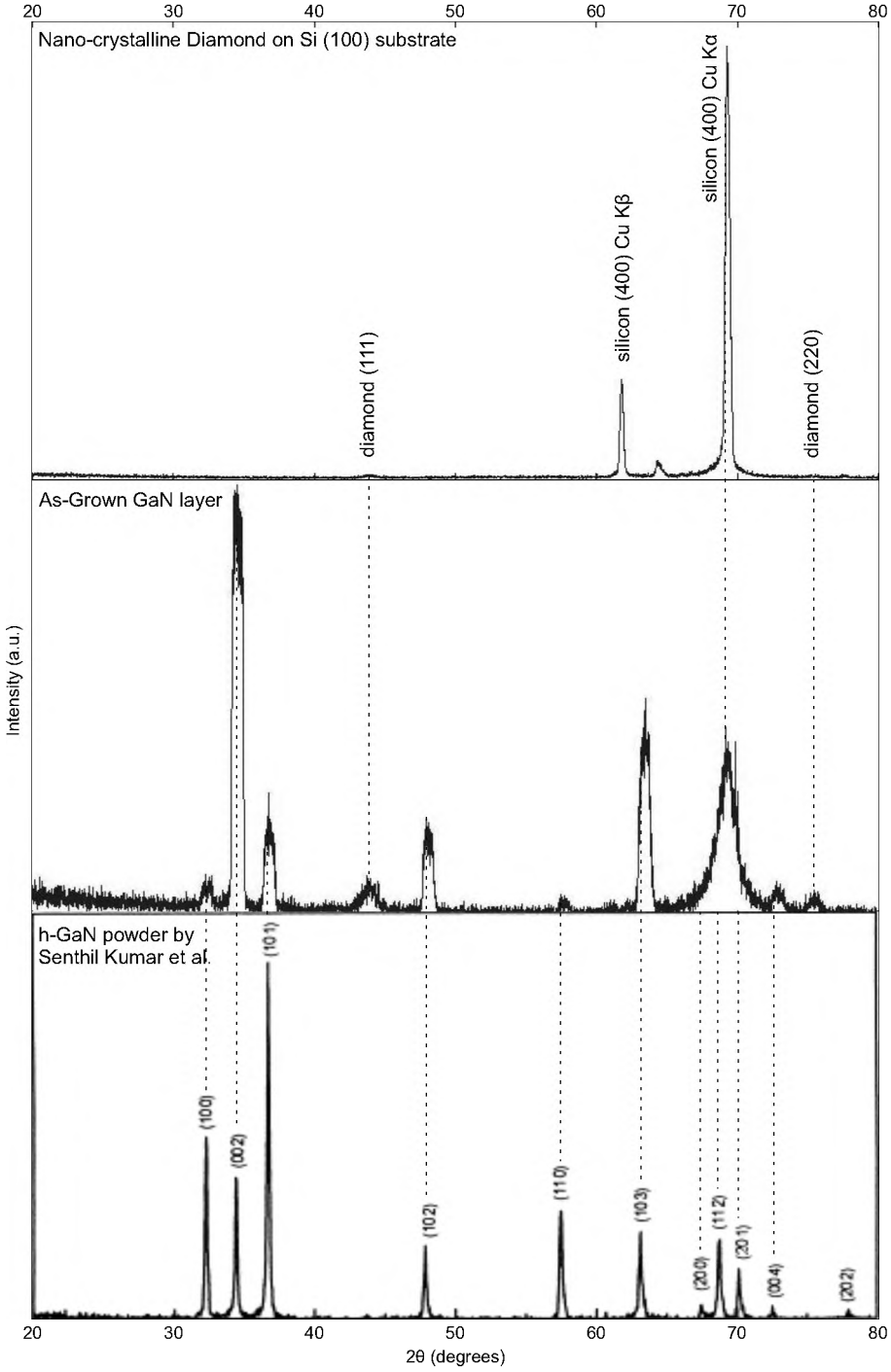

Figure 7.2: $\theta/2\theta$ XRD spectra of the nano-crystalline diamond substrate (above), as-grown GaN layer (middle) and h-GaN powder spectrum from reference [140] (bottom).

to A_1(TO). The mode is observed in this experiment because the incident light was not exactly normal to the (0001) surfaces of the crystals, due to their polycrystalline character [143]. The narrow width of the peaks implies a high crystalline quality, whereas the positions of the E_2(high) and E_1(LO) peaks, respectively at 568 cm^{-1} and 741 cm^{-1}, suggest a very low free carrier concentration in the layer [144]. These positions are in agreement with previous work [145] for GaN (0001) layers (E_2(low) has a phonon frequency of 144

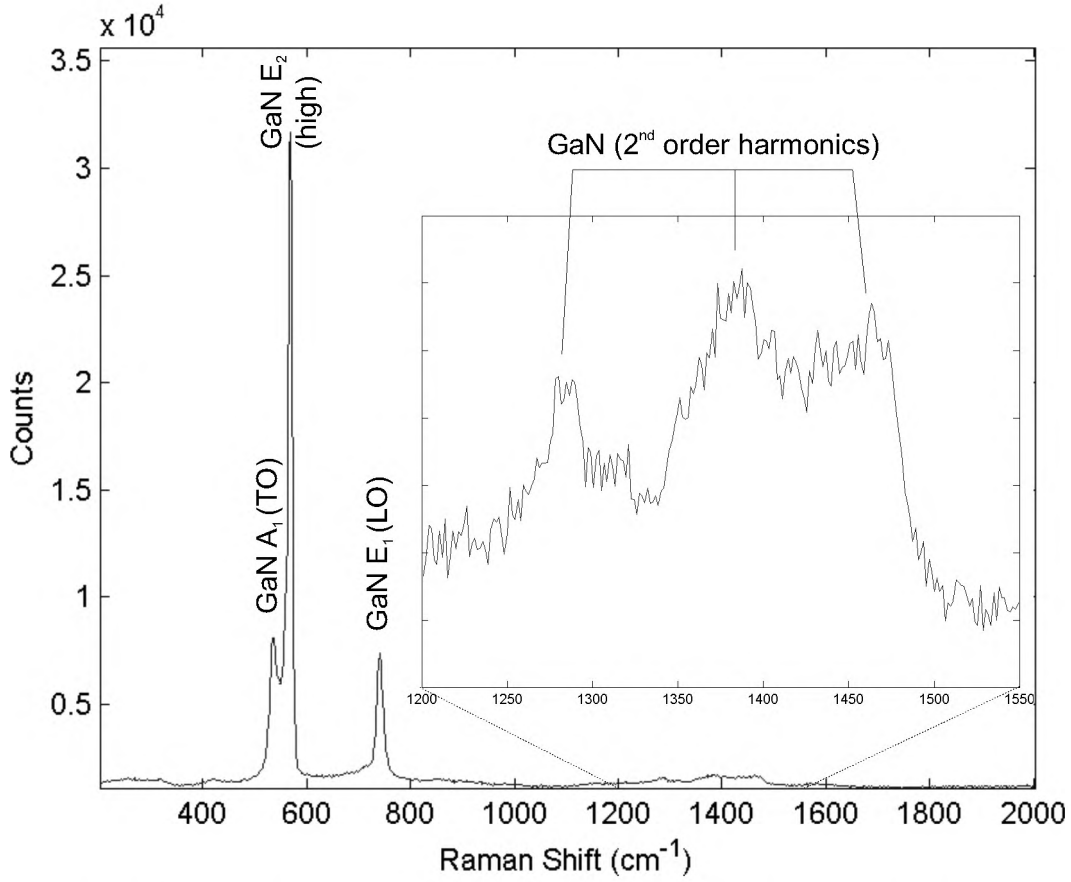

Figure 7.3: Room temperature Raman spectrum in backscattering geometry.

cm^{-1}, and therefore is not included in figure 7.3).

The inset of figure 7.3 shows the second order Raman scattering of the deposited layer. It is in very good agreement with previous work by Murugkar *et al.* [146] and all contributions are attributed to wurtzite GaN. No features of diamond or graphite are observed, which confirms the quality and thickness of the GaN crystal layer.

Subsequently, the effect of the GaN deposition on the diamond quality was investigated. This was done by comparison of Raman spectra taken prior to GaN deposition and taken after deposition from an area where the GaN was removed, as depicted in figure 7.4. The contributions in the spectra are ascribed to diamond (1332 cm^{-1}), graphite (1367 cm^{-1} and 1560 cm^{-1}), and transpolyacetylene (1140 cm^{-1} and 1470 cm^{-1}) [46]. Only the relative intensity of the transpolyacetylene peaks is lower after the growth. Considering that transpolyacetylene is expected to be formed in the grain boundaries, it can be concluded that the nano-crystalline diamond quality has not decreased, presumably even slightly increased, during the GaN growth.

7.3.5 Cathodoluminescence

The acquired CL spectrum is depicted in figure 7.5. The large emission around 2.20 eV (564 nm) is believed to be the yellow luminescence band of GaN (YL GaN). The exact origin of this yellow luminescence in GaN is not understood exactly, but several studies indicate that almost all defects and vacancies in GaN cause yellow luminescence [147].

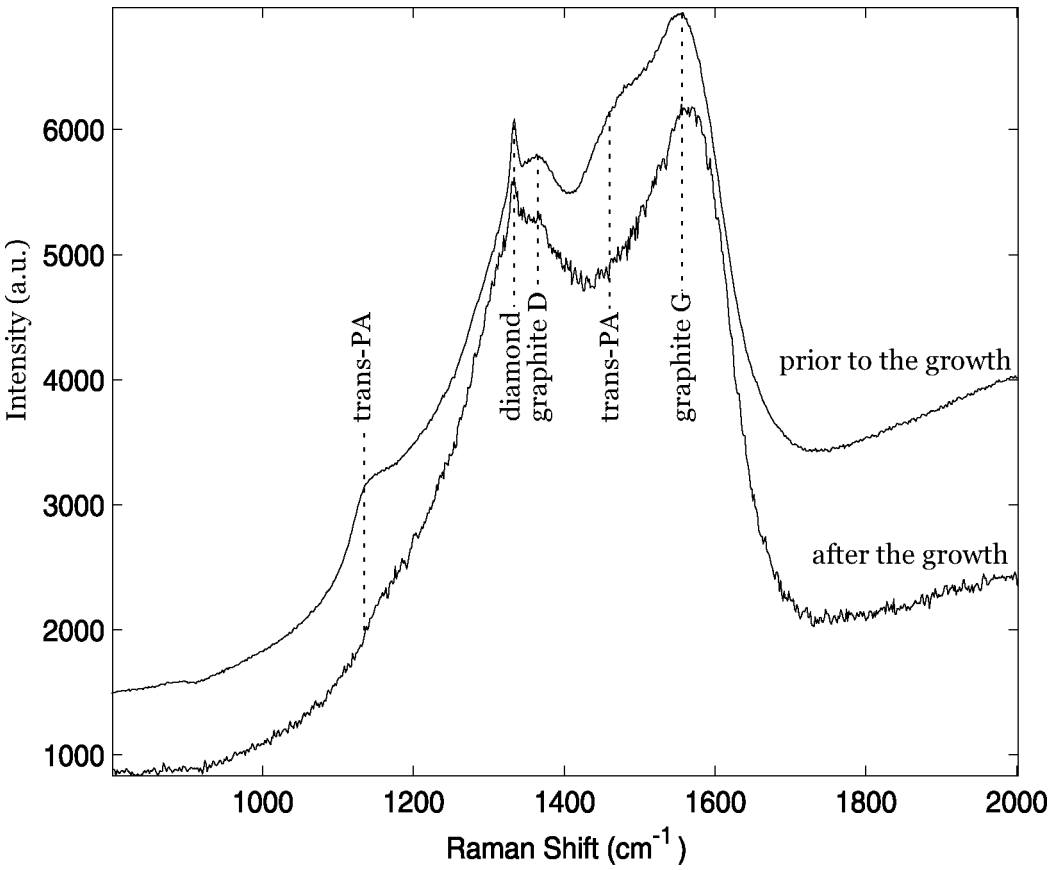

Figure 7.4: Comparison of the diamond quality prior and after the growth of the GaN layer by room temperature Raman spectroscopy.

Here it is ascribed to the incorporation of carbon atoms from the diamond in the GaN crystals [147], as suggested from the decrease in transpolyacetylene concentration in the diamond layer after the growth. It was suggested by Birkle *et al.* [148] that carbon doping also enhances the broad UV-luminescence band around 3.26 eV (380 nm). This band is observed in the spectrum (denoted as UVL GaN) too, supporting the theory of carbon doping in our sample. Other defects in the GaN crystals, for example originating from the lattice mismatch between diamond and GaN, may also enhance the yellow luminescence.

Although the nano-crystalline substrate is excited in the measurement, because GaN is cracked and flaked in some areas during the cooling down, the large amount of grain boundaries and the sp^2-character of the substrate quench the electrons in such a way that any luminescence is prevented from irradiating. Therefore, no diamond luminescence is observed. The other features in figure 7.5 originate from the cathodoluminescence unit and are indicated by P.

Most striking in the cathodoluminescence spectrum, however, is the absence of the band-edge line around 3.44 eV (at 293K, [149]). Apparently, there is no direct transition of donor/acceptor bound excitons or donor-acceptor recombination. This can be related to the large yellow luminescence band, suggesting all excitons follow a recombination route via at least one impurity or defect level, which induces a transition of 2.2 eV. Furthermore, the afterglow of the luminescence (up to 3 seconds at room temperature), after the electron beam was stopped, makes it plausible that excitons are trapped somewhere. For carbon

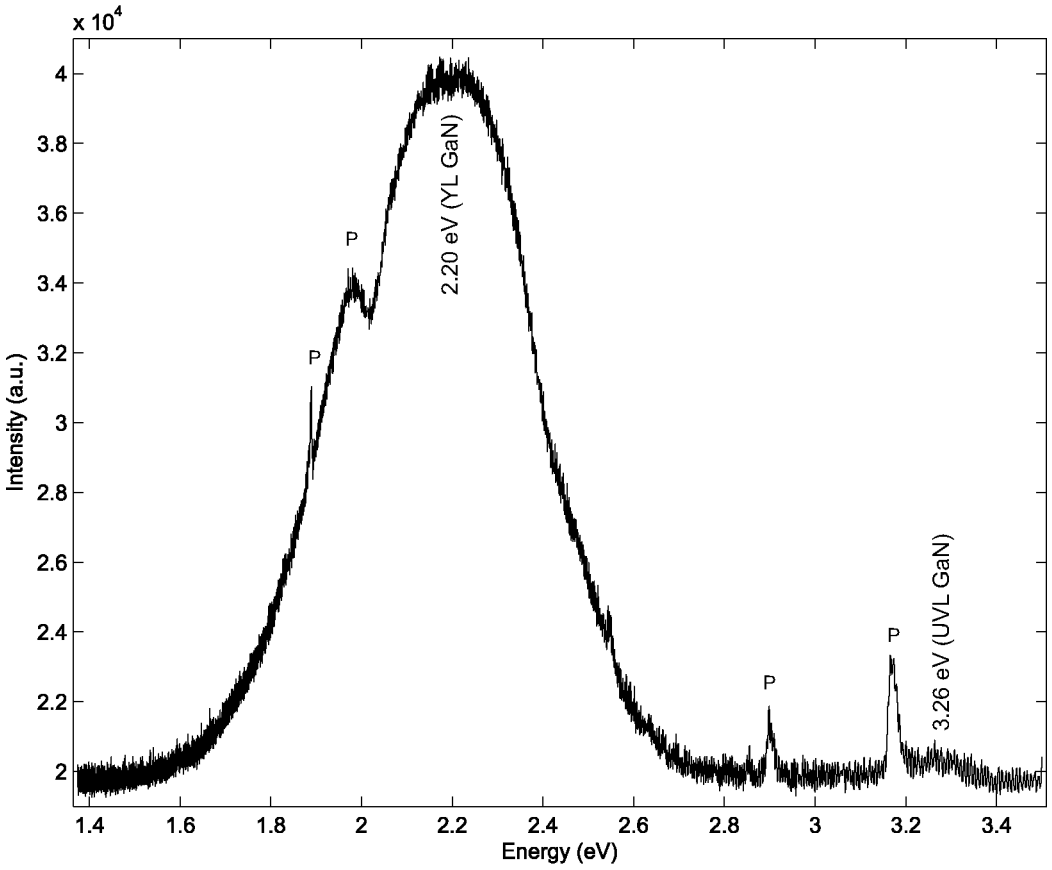

Figure 7.5: Room temperature cathodoluminescence spectrum excited by a 15 keV electron beam. The plasma peaks produced by the CL unit are denoted by P.

doping, this was already investigated by Lopatiuk *et al.* [150]. Another possible location in the polycrystalline GaN is at the grain boundaries between the crystals, which can act as traps for excitons.

7.4 Conclusions

In summary, h-GaN polycrystalline films have been synthesized on nano-crystalline diamond templates which were in turn grown on a silicon wafer. Results obtained from several characterisation techniques reveal a relatively smooth diamond substrate and good structural quality GaN. However, due to the formation of microsized crystals, a high surface roughness has been observed for the polycrystalline GaN layer. The optical quality is still poor, as was concluded from cathodoluminescence measurements. There was no decrease in the nano-crystalline diamond quality.

Evidence was found for preferred orientation, in particular in the [0001] direction. Based on this information, future work will focus on the production of heterogeneous layers of wurtzite GaN on nano-crystalline diamond, which should also lead to better optical quality of the GaN layer.

8

Comparison of GaN and AlN Nucleation Layers for the Oriented Growth of GaN on Diamond Substrates

*In this study, {0001} oriented GaN crystals have been grown on freestanding, polycrystalline diamond substrates using AlN and GaN nucleation layers (NLs). XRD measurements and SEM analysis showed that the application of a thin AlN NL gives the best structural results, because AlN has a thermal expansion coefficient in between GaN and diamond and thus delocalizes the stress to two interfaces. The optical quality of the layers, investigated with Raman microscopy and photoluminescence spectroscopy, is similar. Although no lateral epitaxy is obtained, new insight is gained on the nucleation of GaN on diamond substrates facilitating the growth of GaN epilayers on polycrystalline diamond substrates.

8.1 Introduction

Thermal management is one of the major problems in modern electronics. Smaller spacing between devices, all operating at higher power, increases the produced heat severely. For these devices, especially Gallium Nitride (GaN) with its potential in high-power applications, the spreading of produced heat is essential considering the lowered performance and reduced life-time caused by usage at high temperatures. Adding a diamond layer to the device should lead to a spread of heat away from the device, because of the high

*Published in: G.W.G. van Dreumel, T. Bohnen, J.G. Buijnsters, W.J.P. van Enckevort, J.J. ter Meulen, P.R. Hageman, and E. Vlieg, Diamond Relat. Mater. 19 (2010), 437.

thermal conductivity of diamond, which also has the advantage of being an electric insulator [27]. The diamond layer thus acts as a heat sink and lowers the operating temperature of the device. This perception led to intensified research on a variety of approaches that target the integration of these two materials [50, 52, 58, 63, 73, 74, 151].

In chapter 7, it has been shown that it is possible to grow GaN crystals on nanocrystalline diamond, utilizing a GaN nucleation layer (NL) [151]. However, the formed GaN layer was polycrystalline and consisted of crystals with random orientations with respect to the substrate surface. Furthermore, large amounts of residual stress have been observed in the layers. This stress mostly originates from the difference in thermal expansion coefficient between the GaN and diamond. In this research, an Aluminum Nitride (AlN) interlayer [58] has been employed, which is commonly used for other substrates [80]. For the GaN and AlN nucleation layers, the dependence on nucleation time is investigated and then best samples from both series are compared.

Table 8.1: Overview of the samples grown in this study

Sample	Type NL	Time NL	Time HT GaN
A	GaN	1.0 min	90.0 min
B	GaN	2.0 min	90.0 min
C	GaN	3.0 min	90.0 min
D	GaN	4.0 min	90.0 min
E	GaN	5.0 min	90.0 min
F	AlN	1.0 min	90.0 min
G	AlN	2.0 min	90.0 min
H	AlN	3.0 min	90.0 min
I	AlN	4.0 min	90.0 min
J	AlN	5.0 min	90.0 min

8.2 Experimental

For this studies, hexagonal GaN layers were grown on polycrystalline diamond substrates, acquired from Element Six (Diafilm TM100), in an Aixtron AIX-200 RF MOCVD reactor using trimethylgallium (TMG), trimethylaluminum (TMA) and ammonia gas (NH_3) as precursors for Ga, Al and N, respectively. Prior to growth, each sample was cleaned with isopropanol in an ultrasonic bath and dried overnight at 120 °C. The growth temperatures for the GaN NL, AlN NL and high temperature (HT) GaN were 525 °C, 850 °C and 1170 °C, respectively. The samples were annealed for 1 minute 1170 °C. Hydrogen was used as a carrier gas and the reactor pressure was kept at 50 mbar for the NLs and 35 mbar for the HT-GaN growth. The TMA flow rate was $1.08 \cdot 10^{-5}$ mol/min [58], while the TMG flow rate was $1.37 \cdot 10^{-5}$ and $5.25 \cdot 10^{-5}$ mol/min for the NL and HT-GaN, respectively [151]. The flow rate for ammonia was kept at $1.0 \cdot 10^{-1}$ mol/min, throughout the whole growth process. Table 8.1 summarizes the nucleation and growth times for the series.

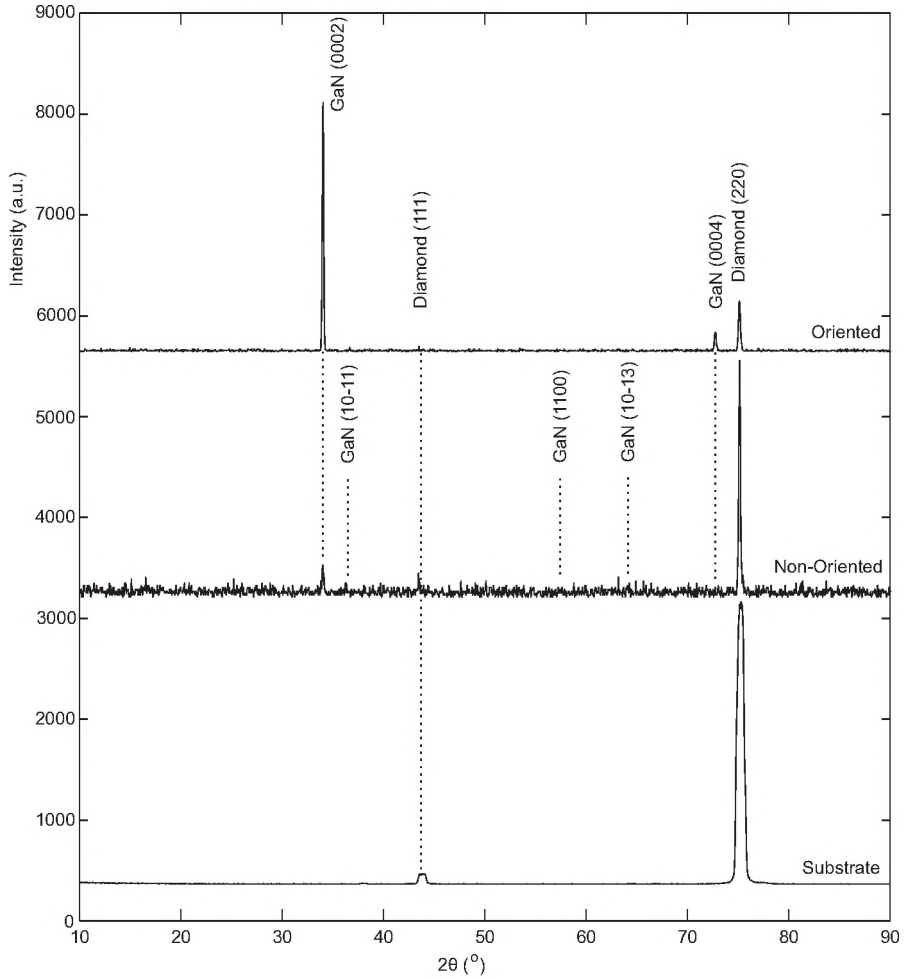

Figure 8.1: Typical $\theta/2\theta$ diffractograms of GaN grown on AlN and GaN NLs for oriented (Samples D, E, F, G and H) and non-oriented (Samples: A, B, C, I and J) layers. A substrate pattern is added for direct comparison and patterns are vertically shifted for clarity.

The morphology of the substrates and the as-grown surfaces was studied by applying scanning electron microscopy (SEM, Jeol JSM 6330F) and the roughness was measured using a Wijco NT-1100 optical profiler in VSI-mode. Rocking curves and $\theta/2\theta$ X-Ray diffraction (XRD) patterns of the layers have been recorded with a high resolution Bruker D8 diffractometer setup using Cu K_α radiation (λ = 1.5418Å), while a Renishaw 1000 micro-Raman spectrometer with an Ar ion laser at wavelength λ = 514.8 nm and 10 mW power was used to investigate the samples in backscattering geometry at room temperature (RT). Photoluminescence spectra (PL) were obtained applying a 325 nm HeCd laser at RT.

8.3 Results and Discussion

8.3.1 Diamond Substrate Characterization

The polycrystalline diamond substrates were delivered pre-polished. According to the manufacturing data, the diamond had a thermal conductivity of >1000 W $m^{-1}K^{-1}$ and

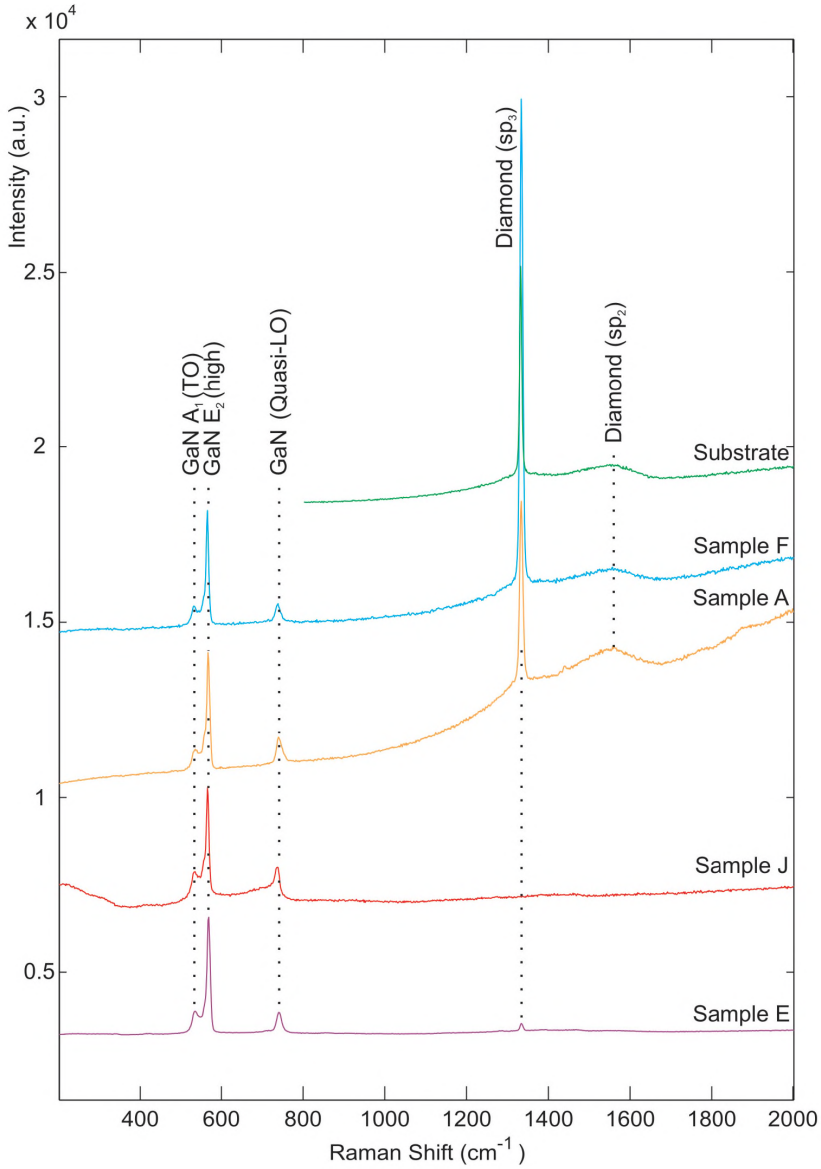

Figure 8.2: Raman spectra of GaN layers grown on GaN and AlN NLs with short (1 minute: A, F) and long (5 minutes: E, J) nucleation times. The diamond substrate spectrum is added for comparison and spectra are vertically shifted for clarity.

a thermal expansion coefficient of $1.0 \pm 0.1 \cdot 10^{-6}$ K^{-1}. Its roughness is determined at R_a = 5.40 nm with profilometry. $\theta/2\theta$ XRD showed that the substrates mainly consisted of (220) oriented grains (figure 8.1, bottom: $2\theta = 75\,^\circ$). Relatively smaller signals were detected for grains with (111), (311) and (400) orientations at 2θ = 42, 92 and 120 °, respectively (not shown in figure 8.1). A Raman spectrum of the substrate is included in figure 8.2 and shows the typical features for good quality polycrystalline diamond, *i.e.* a large sharp sp^3 diamond peak and low diamond sp^2 intensity.

8.3.2 Scanning Electron Microscopy

Figure 8.3 shows SEM-images of the layers grown with a GaN NL (Samples A-E) and an AlN NL (Samples F-J). For the samples A, B and C with 1, 2 and 3 minutes GaN nucle-

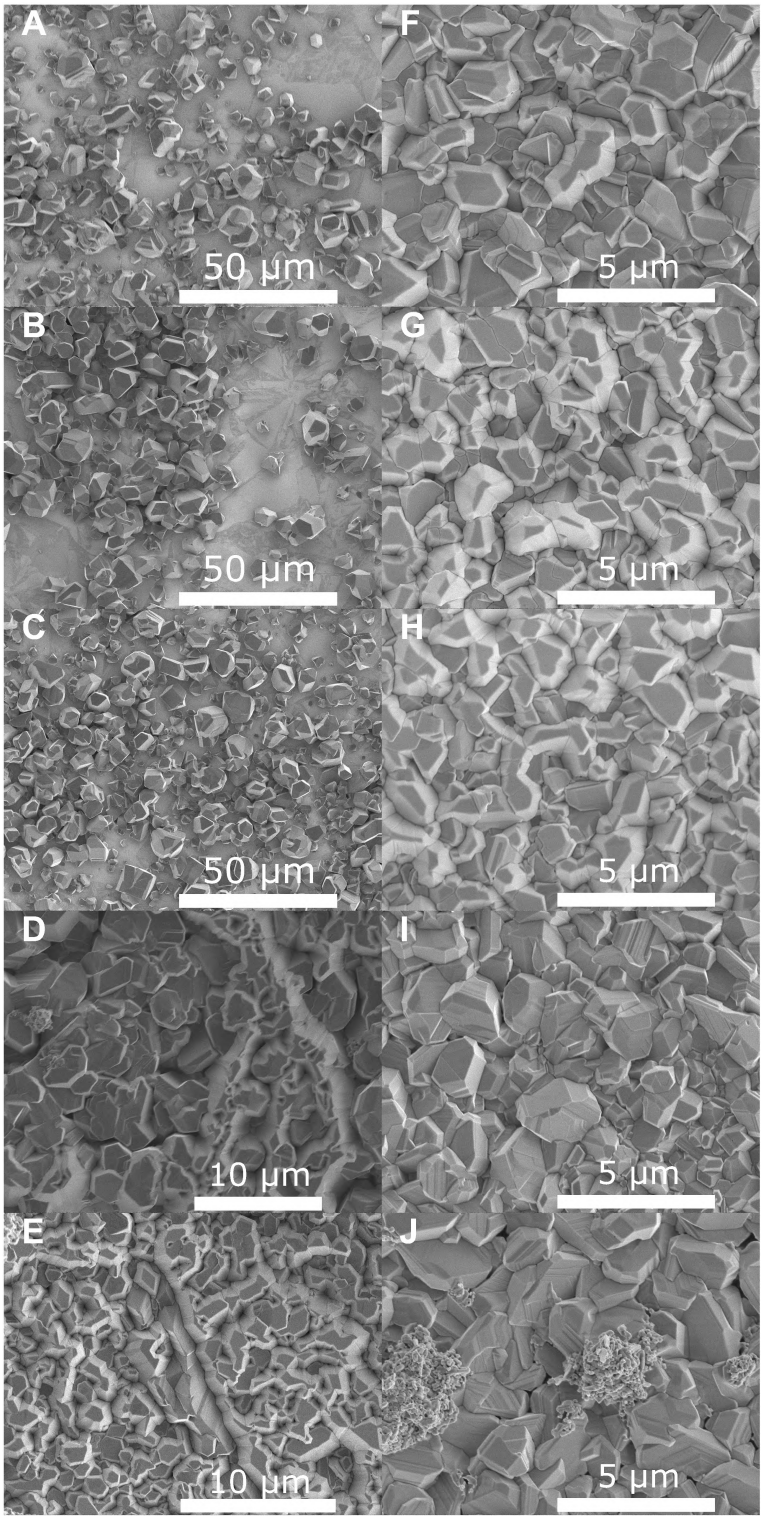

Figure 8.3: SEM images of the samples produced with varying GaN and AlN NLs. Samples are denoted as described in Table 8.1. Note the different scales for different micrographs.

ation layer growth, respectively, large areas of uncovered substrate can still be observed, which probably originates from poor wetting of GaN on the substrate. Thus a low amount of nuclei is formed during nucleation resulting in a few large crystals after 90 minutes of growth. However, on samples D and E more and smaller GaN crystals are formed.

These crystals have a flat top parallel to the substrate, sloped side facets and show six-fold symmetry, suggesting the crystals are (0001) oriented. Apparently, during annealing the original nucleation layer recrystallizes to oriented nuclei as previously described by Koleske *et al.* for sapphire substrates [105].

In contradiction to the GaN NLs, for the layers with an AlN NL numerous small, well oriented islands can be recognized in the SEM images even at short nucleation times, caused by much better wetting of the AlN on the diamond. If the nucleation time is 4 or 5 minutes (Samples I and J) the amount of nanocrystalline material deposited in the nucleation step becomes too large, resulting in recrystallization of nucleation islands on top of the nanocrystalline GaN layer instead of the diamond substrate. The layer is thus too rough to form oriented islands. This assumption is confirmed by investigating samples prepared with only the nucleation and annealing step (not included in figure 8.3).

For samples D and E several wide cracks in the GaN layers can be observed, from which it can be concluded that the amount of nuclei is high enough to form a coherent layer of islands. The oriented layers with AlN NL (F, G and H) also contain some cracks, however, these are much smaller in width and their number is less than in the GaN layers. Probably the stress in the layers is lower for the AlN NL compared to the GaN NL. AlN has a thermal expansion coefficient of $4.2 \cdot 10^{-6}$ K^{-1} [137], which is in between diamond and GaN (1.0 and $5.6 \cdot 10^{-6}$ K^{-1}, respectively [137, 138]) and thus distributes the stress to two interfaces instead of one diamond/GaN interface. The creation of oriented islands instead of closed epitaxial layers is probably caused by a lack of lateral growth compared to the vertical growth rate of the individual crystallites.

8.3.3 $\theta/2\theta$ XRD

In figure 8.1 the oriented layers (top, samples D, E, F, G and H) are compared to the substrate's diffraction pattern (bottom) and the data from the non-oriented layers (middle, samples A, B, C, I and J). It is clear that one hexagonal GaN orientation dominates the $\theta/2\theta$ spectrum for the oriented samples. Only the substrate peaks and the (0002) and (0004) peaks of GaN are detected, indicating a preferential orientation along the c-axis. This is consistent with the SEM observations. The non-oriented layers display much lower intensities and show more features, for instance $(10\bar{1}1)$, (1100) and $(10\bar{1}3)$ orientations of GaN.

8.3.4 Raman Microscopy

In theory, for hexagonal GaN only three Raman active optical phonon modes can be measured in backscattering geometry if the GaN is c-axis oriented, i.e. A_1(TO), E_2(low) and E_2(high) [142]. Often a quasi-LO (mixing of A_1(LO) and E_1(LO) [144, 145]) is also observed when the incident light is not exactly normal to the (0001) surface of the crystals, for instance if the layer has a higher mosaicity due to its polycrystalline character [143].

Results of the Raman measurements are displayed in figure 8.2. The E_2(low) has a phonon frequency of 144 cm^{-1} and is therefore not visible in the spectra. For all samples the above-mentioned A_1(TO), E_2(high) and the quasi-LO are clearly visible, respectively at 535 cm^{-1}, 568 cm^{-1} and 741 cm^{-1}, indicating that no stress is present in the samples either by releaving the stress through the observed cracks (SEM, section 8.3.2) or due to the fact that some layers are not coherent at all. The peak values correspond well with

previous work on GaN (0001) oriented layers of high crystalline quality on sapphire [145] and GaN crystals on nanocrystalline diamond substrates (chapter 7, [151]). Only sample J displays a slightly distorted spectrum and a slightly shifted position of the quasi-LO peak at 738 cm^{-1}. The cause for this difference could not be determined unambiguously, but it most likely originates from a larger carrier concentration ($\alpha \sim 1{\cdot}10^{18}$ cm^{-3} instead of α = $1{\cdot}10^{17}$ cm^{-3}) resulting in LO phonon-plasmon coupling of which the L^+ branche is at 738 cm^{-1} and the L^- branche is just visible at 200 cm^{-1} [144].

Furthermore, the Raman measurements revealed a clear trend for both series: the intensity of the diamond peak (1333.8 cm^{-1}) is lowered with increasing nucleation time. This suggests the nucleation is the essential step to obtain a homogeneous distribution of nucleation islands. As the diamond peak is not shifted and no carbon sp^2 peaks [46] are observed, it can be concluded that the diamond substrate remains its quality throughout the GaN growth process and no graphitic interlayers are formed.

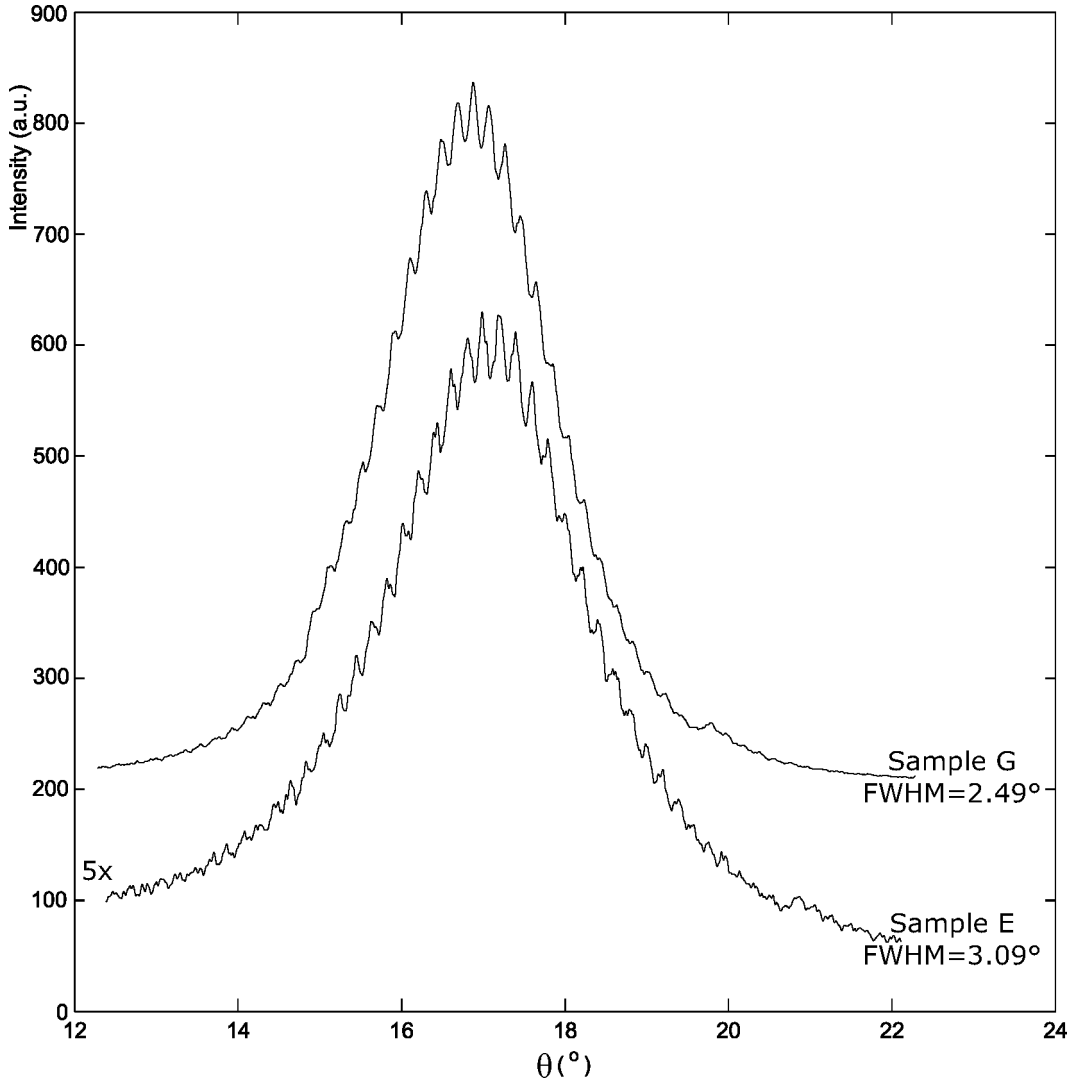

Figure 8.4: (0002) XRD Rocking curves for samples E and G. The intensity of the spectrum of sample E is enhanced 5 times and spectra are vertically shifted for clarity.

8.3.5 Comparison between GaN and AlN NLs

To compare the quality between the layers obtained with optimized nucleation layers for GaN and AlN, $\theta/2\theta$ and (0002) rocking curve XRD scans have been compared for the most oriented samples of both series (*i.e.*, samples E and G). The full-width at half-maximum (FWHM) of the $\theta/2\theta$ (0002) peaks are 0.77 and 0.78 degrees for GaN and AlN samples, respectively. Because both samples consist of slightly tilted, oriented islands, the peaks are much broader than for a single crystal layer. However, with respect to the rocking curve scans, plotted in figure 8.4 with FWHMs of 3.09 and 2.45 degrees respectively, the FWHM of the $\theta/2\theta$ peaks are small. This indicates that the randomness in sheet texture (the mosaicity, *i.e.* the spread of the (0002) orientation with respect to the substrate surface, measured in the direction of the rocking curve) is a few degrees in both samples. The layer with AlN NL has a lower FWHM, suggesting a more in-plane orientation than the sample with the GaN NL. It also has a higher intensity, suggesting it is less rough compared to the GaN NL. This is confirmed by profilometric measurements, giving roughness values of R_a= 900 nm and 360 nm for the samples E and G, respectively.

The band edge photoluminescence is 3.39 eV (FWHM = 53 meV) for sample E and 3.40 eV (FWHM = 56 meV) for sample G determined at RT. Both samples exhibited large yellow luminescence emissions, which is a sign of a large amount of defects [147].

8.4 Conclusions

In summary, hexagonal GaN layers have been grown on freestanding polycrystalline diamond substrates with AlN and GaN NLs. The optimum deposition times for both types of NL are 2 and 5 minutes for the AlN and GaN NL respectively, giving $\{0001\}$ oriented GaN islands after subsequent growth. The structural quality of the GaN layer is better for AlN NLs, as can be concluded from the SEM, rocking curve XRD and profilometric measurements. Raman and PL spectroscopy showed that the optical quality of both layers is very similar, while the diamond substrate is unaffected.

Part IV

Single Crystal Diamond Substrates

9

Realising Epitaxial Growth of GaN on (001) Diamond

* By an extensive investigation of the principal growth parameters on the deposition process, we realised the epitaxial growth of crystalline wurtzite GaN thin films on single crystal (001) diamond substrates by MOCVD. From the influence of pressure, V/III ratio and temperature, it was deduced that the growth process is determined by the mass-transport of gallium precursor material toward the substrate. The highest temperature yielded an improved epitaxial relationship between grown layer and substrate. XRD pole figure analysis established the presence of two domains of epitaxial layers, namely (0001)<10$\bar{1}$0>GaN$\|$(001)[110]diamond and (0001)<10$\bar{1}$0>GaN$\|$(001)[1$\bar{1}$0]diamond, which are 90 ° rotated with respect to each other. The presence of these domains is explained by the occurence of areas of (2×1) and (1×2) surface reconstruction of the diamond substrate. When applying highly misoriented diamond substrates towards the [110] diamond direction, one of the growth domains is suppressed and highly epitaxial GaN on (001) diamond is realised.

9.1 Introduction

GaN-based devices have a unique potential for high-power applications. Recently, this has been demonstrated once more for a GaInN diode laser with 100 W peak power [152], while Wu *et al.* reported output powers for AlGaN/GaN HEMTs which reached a density of 32.2 W mm^{-1} [24]. In theory, even higher power outputs are possible. However, currently GaN devices are hindered to a large extent by self heating problems.

*Published in: G.W.G. van Dreumel, P.T. Tinnemans, A.A.J. van den Heuvel, T. Bohnen, J.G. Buijnsters, J.J. ter Meulen, W.J.P. van Enckevort, P.R. Hageman, and E. Vlieg, J. Appl. Phys. 110 (2011), 013503.

To minimise these specific thermal problems it is vital to extract the heat from the active area in the GaN device. This can be achieved by using alternative substrates that have higher thermal conductivity than the traditional sapphire and silicon substrates applied for GaN growth. Diamond has, by far, the highest thermal conductivity that is known [27]. Therefore, a layer of high thermal conducting diamond between the device and the cooling system can significantly lower the temperature in these high-power structures. The attachment of GaN films onto diamond substrates, acting as heat sinks, would thus be a good solution to increase the power range in which GaN devices can be operated.

For this reason, the last years an increased interest has risen in research targeting the integration of these two materials. Besides investigations on the adding of a diamond layer on existing GaN structures [50, 52], this research involves bonding of GaN on CVD diamond [71, 73, 74], and the application of silicon-on-diamond substrates [63, 153]. Recently, GaN has been deposited directly on several types of diamond substrate [58, 61, 151, 154, 155], leading to the successful fabrication of an AlGaN/GaN HEMT on (111) single crystalline diamond by MBE [62]. Although this diamond (111) substrate offers a nice threefold symmetry as a template for the growth of hexagonal GaN, it is much more difficult to obtain and process in comparison to (001) diamond. Therefore, the formation of high quality epitaxial GaN on (001) diamond by MOCVD is investigated in these studies.

In previous work, while obtaining the best conditions for the nucleation of GaN on polished polycrystalline diamond, it was already shown that the low lateral growth rate of the annealed nucleation islands hinders the formation of a closed layer [154]. Similar problems can be identified in other reports, such as in the MOCVD growth of GaN on nanocrystalline and (110) oriented diamond substrates [58, 151], for the c-oriented AlN deposition on various diamond faces [60, 156] and the closely related GaN and AlN growth on silicon substrates [157, 158]. To overcome this problem of slow lateral growth rate, the influence of several major parameters in GaN growth, like reactor pressure, precursor flow, growth temperature, and substrate misorientation, on the growth rate are investigated. In this way, important information on the growth process of GaN on diamond is obtained.

9.2 Experimental

For this study, the substrates used are 3.0 x 3.0 mm^2 single crystalline CVD diamond substrates, acquired from Element Six, UK. According to the supplier's specifications the substrates have a nominal (001) orientation with a maximum deviation of 3 °. With profilometry, the substrates' roughness is determined at R_a = 3.12 nm. Prior to growth, each sample is cleaned in an ultrasonic bath with $NH_4OH/H_2O_2/H_2O$ solution (1:1:5) subsequently followed by rinsing in H_2O and ultrasonic treatment in $HCl/H_2O_2/H_2O$ solution (1:1:5). Then the sample is again rinsed in H_2O and cleaned in an ultrasonic bath with HF solution, and finally 5 times rinsing in H_2O.

GaN growth is performed in an Aixtron AIX-200 RF MOCVD reactor using trimethylgallium (TMG), trimethylaluminum (TMA) and ammonia gas (NH_3) as precursors for Ga, Al and N, respectively. Hydrogen was used as a carrier gas throughout the whole growth process. The influence of growth parameters is compared with samples prepared with the settings used in our earlier study (sample A, in table 9.1) [154].

Table 9.1: Overview of the samples grown in this studies on nominal (001) diamond substrates

Sample	Thickness GaN film (μm)	Press. (mbar)	NH_3 (mmol/ min)	TMG (μmol/ min)	V/III ratio	Temp. (°C)
A	0.80	35	100	52.5	1870	1170
B	0.78	20	100	52.5	1870	1170
C	0.07	500	100	52.5	1870	1170
D	0.85	35	68	52.5	1275	1170
E	0.58	35	132	52.5	2465	1170
F	1.55	35	100	105.0	935	1170
G	0.82	35	100	52.5	1870	1140
H	0.85	35	100	52.5	1870	1185
I	0.86	35	100	52.5	1870	1215

For all samples the nucleation and annealing steps were identical. An AlN nucleation layer was deposited at 850 °C in 2 minutes, while the pressure was maintained at 50 mbar. The flow rates for NH_3 and TMA during nucleation were $1.0 \cdot 10^{-1}$ mol/min and $1.08 \cdot 10^{-5}$ mol/min, respectively [58]. Annealing was performed in NH_3/H_2 atmosphere under 50 mbar total pressure for 1 minute at 1170 °C. The parameter values applied for the main layer growth are outlined in table 9.1. To ensure the effects of the different parameters on the GaN island growth can still be observed, the growth time for the main layer was kept constant at 20 minutes, and the resulting thickness for each sample is listed in table 9.1 too.

The morphology of the substrates and the as-grown surfaces was studied using scanning electron microscopy (SEM, Jeol JSM 6330F), while a Renishaw 1000 μ-Raman spectrometer with an Ar ion laser at wavelength $\lambda = 514.8$ nm and 20 mW power was used to investigate the samples in backscattering geometry at room temperature (RT). The layer thickness and roughness were measured using a Wijco NT-1100 optical profiler. X-Ray diffraction (XRD) pole figures of the layers were recorded with a high resolution Bruker D8 diffractometer setup using Cu K_α radiation (λ = 1.5418Å). Photoluminescence (PL) spectra of the layers were taken at 5 K. The samples were excited by a continuous-wave 325 nm HeCd laser with a power density of 30 W cm^{-2}. The spectra were resolved by a 1 m monochromator, which was equipped with a UV-enhanced CCD detector.

9.3 Influence on Morphology

9.3.1 Pressure

The influence of pressure in the reactor during the growth of GaN has been investigated frequently in the past, and has been marked as an important parameter for MOCVD growth of GaN [84]. It determines, for instance, at which temperature the transition between 3D and 2D growth mode occurs. De Theije *et al.* found that an increasing pressure

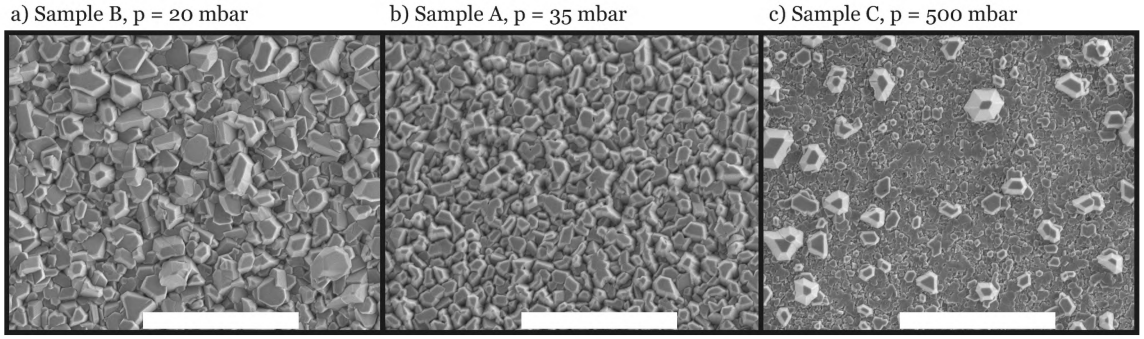

Figure 9.1: SEM images showing the results of the change in reactor pressure during the main GaN layer growth, with increasing pressure from left to right: a) sample B prepared under 20 mbar pressure, b) the reference sample A prepared under 35 mbar, and c) sample C after the growth with 500 mbar reactor pressure. The scale bars represent 5 μm.

in the reactor decreases the transition temperature for growth of GaN on sapphire [159]. Therefore, its influence has been tested first and SEM images of the samples, presented in figure 9.1, show the most significant results. Sample A (middle) is the reference sample obtained after growth at 35 mbar reactor pressure, while on the left side is the sample prepared at 20 mbar reactor pressure (sample B). Where sample A shows an ordered layer with all crystals having a relatively constant height, sample B is disordered with GaN crystals grown on top of another. Furthermore, the shape of the crystals is not so well defined as the obvious hexagonal symmetry (the preferred (0001) orientation for epitaxial growth) observed in the reference sample. It appears this is caused by secondary nucleation of GaN during the growth of the main GaN layer, and that decreasing the pressure in the reactor increases the rate of mass-transport so much that kinetically limited growth is observed [84].

When increasing the pressure, up to a total reactor pressure of 100 mbar, no changes are observed and samples are almost identical to the reference sample. At even higher pressures, the grown film becomes very thin (see table 9.1) and only a few big crystals on top of a layer with small flat islands is observed. Sample C (figure 9.1c) is a typical example obtained at 500 mbar reactor pressure. As hydrogen is the carrier gas during MOCVD growth it is essential to consider the reaction with GaN, certainly at temperatures around 1170 °C. It decomposes GaN into volatile products via the following reactions (chapter 3, [50, 160] :

$$2N_{(surface)} + 3H_2(g) \rightleftharpoons 2NH_3(g); \tag{3.1}$$

$$2Ga_{(surface)} + H_2(g) \rightleftharpoons 2GaH(g). \tag{3.2}$$

The small film thickness of samples grown at high reactor pressure is probably caused by the increase in hydrogen partial pressure in the reactor due to the higher overall pressure. This hydrogen partial pressure changes the ratio between GaN growth and the etching of GaN by hydrogen more towards the latter [84] and thus the resulting GaN layer remains very thin.

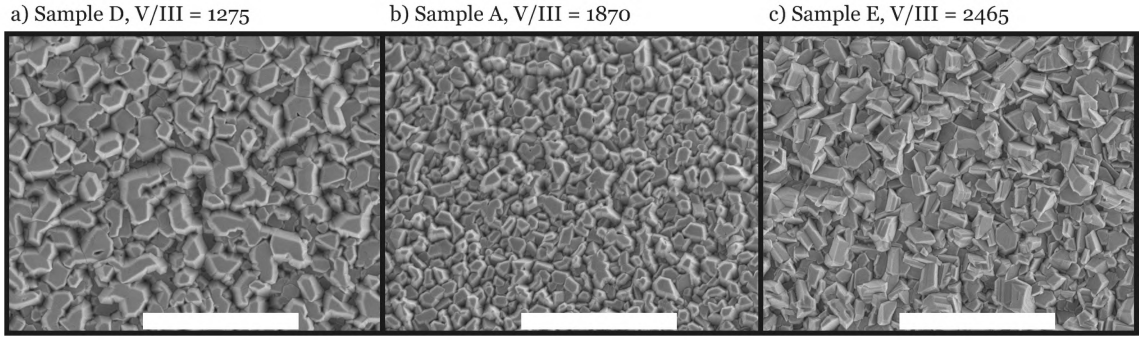

Figure 9.2: SEM images taken from the series in V/III-ratio with increasing NH_3 flow: a) sample D grown with 68 μmol/min NH_3 (V/III = 1275), b) the reference sample A (100 μmol/min NH_3, V/III = 1870), and c) sample E, grown with 132 μmol/min NH_3 (V/III = 2465). The scale bars represent 5 μm.

9.3.2 V/III-ratio

Alteration of the V/III ratio is reported to give good control on the early stages of GaN growth [161], and has been shown to greatly influence the characteristics of the grown epilayer [162]. Because of the variation in lateral growth speed with V/III ratio it is also commonly employed as a steering parameter in lateral epitaxial overgrowth [163]. In this study, its influence is tested by altering the amount of NH_3. Sample D is prepared with less NH_3 (thus lower V/III ratio), while in sample E the NH_3 flow and V/III ratio are increased. The overall amount of gas in the reactor is kept constant by compensating the change in ammonia with the carrier gas flow. Sample A is the reference sample.

Figure 9.2 shows that the preferred (0001) orientation of the GaN crystals with respect to the substrate is lost when more ammonia is added (from left to right). As a result, the crystals show a more or less random orientation, devoid of any epitaxial relationship, due to the excess ammonia.

Sample D (figure 9.2a) however, prepared with a decreased ammonia flow and thus lower V/III ratio, looks quite similar to the reference sample. Profilometric measurements of both samples show the growth rate to be very similar (0.80 and 0.85 μm for samples A and D, respectively) and the (0001) oriented top faces of the GaN crystals are smooth as observed in SEM. On the other hand, the GaN islands in sample A have much steeper edges than the almost trapezoid form of the crystals in sample D. This is directly visible in the SEM images (figure 9.2a, b), where the sides of the crystals (white) are in clear contrast with the top face (grey). However, as the nucleation density differs much between the samples, no real dependence on the lateral growth rate can be obtained.

Furthermore, counterintuitively the grown layer in sample E has a smaller thickness although more growth material (ammonia) is present in the reactor as compared to the reference sample. The thickness remains constant with less ammonia. An extra sample (F) has been prepared with twice as much TMG and the result is compared with the reference sample in figure 9.3. It depicts a similar morphology as sample D but the layer is doubled in thickness due to the increased TMG flow, 1.55 and 0.74 μm respectively. This shows that the growth rate is mainly dependent on the gallium concentration in the reactor. In this gallium-limited growth regime the growth rate decreases with increasing ammonia flow although the TMG flow is not changed. A possible cause for this effect is the raised viscosity due to the high ammonia content in the gas phase. This leads to

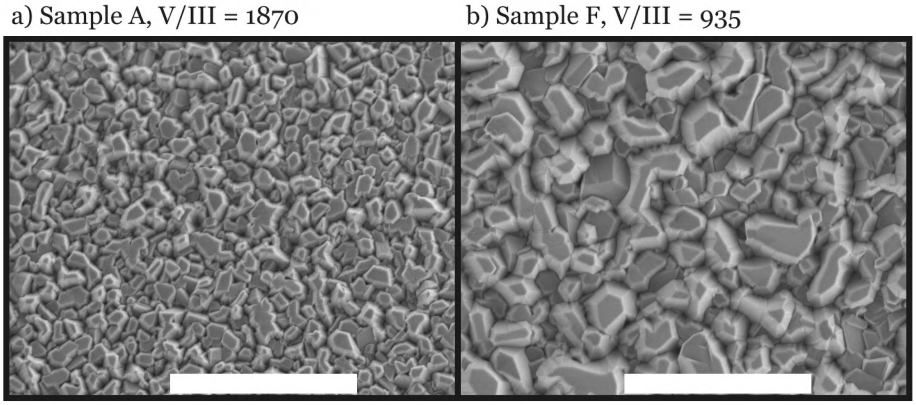

Figure 9.3: SEM images from the reference sample A (a) and sample F prepared with a double amount of TMG present in the reactor (b). The V/III ratio decreases from V/III = 1870 for sample A to V/III = 935 for sample F with TMG flows of 52.5 and 105 mmol/min, respectively. The scale bars represent 5 μm.

reduced mass-transport in the diffusion layer, present just above the sample, and to a lower growth rate [84, 164]. It suggests the GaN growth under the reference conditions is mass-transport limited. Furthermore, a higher amount of ammonia can also result in a site blocking effect: ammonia will compete with gallium and prevent it from attaching to sites where it is adsorbed. The areal density of sites blocked by ammonia adsorption will increase with increasing ammonia partial pressure, thus decreasing the overall growth rate [165].

Although the morphology of the crystals is not altered significantly by the decrease in ammonia flow or increase in TMG flow, it is clearly visible from both figures 9.2 and 9.3 that a smaller amount of GaN crystals is obtained when growing at lower V/III ratio. The crystals are also much larger than in the reference sample, and there is almost no height difference between the individual GaN crystals in these samples. Because no renucleation is observed, the lower amount of crystals can only be caused by a decrease in the island density produced during annealing of the nucleation layer with the decreased V/III ratio. For all samples (A, D, and F), the GaN layer fully covers the diamond substrate and no space is left between the crystals. This suggests that the deposited islands expand as far as possible until another island is reached and the lateral growth is thus sufficient to form an epitaxial layer. Apparently, the islands can not coalesce due to some barrier, like the extra energy necessary to produce dislocations at grain boundaries between adjacent crystallites [166–168].

9.3.3 Growth Temperature

The results obtained by the series in pressure and V/III ratio indicate that the growth of GaN on diamond is determined by the diffusion of gallium gas phase precursor material through the boundary layer onto the surface. If so, the growth rate should be independent on growth temperature [84], and thus this influence is tested next.

Figure 9.4 displays the SEM results for the specimens grown in this series with 1140 °C (sample G), 1170 °C (sample A), 1185 °C (sample H), and 1215 °C (sample I) growth temperature, respectively. All samples have constant GaN layer thickness of about 0.83 μm, thus any differences observed among the layers are directly related to the dif-

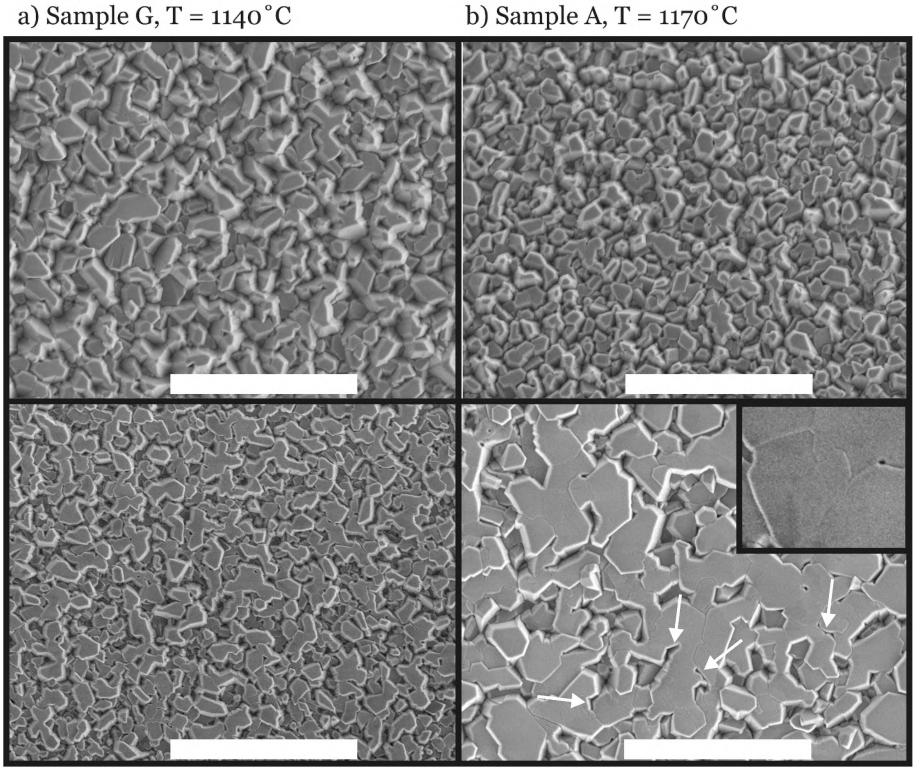

Figure 9.4: SEM images of the series in growth temperature: a) sample G, grown at 1140 °C, b) reference sample A prepared at 1170 °C, c) sample H deposited at 1185 °C, and d) sample I, grown at a temperature of 1215 °C. The scale bars represent 5 μm. The inset shows an example of the observed low angle grain boundaries.

ference in lateral growth rate by the change in temperature. The constant thickness again shows GaN growth on diamond is mass-transport limited just like the growth of GaN on sapphire and other III-V compounds [169].

First, a sample (G) is prepared at 1140 °C, depicted in figure 9.4a. It shows a GaN layer with less crystals in comparison to the reference sample A (1170 °C, figure 9.4b). Although the annealing time at the growth temperature was compensated for the different time in ramping to reach this final temperature, the lower nucleation density (resulting in less crystals) can originate from a small deviation in total annealing time.

By increasing the growth temperature to 1215 °C, which is the limit of the reactor applied, a prominent difference in the morphology of the sample (I, figure 9.4d) is observed as compared to the reference sample. Now, large areas of coalesced islands are formed indicating a high lateral growth rate during crystal growth. This is consistent with the behaviour previously reported by de Theije *et al.*, who demonstrated the large influence of growth temperature on the formation of a coalesced epitaxial layer [159]. Here, the SEM image shows that the GaN islands have different altitudes and some have overgrown others in the lateral direction.

From the intermediate sample (H), depicted in figure 9.4c and grown at 1185 °C, it can be concluded that the transition to the high lateral growth is gradual. Sample H shows the nucleation density is constant with respect to the temperature [159]. The large crystallite size in the high temperature sample I is thus a consequence of advanced coalescence and

overgrowth.

Although the largest crystallites are formed at the highest growth temperature, large-angle grain boundaries are present between the islands, as indicated by the white arrows in figure 9.4d (sample I). Apparently, with increased temperature the energy barrier to include material in the grain boundary can be overcome (samples H and I). This leads to the formation of dislocations at the interface between two neighboring islands during the subsequent merging of these islands. This is different to the samples grown at lower temperature where indivual 3D islands are formed (samples A, B, D, F, and G). In addition to the large-angle grain boundaries also low-angle grain boundaries can be observed in the SEM image of sample I (inset of figure 9.4d), as the boundary between two coalesced islands is still visible too.

Only in sample I cracks in the GaN layer are observed (figure 9.6). These cracks originate from stresses built up during cooling as a result of the difference in thermal expansion coefficient between the (001) diamond substrate and the GaN with $\beta = 1{\cdot}10^{-6}$ K^{-1} and $\beta = 6.2{\cdot}10^{-6}$ K^{-1} respectively [137–139]. The presence of the cracks in the layer also results from the increased coalescence of the GaN islands, because cracks can only occur if the stress is built up over large areas. With no coalescence, the stresses are local and the GaN islands can cope with it. In addition, cracks also imply a good adhesion of the grown layer to the substrate, otherwise delamination would occur.

9.3.4 Texture Analysis

To further understand the formation process and epitaxial relationship, the in-plane orientation of the GaN layer with respect to the substrate was investigated by using XRD pole figure analysis. If the orientation of the GaN islands is randomly distributed, no specific X-ray peaks can be identified and only a circle of increased intensity will be observed when measuring the reflection from a plane, not being (0001), over 360 °. However, in the case of GaN, with its six-fold symmetry, a single preferred in-plane orientation will lead to six peaks, each separated by 60 °. For this purpose, an extra sample was grown under equal conditions as sample I (table 9.1), but with a longer growth time of 60 minutes to ensure sufficient thickness for XRD pole figure analysis. SEM and profilometry showed the obtained morphology was similar as presented in figure 9.4d, but now with a layer thickness of 2.92 μm.

The XRD pole figure, depicted in figure 9.5a, was obtained using the Schulz reflection method [170] for the $(10\bar{1}1)$ reflection of the GaN layer, thus with optimised parameters ω = 18.38 °, 2Θ = 36.76 ° and χ = 55 - 70 °, and ϕ = 0 - 360 °. In the displayed plot, twelve peaks of high intensity can be distinguished with 30 ° relative difference. Considering the six-fold symmetry of GaN, resulting in six reflection peaks separated by 60 °, this means that there are two preferred orientations of GaN on (001) diamond. These domains are rotated 30 ° with respect to each other and are denoted I and II in figure 9.5a for convenience of discussion. The measured XRD pole figure data are recapitulated in table 9.2. In figure 9.6, which is a small section of sample I, the different orientations, reflected by the $\{1\bar{1}01\}$ side faces, can be observed clearly. Possibly, this 30 ° difference in orientation of the two domains is the reason why adjacent islands do not coalesce in the samples discussed in sections 9.3.1 and 9.3.2 and explains the large-angle grain boundaries in the SEM images (subsection 9.3.3). The low-angle grain boundaries observed in SEM originate from the spread within one orientation, typically 1-1.5 ° in the ϕ direction.

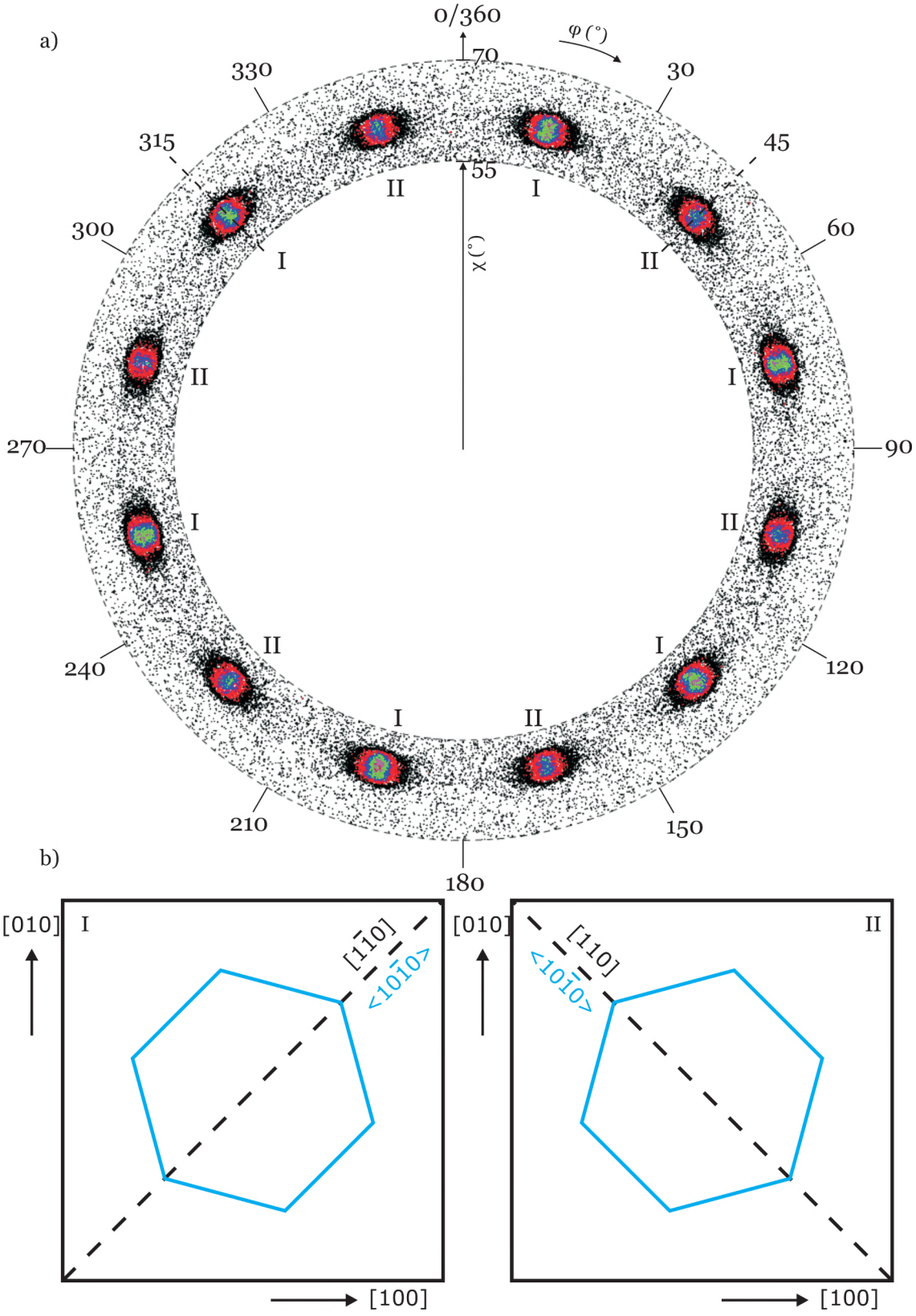

Figure 9.5: Pole figure obtained from the (10$\bar{1}$1) Bragg reflection of the GaN layer (a), and the preferred orientations with respect to the (001) diamond substrate (b).

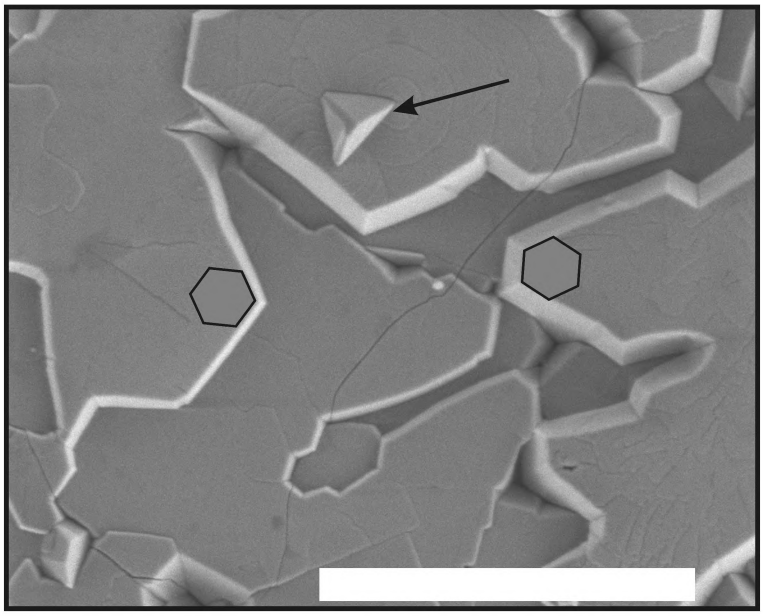

Figure 9.6: Close up of the sample I, prepared at 1215 °C, depicting the two growth domains in the GaN layer. Two cracks can be recognised as well. The scale bar represents 5 μm.

The full determination of the in-plane texture requires the plot of two sets of pole figures or the substrate orientation to be known with respect to the rotation axis. Here, the latter is used, because the diamond substrate was mounted with the [100] diamond direction parallel to the χ-rotation axis and the [010] direction along the ω-rotation axis with an estimated mounting error of 1 °. As the $(10\bar{1}1)$ reflection peaks 2 and 11 are observed at positions ϕ = 45.1 ° and ϕ = 315.2 ° respectively, it follows that the two GaN growth domains are aligned with their $<10\bar{1}1>$ along the [110] and $[1\bar{1}0]$ diamond directions as depicted in figure 9.5b. The two growth domains thus are oriented 90 ° with respect to each other, which corresponds to the four-fold symmetry of the (001) diamond surface. These results are in good agreement with comparable heteroepitaxial systems like GaN on (001) Si [171], AlN on (001) Si [172], and AlN on (001) diamond [173, 174]. In all cases two growth domains rotated 90 ° with respect to each other were found, with the $<10\bar{1}1>$ crystal domains aligned along the [110] and $[1\bar{1}0]$ directions of the underlying substrate. Therefore, it can be concluded that the growth of GaN on (001) diamond is similar to the forementioned systems and the predominant epitaxial orientation of growth domain I is $(0001)<10\bar{1}0>$GaN$\|(001)[1\bar{1}0]$diamond and $(0001)<10\bar{1}0>$GaN$\|(001)$[110]diamond for domain II.

The pole figure provides additional useful information on the GaN layer. From the peak position in the χ-direction for instance, an estimate of the stress in the GaN layer can be determined. On average the twelve peaks are positioned at an angle of χ = 61.2 ° with a spread of 0.6 ° along the rotation of ϕ. This spread is an indication of the misalignment of the diamond substrate, but this effect is cancelled out by the ϕ rotation in the average. From the lattice parameters of stress free bulk GaN (a = 3.189Å and c = 5.186Å [139]), the theoretical angle of the $(10\bar{1}1)$ plane with respect to (0001) is calculated to be 61.96 °. Because the theoretical angle is larger than the experimental value, it can be deduced that the ratio c/a is lower in the grown layer, which implies an amount of tensile stress parallel to the surface. This stress can partly be explained by the difference of the thermal

Table 9.2: Overview of the reflection peaks observed in the XRD pole figure depicted in figure 9.5a

Number	Domain	Position ϕ (°)	Position χ (°)
1	I	14.7 ± 0.6	61.3 ± 0.7
2	II	45.1 ± 0.7	61.2 ± 0.6
3	I	74.6 ± 0.6	60.9 ± 0.6
4	II	105.0 ± 0.6	60.9 ± 0.6
5	I	134.9 ± 0.5	60.9 ± 0.6
6	II	165.2 ± 0.5	60.9 ± 0.5
7	I	195.0 ± 0.8	60.9 ± 0.7
8	II	225.3 ± 0.7	61.0 ± 0.6
9	I	255.1 ± 0.6	61.3 ± 0.7
10	II	285.1 ± 0.5	61.5 ± 0.5
11	I	315.2 ± 0.8	61.8 ± 0.5
12	II	345.1 ± 0.6	61.5 ± 0.6

expansion coefficients of GaN (β_{GaN} = 6.2·10^{-6} K^{-1} and $\beta_{diamond}$ = 1·10^{-6} K^{-1}). During cooling down this leads to a strain increase of

$$\Delta\epsilon = \Delta T \cdot (\beta_{diamond} - \beta_{GaN}), \tag{9.1}$$

with ΔT the difference in temperature (1190 °C). For the present case, this gives a tensile strain of $\Delta\epsilon$ = - 6.2 ·10^{-3}, which corresponds with an increase of $a-$axis length of Δa = 0.020Å. Assuming a constant c-axis length the angle between the $(10\bar{1}1)$ and (0001) planes should become 61.81 °, which only partially explains the observed value of χ = 61.2 °.

It should be mentioned here that the observed epitaxial growth of GaN on diamond is quite surprising in view of the fact that the surface symmetry of GaN does not correspond with the four-fold symmetry of the (001) diamond plane. In addition, the lattice mismatch

$$f = 100 \cdot \frac{\left|a_{GaN} - a\sqrt{2}_{diamond}\right|}{(a\sqrt{2}_{diamond})} = 36.8\% \tag{9.2}$$

is extremely large. Here, a_{GaN} is 3.189Å, and $a\sqrt{2}_{diamond}$ (with $a_{diamond}$ = 3.567Å) is the unit translation of diamond along <110>.

9.4 Influence on Structural Properties

To further investigate the structural properties of the GaN layers, for each sample a μ-Raman spectrum was acquired. All spectra have an intense peak at 1332.3 cm^{-1} (FWHM = 6.0 cm^{-1}) attributed to diamond and an area in which the GaN modes are observed. As

the diamond peak is not shifted with respect to bare diamond and no carbon sp^2 peaks [46] are observed, it can be concluded that the diamond substrate keeps its quality throughout the GaN growth process and no graphitic interlayers are formed, as is consistent with earlier work (chapter 7, [151]). Based on the Raman signals in the GaN area (200 cm^{-1} - 800 cm^{-1}) the spectra obtained can be classified in two categories, for each of which a typical measurement is displayed in figure 9.7.

The spectrum of sample D is typical for the GaN layers in experiments A, C, D, F, G, H, and I. It shows the two Raman active optical phonon modes that, in theory, can be measured in this wavenumber range for hexagonal GaN in backscattering geometry if the GaN is c-axis oriented, i.e. A_1(LO) and E_2(high) [142]. The E_2(low) can, in principle, also be observed in hexagonal GaN but it has a phonon frequency of 144 cm^{-1} and therefore is not visible in the displayed spectra. The A_1(LO) phonon mode is here denoted as GaN (Quasi-LO) because of its potential mixing with E_1(LO) to produce a carrier concentration dependent coupled longitudinal optical mode [144, 145].

For all the samples in this category, the above-mentioned E_2(high) and the quasi-LO are clearly visible, respectively at 565.5 cm^{-1} and 734.4 cm^{-1}, indicating that some stress is present in the samples. The peak wavenumber for the E_2(high) is slightly lower than the value obtained for bulk GaN, thus demonstrating a small tensile stress in the layer, which is estimated at 0.4 GPa from the relation [175]

$$\Delta\omega = 6.2 \cdot \sigma, \tag{9.3}$$

where $\Delta\omega$ is the determined Raman shift and σ is the stress in GPa.

For the remaining samples (B and E) the spectrum is slightly different and, as an example, the acquired Raman spectrum for sample B is displayed. For these layers, an extra peak is detected at 535 cm^{-1}, which is attributed to A_1(TO). Often the A_1(TO) is observed when the incident light is not exactly normal to the (0001) surface of the GaN crystals, for instance if the layer is tilted, if it has a higher mosaicity [143], or when the layer is polycrystalline and consists of differently orientated crystals. Here, the latter is the case, as follows from the SEM images (figures 9.1a and 9.2c).

Furthermore, the spectrum of sample B displays a small distortion and a slightly shifted position of the quasi-LO peak at 737.9 cm^{-1}. The cause for this difference could not be determined unambiguously, but it most likely originates from a larger carrier concentration (about $\alpha = 1.5 \cdot 10^{17}$ cm^{-3}) resulting in LO phonon-plasmon coupling of which the L^+ branch is at 738 cm^{-1} and the L^- branch is just visible at 244 cm^{-1} [144].

9.5 Influence on Optical Properties

Next, the optical properties are investigated using photoluminescence (PL) spectroscopy. All spectra show the same features, only distinguished by changes in the relative intensity. No features from the diamond substrate are observed and a typical PL spectrum is depicted in figure 9.8.

On the right side of the plot, a set of two distinct peaks are observed. Here, the peak at 3.466 eV has higher intensity than the emission found at 3.388 eV, but from other spectra it was deduced that the intensities are not related to each other. The peak distinguished at

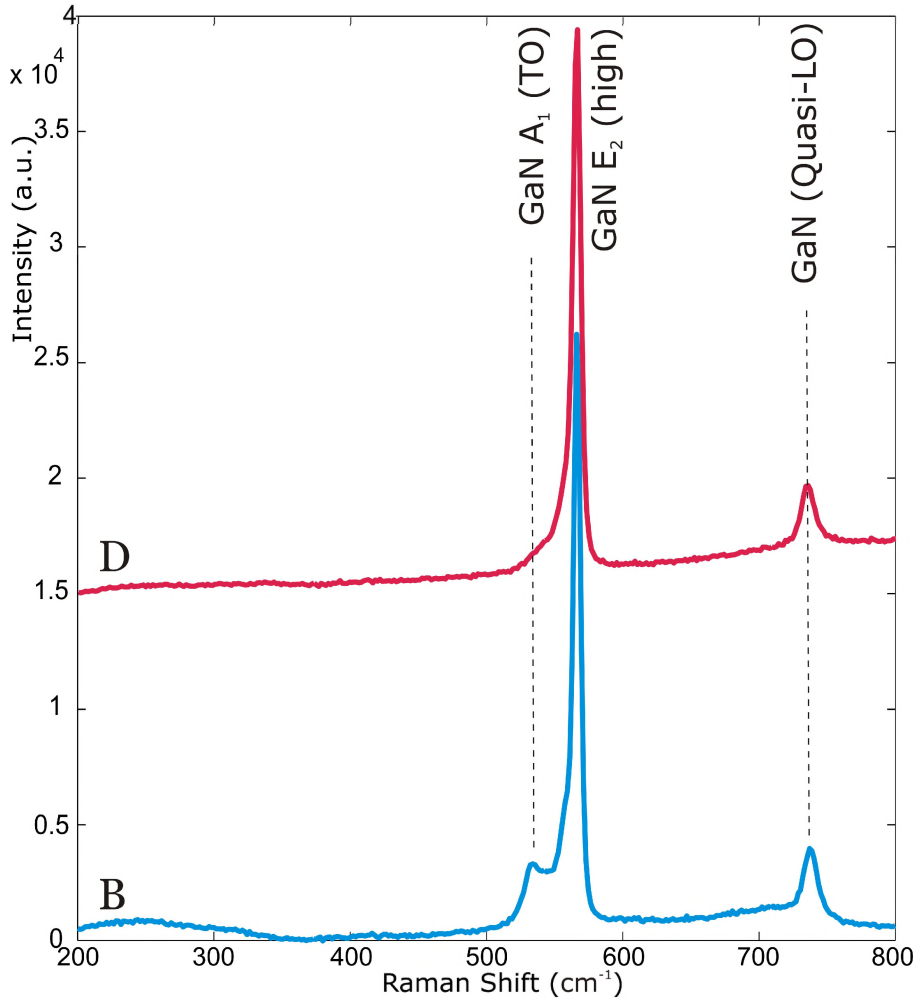

Figure 9.7: Raman spectra from typical ordered (D) and disordered (B) samples.

3.466 eV with a FWHM of 36 meV is ascribed to the donor bound exciton (DBE) emission of wurtzite GaN [149], but the position here is slightly lower than normally found, indicating tensile stress in the GaN [176]. This is consistent with the findings discussed in sections 9.3.4 and 9.4. The second peak cannot be related to acceptor bound recombination (ABE) because the energy distance (78 meV) from the DBE peak is too large. Instead it is attributed to the less commonly observed Y_2 line [147], normally detected at 3.40 meV, but again the emission can be shifted towards lower energy due to tensile stress. The Y_2 line is reported to be influenced by acceptor doping [147] (like carbon) and is strongly related to stacking faults parallel to the substrate/film interface [177, 178], which originate from the overgrowth in the lateral direction of GaN islands with different altitudes, as described above in section 9.3.3.

The broad peak in the lower energy section of figure 9.8 actually consists of two systems. The main band is mostly likely related to carbon doping in the GaN layer, which is known to produce a broad emission focused around 3.07 eV [147]. Additionally, a system with three peaks is observed in most layers. It was found that this system is much more resolved when the DBE peak of GaN has a relatively high intensity, and it is attributed to donor-acceptor pair (DAP) transitions. Indeed, the higher intensity of the DBE line suggests a higher concentration of donors, which also participate in the donor-

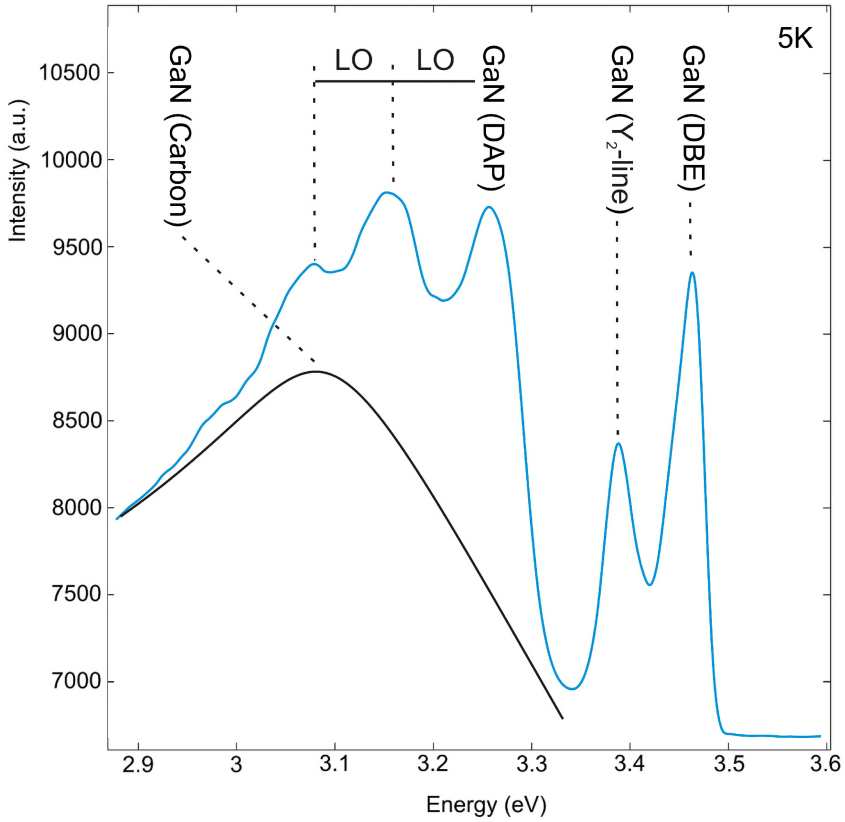

Figure 9.8: Typical PL spectrum for the growth of GaN on nominal (001) diamond, taken from sample H. The black line displays the assumed contribution of luminescence by carbon doping to the spectrum.

acceptor pair recombination. The DAP transitions are usually enhanced in films which are not simply $n-$ or $p-$doped, but have rather compensated character, showing the presence of both donors and acceptors. In addition, there is a very effective coupling of the DAP and the DBE to longitudinal optical (LO) phonons of the DAP with energy of about 92 meV. Due to this coupling of photons with the LO-phonons, not only the direct transitions are seen in figure 9.8, but also their LO-phonon replicas, $i.e.$ transitions with simultaneous emission (or absorption) of a photon and one or more phonons [179].

9.6 Off-axis Substrates

As demonstrated in section 9.3.4, the growth of GaN on nominal (001) diamond produces two growth domains with a 90 ° angular difference in orientation caused by the four-fold symmetry of the substrate. The same phenomenon has been observed in the epitaxial growth of GaN on (001) Si. The reason for this is the fourfold symmetry of the substrate and the possibility for GaN with its sixfold symmetry to grow with two preferred rotational alignments on this surface if AlN seed layers are applied. Considering the large resemblance between the silicon and diamond lattice structures, it can be expected that also here surface reconstruction plays an important role. For (001) Si in conditions >1000 °C, it was found that the surface reconstructs in a (2×1) and (1×2) reconstruction reducing the fourfold symmetry of the crystal surface to a twofold symmetry [180]. Indeed, for

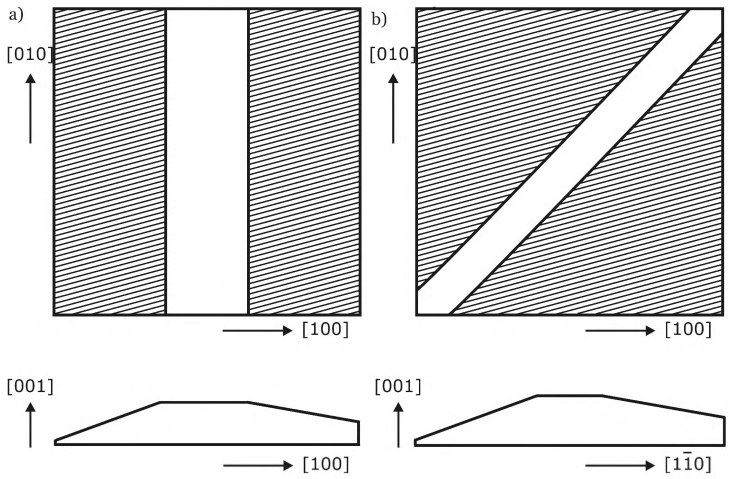

Figure 9.9: Schematic representation of the vicinal substrates used in this study. Top and side views of the polished diamond with the off-axis orientation towards [100] direction (a) and towards [1$\bar{1}$0] direction (b).

diamond both modelling [181, 182] and experimental observation by scanning tunneling microscopy [183, 184] have shown the hydrogen terminated surface and (2×1) and (1×2) dimer formation too [32]. The dimers formed by reconstruction of the diamond or Si surface are aligned along the [110] or the [1$\bar{1}$0] directions and the reconstructed domains are separated by one monolayer in height. Because the diamond substrates are not atomically flat, both reconstruction orientations can occur in close approximation of each other, leading to a random distribution of the two GaN growth domains. However, if one of these surfaces, either with the (1×2) or the perpendicular (2×1) reconstruction, is suppressed the other can be used for single crystalline GaN growth. This suppression can be achieved by forming biatomic steps using off oriented substrates [185], or by applying tensile or compressive strain on the substrate [186]. While the latter method is difficult to apply, the first can be tested much easier by polishing an angle on the (001) diamond substrate.

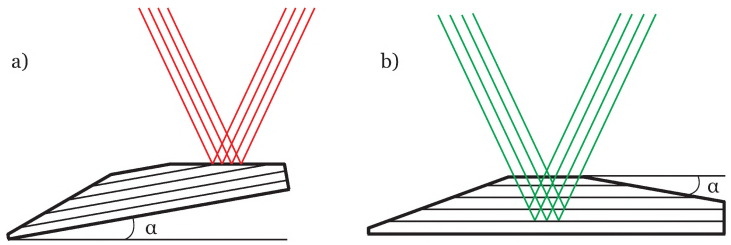

Figure 9.10: Schematic representation of the two-step determination of the angle α of misoriented facets in this study. Alignment of the sample surface using the laser beam (a) and subsequent measurement of the X-ray reflection from (004) diamond lattice planes (b).

9.6.1 Substrates

For this purpose, nominal (001) diamonds, supplied by Element Six with a maximum deviation of 3 ° from the (001) plane, have been polished by a commercial company (Wiediam VOF, Wanroy, The Netherlands) to add off-axis facets to the substrate. Each

Table 9.3: Overview of the samples used in this studies on vicinal (001) diamond substrates

Sample	Off-axis Angle α (°)	Vicinal Direction Towards
J	2.0	[100]
K	2.2	[100]
L	2.7	[100]
M	3.6	[100]
N	6.5	[100]
O	8.3	[100]
P	2.6	[110]
Q	2.7	[110]
R	5.9	[110]
S	6.7	[110]
T	9.0	[110]
U	11.0	[110]

diamond has been polished to have two off-axis facets and one nominal facet for comparing the growth results with the forementioned series. Eventhough it is very difficult to establish a predefined angle, substrates with various mis-orientation angles towards different crystallographic planes are prepared, as depicted schematically in figure 9.9. After polishing, the diamonds are cleaned in boiling H_2SO_4, subsequently followed by heated aqua regia, rinsing in H_2O (4×) and isopropanol (3×). Finally, just before the MOCVD growth, the substrates are cleaned following the procedure described in section 9.2.

Because of the uncertainty in the substrate orientation for both the 'nominal' surfaces and the added off-axis facets, first the misorientation between the surface and the (001) lattice plane is determined for each facet. For this, the diamond sample is mounted on a goniometer head inside the XRD setup and aligned with a laser in such a way that the position of the reflected beam does not vary upon rotation of the sample (figure 9.10a). Then, the optimised ω, 2Θ, and χ for the Bragg-Brentano reflection of the (004) diamond plane are determined, as schematically shown in figure 9.10b. The extra angular difference between ω and half of the 2Θ value is then used in combination with the measured χ value to calculate the vicinal angle of the facet. The angles of a representative selection of the samples are summarised in table 9.3. The error in the obtained angles is estimated at 0.1 °. As it is more difficult to polish a vicinal facet towards the [100] direction, the off-axis angle of these specimens is on average lower than of those polished towards the [110] direction.

9.6.2 Vicinal Direction Towards [100]

For this part of the studies the same growth conditions were used as listed for sample I in table 9.1. SEM images of the results are depicted in figure 9.11. The two images at the top of the figure (samples J and L) display the morphology of the 'nominal' sections of the sample (the central section in figure 9.9A). It shows that the layers are slightly less

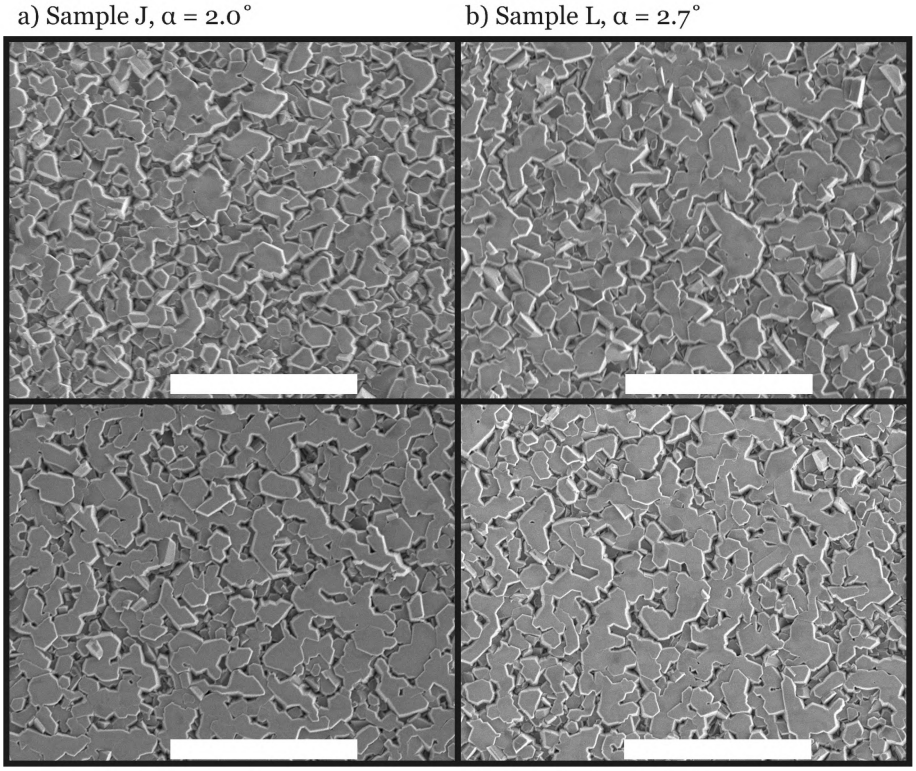

Figure 9.11: SEM images of the series in vicinal angle towards the [100] direction: a) sample J, grown on a facet with 2.0 ° misorientation, b) sample L prepared on a 2.7 ° misoriented substrate, c) sample M, deposited at a vicinal angle of 3.6 °, and d) sample O, grown at an off-axis facet of 8.3 °. The scale bars represent 5 μm.

coalesced as described for sample I. This can be due to a less optimal contact between the substrate and the susceptor in the MOCVD reactor during growth, for instance caused by increased roughness of the backside of the substrate, which in turn leads to a lower temperature at the substrate surface and thus to a decrease in lateral growth as seen in section 9.3.3.

The samples M and O (with vicinal angles 3.6 and 8.3 °) are displayed to demonstrate the large simularity between layers grown on the substrates with higher off-axis angles. When comparing the SEM images, it can be concluded that increasing the misorientation >3 °, the average size of the top layer of GaN islands is increased, probably due to more step flow growth induced by the extra steps as a consequence of the off-axis surface. Again, it was observed that crystals with larger height overgrow the neighbouring islands laterally. By inspection of the orientation of the inclined $\{1\bar{1}01\}$ side facets, both growth domains are identified in the GaN crystals for all experiments.

9.6.3 Vicinal Direction Towards [110]

Finally, GaN layers on (001) diamond substrates with vicinal orientation towards [110] are prepared by applying the conditions used for the growth of sample I (table 9.1). Sample P (figure 9.12a) shows the layer produced on 'nominal' diamond, as a standard for comparison of the results. With increasing misorientation the GaN islands become larger,

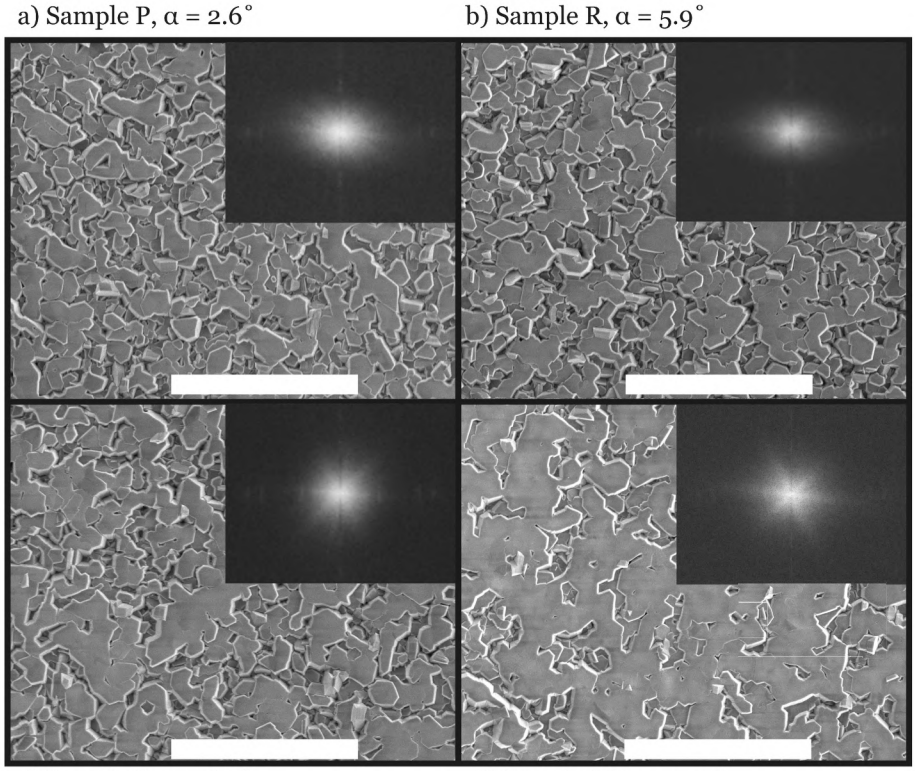

Figure 9.12: SEM images of the GaN growth on misoriented diamond surface towards the [110] direction: a) 2.6 ° for sample P, b) 5.9 ° for sample R, c) sample S, deposited on a 6.7 ° misoriented substrate, and d) sample U, grown at a vicinal angle of 11.0 °. The insets show the calculated Fourier Transform of the corresponding SEM image. The scale bars represent 5 μm.

as depicted for samples R and S, which is also observed in the previous section. However, now the distribution between the two growth domains (I and II, section 9.3.4) is changed in comparison to samples on nominal (001) diamond, where the relative population is about 50% for either growth domain. This was deduced from the relative occurences of the different orientations of the inclined $\{1\bar{1}01\}$ side faces of the crystallite layers. The layer of sample U (figure 9.12d), obtained with 11.0 ° angle towards [110], consists of large areas of single domain hexagonal GaN.

Figure 9.13 shows a SEM image of GaN deposited near the transition from a 2.6 ° to an 11.0 ° misorientated surface (samples P and U). The black line indicates the $[1\bar{1}0]$ direction of the diamond along which the steps orient. Here, it is clearly visible that at the misorientation of 2.6 ° two growth domains are present in the layer, while for the 11.0 ° off-axis surface an abrupt transformation to only one growth domain is displayed and the side faces of the GaN islands are aligned parallel to the $[1\bar{1}0]$ line. The film at this location of the sample is not as well coalesced as observed in figure 9.12, probably caused by temperature effects. Furthermore, the growth can be influenced by extra roughness in the diamond surface due to grooves along the [100] direction resulting from the polishing [187], as confirmed by optical microscopy. Some twinning in the GaN is observed in all samples in this studies, which may be attributed to these polishing effects. An example is indicated by the arrow in figure 9.6. Possibly, some debris from the polishing was also still present at the surface, prior to growth, causing these defects.

Corresponding to reported growth on vicinal (001) Si, the dominance of one growth domain on highly misoriented substrates is likely attributed to the increase of the number of double steps on the substrate surface [185]. As mentioned above, the diamond surface is reconstructed, by (2×1) and (1×2) dimers, at high temperatures. When the miscut is relatively low, only single-height-atomic steps are expected to occur on the surface, and these are known to produce a 90° rotation of the dimers on every next terrace, due to the diamond lattice structure of the substrate [188]. This leads to the growth of the two different growth domains of GaN. However, when the miscut angle is increased, the surface will contain more double-height-atomic steps and the dimer direction does no longer change on adjacent terraces. This implies that the GaN islands nucleated on neighbouring terraces will be aligned in the same direction and single domain (0001) GaN is obtained. As stable steps on reconstructed (001) diamond surfaces are aligned along the dimer [110] and [1$\bar{1}$0] directions, double height steps are not easily formed on diamonds with vicinal direction toward [100]. Therefore, for these substrates both surface reconstruction domains persist and no single crystal GaN will be formed, regardless of the misorientation angle.

Alternatively, the growth of single domain GaN can also be enhanced by the orientation of the substrate steps. Similar to growth via pseudoepitaxy ([189]) the steps can act as nucleation sites for the GaN growth, because addition of growth material is energetically more favorable there. However, the substrates with vicinal direction toward [110] have a distinguished advantage over the diamonds misoriented toward the [100] direction. Substrate steps on the latter are kinked, leading to nuclei oriented in two perpendicular directions, while the steps on substrates with vicinal direction toward [110] are straight. This leads to nuclei that are aligned in one direction, parallel to the steps, as is observed in figure 9.13. With increasing miscut angle the terrace width becomes smaller and more steps are available, enhancing the probability to form aligned GaN nuclei. This results in subsequent single domain growth of GaN on diamond substrates with larger vicinal angles toward the [110] direction.

9.6.4 Quality of the GaN Layers on Vicinal (001) Diamond

Due to the small sample size and the short growth time of 20 minutes, it was not possible to confirm the single domain structure of GaN for the highly misoriented facets towards the [110] diamond direction by XRD pole figure analysis. Our evidence is based on the orientation of the $\{1\bar{1}01\}$ side facets of the GaN layers with respect to the <100> diamond directions (figure 9.12) and it is supported by the calculated Fourier Transform (FT) of the SEM images (figure 9.12, insets). With increasing vicinal angle, the FT shows increased intensity for only six directions. This demonstrates that only one domain is preferred if a GaN layer is prepared on highly misoriented (001) diamond substrates.

Raman measurements for all GaN layers deposited on misoriented substrates produced spectra similar to the signal depicted in figure 9.7B. The A_1(TO) relative peak intensity is increased with increasing vicinal angle, and is independent of the orientation of the miscut. This is obviously caused by the fact that the incident light was not aligned exactly normal to the (0001) surface of the GaN film. Furthermore, for the layers on [110] misoriented diamond, the peak position of the E_2(high) phonon mode moves towards the bulk GaN value of 568 cm^{-1} for higher vicinal angles. It appears that the stress developed during cooling of the sample from the growth temperature is released more in the largely

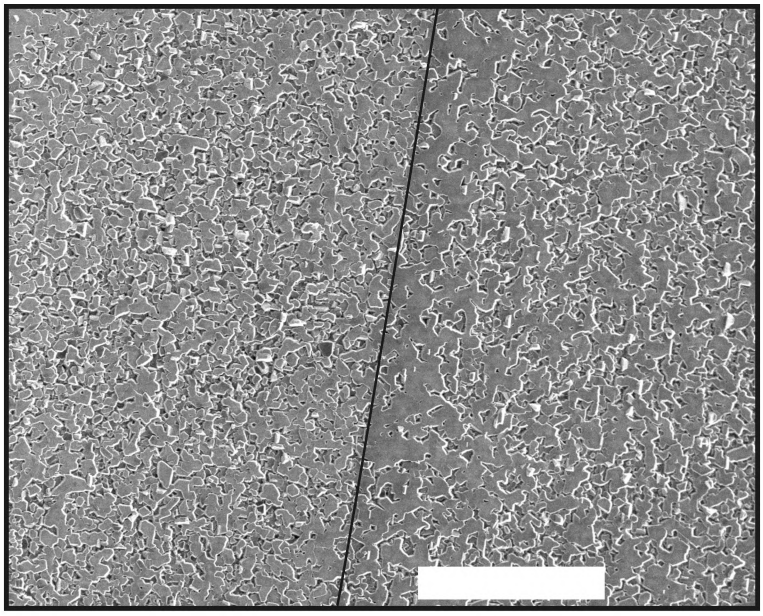

Figure 9.13: SEM image of a GaN layer grown on a diamond surface misoriented towards the [110] direction. The black line, which runs parallel to the [1$\bar{1}$0] direction, indicates the transition from a slightly to a highly misoriented substrate. Left of the black line the misorientation is 2.6 °, while on the right side the off-axis angle is 11.0 °. The scale bar represents 20 μm.

coalesced GaN layers, as is also deduced from crack formation in the layer.

The optical properties for the wurtzite GaN layers grown on vicinal diamond have been studied intensively with PL spectroscopy and will be the subject of a forthcoming research article.

9.7 Conclusions

This research describes the influence of multiple growth parameters on the preparation of epitaxial GaN layers on (001) diamond by MOCVD. SEM and growth rate measurements of the obtained heterostructures show that the growth of GaN is determined by mass-transport of gallium precursor material toward the substrate. Lateral growth of the 3D GaN nuclei and subsequent coalescence is enhanced by increasing V/III ratios and growth temperature. X-ray pole figure analysis reveals two preferential growth orientations of the GaN layers on the (001) diamond surfaces, namely (0001)<10$\bar{1}$0>GaN||(001) [110]diamond and (0001)<10$\bar{1}$0>GaN||(001)[1$\bar{1}$0]diamond, 90 ° rotated with respect to each other. This is a consequence of the 'incompatible' four-fold symmetry of the substrate and the hexagonal symmetry of the (0001) GaN contact face. Raman spectroscopy showed that the structural quality of the GaN layers on diamond is very similar to epitaxial GaN layers obtained on other materials, while the diamond substrate remains unaffected. PL spectroscopy showed an intense broad band caused by carbon doping as well as the presence of both donors and acceptors.

The growth on vicinal diamond faces, prepared with various miscut angles towards the [100] and [110] directions, supports the hypotheses that surface reconstruction by (2×1) and (1×2) dimer formation determines the preferred alignment. An epitaxial single crystal GaN layer is formed on vicinal (001) diamond faces which are highly misoriented

toward [110]. This is explained by the occurence of di-atomic steps resulting in one type of reconstruction domain with the C-C dimers aligned in one direction all over the diamond substrate surface. Furthermore, the small distance between steps on the substrate at high miscut angle can contribute to the enhanced preference for the observed single orientation, parallel to the diamond step-edge.

The main conclusion of this work is that the possibility of growing single crystalline GaN layers on (001) diamond substrates holds much promise for the development of high power GaN-based devices.

10

Summary

This thesis addresses the direct growth of GaN layers onto diamond substrates by MOCVD for the application of high power and high frequency device structures to enhance the temperature range for which GaN can be employed.

Gallium Nitride (GaN) is the most important semiconductor material for electronic devices since silicon. It consists of gallium and nitrogen atoms, which produce a strong chemical bond within the solid and it has high chemical stability and wide bandgap energy, making it very suitable for high-power high-temperature applications in harsh environment.

GaN can be applied in transistors, LEDs and laser diodes. The transistors are based on the spontaneous and piezoelectric properties of the wurtzite structure of GaN and its alloys. Effectively, the lack of inversion symmetry along the c-axis enables the formation of a 2D electron gas near the interface of the heterostructure providing the low-resistive conduction of electrons through the transistor. The latter applications address GaNs wide bandgap for the development of short-wavelength laser diodes and light emitters in optical storage and full-color displays.

Intrinsic advantages for GaN-based applications are their improved temperature performance, high-breakdown voltages and high carrier velocities leading to higher efficiencies in comparison to their silicon equivalents. It is even possible to reach higher power outputs, however, currently GaN devices are hindered by self heating problems. Due to the high frequencies and powers at which the devices operate, a lot of heat is produced within the structure. Furthermore, it is the current tendency to produce smaller devices and to place the electronics onto smaller overall areas, which also has a negative effect on heat dissipation. To minimise these specific thermal problems it is vital to extract the

heat from the active section of the devices. This can be achieved by using alternative substrates that spread the produced heat, like diamond, which has the highest available thermal conductivity.

Adding a diamond layer on an existing GaN structure is the most direct approach to enhance the thermal stability of that structure. Despite the many different techniques that have been explored, no method for the deposition of diamond on GaN has been developed in which the GaN remains unaffected and a flawless polycrystalline diamond layer is obtained. This is caused by the high deposition temperatures necessary for diamond growth, which results in thermal decomposition of the GaN substrate. However, the research of commercially available alternatives, as mentioned in chapter 3, has demonstrated that the application of diamond for thermal management purposes is very effective, eventhough a thermal barrier remains between the active device structure and the diamond heat sink.

Chapter 7 comprises a first step in preparing heterogeneous layers and GaN devices with a diamond heat sink as a substrate, facilitating the thermal management of these devices. It describes the synthesis of hexagonal, polycrystalline GaN films on nano-crystalline diamond templates which were in turn grown on a silicon wafer. The results obtained from several characterisation techniques reveal a relatively smooth diamond substrate and good structural quality GaN and thus it shows that the growth of GaN films onto synthetic diamond substrates is feasible, when applying the correct buffer layer and growth parameters. XRD measurements show that the GaN formed is of wurtzite structure and polycrystalline, but the high intensity of the (0002) diffraction peak indicates a preferential crystallite orientation. This preferred [0001] GaN orientation is confirmed by SEM and Raman analysis. The optical properties of the deposited GaN layer are investigated using cathodoluminescence and show a large yellow luminescence peak indicating poor optical quality. Importantly, no decrease is observed in the nano-crystalline diamond quality.

The influence of different nucleation layers and nucleation time is tested and described in chapter 8 by growing $\{0001\}$ oriented GaN crystals on freestanding, polycrystalline diamond substrates using AlN and GaN nucleation layers. The optimum deposition times are 2 and 5 minutes for the AlN and GaN nucleation layer respectively, giving $\{0001\}$ oriented GaN islands after subsequent growth. The structural quality of the GaN layer is better for AlN nucleation layers, as can be concluded from the SEM, rocking curve XRD and profilometric measurements because AlN has a thermal expansion coefficient in between GaN and diamond and thus delocalizes the stress to two interfaces. The optical quality of the layers, investigated with Raman microscopy and PL spectroscopy, is similar for both types of nucleation layer. Although no lateral epitaxy is obtained, new insight is gained on the nucleation of GaN on diamond substrates facilitating the growth of GaN epilayers on polycrystalline diamond substrates. Again, the diamond substrate remains unaffected.

Finally, in chapter 9 the effect of the principal growth parameters on the deposition process is investigated and the epitaxial growth of crystalline wurtzite GaN thin films on single crystal (001) diamond substrates by MOCVD is established. From the influence of pressure, V/III ratio and temperature, it is deduced that the growth process is deter-

mined by the mass-transport of gallium precursor material toward the substrate (SEM and growth rate measurements). The temperature series also show an improved epitaxial relationship between grown layer and substrate for increasing growth temperature. XRD pole figure analysis reveals the presence of two domains of epitaxial layers, namely (0001)<10$\bar{1}$0>GaN‖(001)[110]diamond and (0001)<10$\bar{1}$0>GaN‖(001)[1$\bar{1}$0]diamond, which are 90° rotated with respect to each other. The presence of these domains is a consequence of the 'incompatible' four-fold symmetry of the substrate and the hexagonal symmetry of the (0001) GaN contact face and is explained by the occurence of areas of (2×1) and (1×2) surface reconstruction of the diamond substrate. Raman microscopy showed that the structural quality of the GaN layers on diamond is very similar to epitaxial GaN layers obtained on other materials, while in PL spectroscopy an intense broad band is observed, caused by carbon doping, as well as the presence of both donors and acceptors.

The growth on vicinal diamond faces, prepared with various miscut angles towards the [100] and [110] directions, support the hypothesis that surface reconstruction by (2×1) and (1×2) dimer formation determines the preferred alignment. An epitaxial single crystal GaN layer is formed on vicinal (001) diamond faces which are highly misoriented toward [110]. This is explained by the possible occurence of di-atomic steps resulting in one type of reconstruction domain with the C-C dimers aligned in one direction all over the diamond substrate surface. Furthermore, the small distance between steps on the substrate at high miscut angle can contribute to the enhanced preference for the observed single orientation, parallel to the diamond step-edge.

The main conclusion of this work is that the possibility of growing single crystalline GaN layers on (001) diamond substrates holds much promise for the development of high power GaN-based devices.

11

Samenvatting

In dit proefschrift wordt de mogelijkheid onderzocht voor de directe groei van GaN op diamantsubstraten met behulp van MOCVD om uiteindelijk het temperatuursgebied waarbinnen GaN structuren kunnen worden gebruikt verder te vergroten.

Gallium Nitride (GaN) is de belangrijkste halfgeleider voor electronische toepassingen sinds de ontwikkeling van silicium componenten. Het bestaat uit gallium en stikstof atomen, die zorgen voor een sterke chemische binding, chemische stabiliteit en een grote bandgap. Dit maakt GaN erg geschikt voor toepassingen waarbij hoge vermogens en/of hoge gebruikstemperaturen vereist zijn en voor gebruik onder extreme omstandigheden.

GaN vindt toepassing in transistoren, LEDs en laserdiodes. De transistoren zijn gebaseerd op de spontane en piëzo-electrische eigenschappen van de wurtzite kristalstructuur van GaN en GaN-legeringen. Feitelijk zorgt het gebrek aan inversie symmetrie in de richting van de c-as voor de vorming van een 2D electron gas op het overgangsvlak binnen een heterostructuur. Op dat vlak kunnen de electronen zich dan met lage weerstand door de transistor bewegen. Bij de andere bovengenoemde toepassingen wordt de grote bandgap van GaN gebruikt voor de ontwikkeling van laserdiodes met korte golflengten, voor de opslag van data met licht en voor full-color schermen.

Op GaN gebaseerde toepassingen presteren beter bij hogere temperaturen, hebben een hoge doorslagspanning en ladingsdragers met hoge snelheden. De efficientie van deze toepassingen is dan ook hoger in vergelijking met gelijke toepassingen van silicium. Theoretisch kan het geleverde vermogen van GaN structuren nog verder verhoogd worden. Echter, op dit moment wordt dit met name beperkt door zelfverhitting. Doordat de structuren werken bij hoge frequenties en vermogens, wordt veel warmte geproduceerd. Bovendien worden steeds kleinere structuren gemaakt en wordt electronica op een steeds

kleiner oppervlak aangebracht, hetgeen ook een negatieve invloed heeft op de warmte verspreiding. Om deze thermische problemen te minimaliseren is het essentieel om de warmte goed af te voeren van de actieve gebieden van een structuur. Dit kan worden bewerkstelligd door het gebruik van alternatieve substraten die warmte beter verspreiden, zoals diamant dat de hoogst beschikbare thermische geleiding heeft.

Het aanbrengen van een laag diamant op een bestaande GaN structuur is de eenvoudigste manier om de thermische stabiliteit van die structuur te verhogen. Hoewel verschillende mogelijkheden hiervoor zijn onderzocht, is er nog geen methode gevonden waarbij GaN onaangetast blijft tijdens het proces en tevens een perfecte laag van diamant wordt afgezet. De oorzaak hiervan is de hoge temperatuur waarbij diamant wordt gevormd, die ertoe leidt dat GaN ontbindt. Daarnaast bestaan er commercieel beschikbare alternatieven (zoals beschreven in hoofdstuk 3) waarbij een extra barrière bestaat tussen het actieve gebied van de structuur en het diamant. Ondanks deze barrière is aangetoond dat het gebruik van diamant voor koeling zeer effectief is.

Hoofdstuk 7 beschrijft een eerste stap in de vervaardiging van heterogene lagen en GaN structuren op een diamanten substraat, waarbij het diamant als heatsink wordt gebruikt. Polykristallijne lagen van hexagonaal GaN zijn gesynthetiseerd op een nanokristallijne diamanten ondergrond, die op zijn beurt is afgezet op een silicium wafer. De resultaten die zijn verkregen met de verschillende karakterisatietechnieken laten een relatief gladde diamantlaag en GaN van goede structurele kwaliteit zien. Dit toont aan dat de groei van GaN op substraten van synthetisch diamant mogelijk is, wanneer een goede bufferlaag en de juiste groeiparameters worden gekozen. XRD metingen bevestigen dat de gevormde GaN laag een wurtziet structuur heeft en polykristallijn is. De hoge intensiteit van de (0002) diffractie piek geeft echter aan dat dit de voorkeursoriëntatie van de kristallen is. Dit wordt ondersteund door verdere analyse met SEM en Raman microscopie. De optische eigenschappen van de gegroeide GaN laag zijn onderzocht met kathodeluminescentie. Dit resulteerde in een spectrum met veel gele luminescentie, hetgeen wijst op een lage optische kwaliteit in de gevormde heterostructuur. Er is geen verslechtering van het nano-kristallijne diamant waargenomen.

De invloed van AlN en GaN nucleatielagen en verschillende nucleatietijden is getest door $\{0001\}$ georiënteerde GaN kristallen te groeien op vrijstaande, polykristallijn diamanten substraten. Dit is beschreven in hoofdstuk 8. De optimale depositietijden van beide nucleatielagen zijn bepaald op 2 en 5 minuten voor respectievelijk AlN en GaN. Beide lagen geven een $\{0001\}$ georiënteerde GaN laag na verdere groei, maar de structurele kwaliteit van het GaN is beter bij gebruik van AlN nucleatielagen. Dit is bepaald met behulp van SEM, rocking curve XRD en profilometrische metingen, en wordt veroorzaakt doordat AlN een thermische expansiecoëfficient heeft die tussen de coëfficienten van GaN en diamant ligt, waardoor de spanning wordt verdeeld over 2 overgangsvlakken. De optische kwaliteit is echter vergelijkbaar voor beide typen nucleatielagen. Hoewel geen laterale epitaxie is verkregen, biedt dit wel nieuwe inzichten in de nucleatie van GaN op diamant voor de groei van gesloten GaN lagen. Wederom is het diamant substraat intact gebleven.

Ten slotte behandelt hoofdstuk 9 de invloed van de belangrijkste parameters op het

groeiproces en is een epitaxiale laag van kristallijn GaN op een mono-kristallijn (001) diamant substraat gegroeid met behulp van MOCVD. Uit de gevolgen van veranderingen in druk, V/III-verhouding en temperatuur op de structuur van de laag kan worden afgeleid dat het groeiproces wordt bepaald door de snelheid van het massatransport van gallium precursor materiaal naar het oppervlak waarop de groei plaatsvindt (SEM en groeisnelheidsbepalingen). De serie met oplopende groeitemperatuur laat bovendien de ontwikkeling van een verbeterde epitaxiale relatie tussen substraat en gegroeide laag zien. Analyse van de XRD pole figure geeft daarbij aan dat er twee groeidomeinen bestaan binnen de gegroeide laag: (0001)<10$\bar{1}$0>GaN$\|$(001)[110]diamant en (0001)<10$\bar{1}$0>GaN$\|$ (001)[1$\bar{1}$0]diamant, die 90 ° zijn gedraaid ten opzichte van elkaar. De aanwezigheid van deze domeinen wordt veroorzaakt door de verschillende symmetrieën van substraat (viervoudige symmetrie) en wurtziet GaN (zesvoudig) en wordt verder verklaard met behulp van (2×1) en (1×2) oppervlaktereconstructie van het diamantsubstraat. Ramanmicroscopie laat zien dat de structurele kwaliteit van deze GaN lagen op diamant vergelijkbaar is met epitaxiale GaN lagen op andere substraten. Met fotoluminescentie spectroscopie is een intense brede band gemeten die wordt veroorzaakt door koolstofdoping in de lagen. Daarnaast is de aanwezigheid van zowel donors als acceptors aangetoond.

Vervolgens zijn vicinale diamantoppervlakken vervaardigd door een mis-georiënteerd facet naar de [100] of [110] richting te slijpen. De groei op deze diamantoppervlakken ondersteunt de hypothese dat de oppervlaktereconstructie via (2×1) en (1×2) dimeren bepalend is voor de voorkeursrichtingen van de twee groeidomeinen. Een epitaxiale monokristallijne GaN laag is afgezet op een van deze vicinale (001) diamantoppervlakken met een hoge misoriëntatie naar de [110] richting. Dit wordt verklaard door de aanwezigheid van di-atomaire stappen op het oppervlak, waardoor slechts één oppervlaktereconstructie over het hele substraat aanwezig is en alle C-C dimeren in één richting georiënteerd zijn. Verder kan de kleine afstand tussen de treden op het diamantoppervlak (een gevolg van de hoge misorientatie) er toe leiden dat de orientatie parallel aan de treden een grotere voorkeur geniet, zoals is waargenomen met SEM.

De belangrijkste conclusie van dit proefschrift is dat de groei van monokristallijne GaN lagen op (001) diamant substraten mogelijk is en dus de ontwikkeling van hoogvermogen GaN-gebaseerde structuren met optimale koeling realiseerbaar blijft.

12

List of Publications

1."Realising Epitaxial Growth of GaN on (001) Diamond", G.W.G. van Dreumel, P.T. Tinnemans, A.A.J. van den Heuvel, T. Bohnen, J.G. Buijnsters, J.J. ter Meulen, W.J.P. van Enckevort, P.R. Hageman, and E. Vlieg, J. Appl. Phys. 110 (2011), 013503.

2."Enhancement of the nucleation of smooth and dense nanocrystalline diamond films by using molybdenum seed layers", J.G. Buijnsters, L. Vazquez, G.W.G. van Dreumel, J.J. ter Meulen, W.J.P. van Enckevort and J.P. Celis, J. Appl. Phys. 108 (2010), 103514.

3. "Enhanced growth rates and reduced parasitic deposition by the substitution of Cl-2 for HCl in GaN HVPE.", T. Bohnen, H. Ashraf, G.W.G. van Dreumel, S. Verhagen, J.L. Weyher, P.R. Hageman and E. Vlieg, J. Cryst. Growth, 312 (2010), 2542-2550.

4. "Comparison of GaN and AlN nucleation layers for the oriented growth of GaN on diamond substrates.", G.W.G. van Dreumel, T. Bohnen, J.G. Buijnsters, W.J.P. van Enckevort, J.J. ter Meulen, P.R. Hageman and E.Vlieg, Diam. Relat. Mater., 19 (2010), 437-440.

5. "Growth of scandium aluminum nitride nanowires on SCN(111) films on 6H-SiC substrates by HVPE.", T. Bohnen, G.W.G. van Dreumel, P.R. Hageman, R.E. Algra, W.J.P. van Enckevort, E. Vlieg, M.A. Verheijen and J.H.Edgar, Phys. Stat. Sol. A, 206 (2009), 2809-2815.

6. "On the nucleation, coalescence, and overgrowth of HVPE GaN on misoriented sapphire substrates and the origin of pinholes.", T. Bohnen, A.E.F. de Jong, W.J.P. van Enckevort, J.L. Weyher, G.W.G. van Dreumel, H. Ashraf, P.R. Hageman and E. Vlieg, J. Cryst. Growth, 311 (2009) 4685-4691.

7. "ScAlN nanowires: A cathodoluminescence study.", T. Bohnen, G.R. Yazdi, R. Yakimova, G.W.G. van Dreumel, P.R. Hageman, E. Vlieg, R.E. Algra, M.A. Verheijen and J.H. Edgar, J. Cryst. Growth, 311 (2009), 3147-3151.

8. "Growth of GaN on nano-crystalline diamond substrates.", G.W.G. van Dreumel, J.G. Buijnsters, T. Bohnen, J.J. ter Meulen, W.J.P. van Enckevort, P.R. Hageman and E.Vlieg, Diam.Relat. Mater., 18 (2009), 1043-1047.

9. "Thick GaN layers grown by HVPE: Influence of the templates.", H. Ashraf, J.L. Weyher, G.W.G. van Dreumel, A. Gzregorzyck and P.R. Hageman, J. Cryst. Growth, 310 (2008), 3957-3963.

13

Dankwoord

Zo, nu ga ik het laatste en waarschijnlijk minst serieuze hoofdstuk van dit hele proefschrift schrijven. Daarna zit mijn tijd op de universiteit er zo ongeveer wel op, dus dit is een goed moment om maar eens een hele stapel mensen te gaan bedanken voor die twaalf jaar dat ik hier heb gestudeerd en aan mijn promotie heb gewerkt. Die (eigenlijk té) lange tijd heeft me ook een gigantische lijst goede en heel goede vrienden opgeleverd om maar niet te spreken van een compleet peloton andere bekenden die daarbij komen. Maar goed, bij voorbaat alvast een disclaimer, uiteraard in kleine lettertjes:

Alle tekst (inclusief bijlagen) van dit hoofdstuk is met grote zorgvuldigheid samengesteld. Voor mogelijke onjuistheid en/of onvolledigheid van de hierin verstrekte informatie kan ik geen aansprakelijkheid aanvaarden, evenmin kan aan de inhoud van dit hoofdstuk (inclusief bijlagen) rechten worden ontleend. De inhoud van dit hoofdstuk (inclusief bijlagen) kan vertrouwelijke informatie bevatten en is uitsluitend bestemd voor de geadresseerde van dit hoofdstuk. Indien u niet de beoogde ontvanger van deze tekst bent, verzoek ik u dit hoofdstuk uit het boekje te verwijderen, eventuele bijlagen niet te openen en wijs ik u op de onrechtmatigheid van het gebruiken, kopiren of verspreiden van de inhoud van deze tekst (inclusief bijlagen). Tevens aanvaard ik geen enkele aansprakelijkheid voor directe of indirecte schade ontstaan door de inhoud van de informatie in dit hoofdstuk.

En dan kan de grote opsomming beginnen! Zoals het een goede slechte film betaamt, zal ik dit dankwoord 'in-order-of-appearance' (iooa) schrijven, niet om iemand te bevoor- of te benadelen, maar gewoon omdat de mensen die ik het langst ken ook wel eens vooraan mogen staan. Aangezien ik niet in rencarnatie geloof, is het beste startpunt in dit geval mijn geboorte: Dus, bij deze wil ik dertig jaar na dato de kraamhulp alsnog bedanken voor de geleverde assistentie daarbij. En met iets minder gekheid (want het zal er wel nooit helemaal afgaan) vind ik het belangrijkste natuurlijk om ons pap en mam te bedanken voor hun constante, onvoorwaardelijke steun. Ook al waren er momenten dat er geen land met me te bezeilen of geen enkele vooruitgang in de studie te bespeuren was, jullie hebben me altijd de mogelijkheid gegeven het zelf op te lossen en me nergens in tegengehouden. Uiteindelijk heb ik daarom deze eindstreep toch netjes binnen redelijke tijd bereikt. Voor Rianne, Marieke en Willem (en later Robert, Stefan en Floortje, en Tom, Tiny en Chris) geldt zeker hetzelfde. Ondanks dat het overduidelijk was dat ik geen simpele uitleg kon geven over wat ik nou aan het doen was, hebben jullie altijd interesse getoond in alles waar ik mee bezig was. Ik hoop jullie ooit nog eens duidelijk uit te kunnen leggen waaraan ik al die tijd nou gewerkt heb, al hoop ik dat het lezen van dit hele boekje al duidelijk genoeg

is! De bovenstaande disclaimer is hierbij speciaal voor jullie op alle voorgaande paginas van toepassing In ieder geval, bedankt!

Eigenlijk kan ik nu hetzelfde verhaal (met de uitzondering van de regels over mijn geboorte) hier gewoon nog eens copy-pasten want dat is wel de beste manier om aan te geven dat constante interesse en steun ook geldt voor alle vrienden die ik overgehouden heb aan de middelbare school en mijn studiejaren "I wanna thank my friends.."). In het kader van de iooa wil ik als eerste hier dus Patrick, Frank, Eefke, Evita en Fremco bedanken. Ondanks dat we redelijk uit elkaar zijn gegaan, blijven we gelukkig nog steeds in contact en dat hoop ik ook zo te houden.. Van de vele vrienden vanuit de studietijd en neven activiteiten wil ik er een aantal zeker bij naam noemen (ditmaal iooa en ook nog eens in alfabetische volgorde (iav) en in de hoop dat ik niet te veel mensen vergeet en boos maak..): Arjan, Harm, Tom, Jeroen, Dick, Irmgard, Jordy, Marlinda, Michiel, Sanne, Rik, Morten, waar ik veel tijd mee heb doorgebracht de afgelopen jaren, bedankt! Voor de persoonlijke benadering: Ondanks dat het overduidelijk was dat ik geen simpele uitleg kon geven over wat ik nou aan het doen was hebben jullie altijd interesse getoond in alles waar ik mee bezig was. Ik hoop jullie ooit nog eens duidelijk uit te kunnen leggen waaraan ik al die tijd nou gewerkt heb, al hoop ik dat het lezen van dit hele boekje al duidelijk genoeg is! De bovenstaande disclaimer is hierbij speciaal voor jullie op alle voorgaande paginas van toepassing Daarnaast: Nogmaals bedankt voor de geweldige tijd in de vorm van feesten, partijen (waarvoor ze ook te boeken zijn!) en het gezellig samenzijn in de tussenliggende periodes tijdens mijn studie en promotie! (tot nu toe bedankt, het is geen afscheid, hoop ik..)

Aan het eind van mijn studie heb ik nog een jaar stage gelopen op de Vaste Stof Chemie afdeling. Van Paul, Willem, Hugo en Elias heb ik in die periode veel geleerd wat me later erg goed van pas is gekomen. Hartstikke bedankt daarvoor! Meer bedankjes zijn echter wel op zijn plaats, vooral met het oog op mijn periode als promovendus. De baas natuurlijk als eerste: Elias, bedankt voor de begeleiding en je open-deur-beleid. Niet dat ik anders wél de deur plat zou hebben gelopen, maar wetende dat er altijd een mogelijkheid was om binnen te lopen en een vraag te stellen of een discussie te kunnen aangaan geeft echt vertrouwen. Willem, dankzij jouw scherpe analyses en hulp heb ik veel interessante proeven kunnen doen waar mooie artikelen uit zijn gekomen. Het vele contact dat we hadden en de humor daarbij heeft veel bijgedragen aan het plezier dat ik tijdens mijn promotie heb gehad. Verder was het erg fijn met je samen te werken bij (werk)colleges en practica, waarvoor dank. Ook de manier waarop iedereen met elkaar omgaat binnen de Vaste Stof Chemie afdeling was erg prettig. Daarom nog een rits namen die ik wil bedanken voor die goede sfeer bij VSC: Elisabeth, Ismail, Jan van K., Maurits, Mendel, Natalia, Paul T., Alea, Arno, Fieke, Jan S., Rene, Rienk, Vedran, Wim en alle studenten.

Hierboven heb ik al de mogelijkheid gehad om Elias en Willem te bedanken voor hun bijdrage aan mijn promotieonderzoek, maar ik heb nog veel meer officile en onofficile begeleiding gekregen, want mijn aanstelling was niet alleen een combinatie van diamant en GaN, maar ook een samenwerking tussen twee afdelingen: Applied Materials Science (AMS) en Applied Molecular Physics (AMP) ("I wanna thank my sponsors.."). Dat leverde twee keer zoveel presentaties en werkbesprekingen op, maar elk nadeel heb zijn voordeel: Dus ik mocht ook profiteren van twee afdelingsuitjes per jaar en een aanzienlijke hoeveelheid conferenties. Omdat mijn bureau bij AMS stond was ik daar (bijna) dagelijks te vinden en daarom wil ik mijn afdelingsgenoten van AMS als eerste bedanken! Paul en John, jullie zijn zo gek geweest om mij aan te nemen, daarom kan ik

niet anders dan jullie het meest bedanken. Paul, van jou heb ik veel mogen leren op het gebied van GaN, MOCVD, PL, wielrennen met de grote plaat en het verdedigen van een voetbalclub die net weer kansloos heeft verloren. Bedankt ook voor de espresso-breaks, ouwe-lullen-gitaarmuziek, en de leuke uitstapjes naar Scheveningen, Montreux en Jeju (Zuid-Korea), waar we nog gezellig in een vakantiehuisje hebben gezeten en de plaatselijke bevolking hebben wijsgemaakt dat in Nederland drie mannen één huwelijk kunnen hebben. Daarnaast heb ik mijn reparatie-repertoire kunnen uitbreiden met de Tweede-Hageman-methode: Een proces waarbij elektronische onderdelen een corrigerende tik krijgen, meestal gebruikmakend van een hamer, de achterkant van een schroevendraaier of soortgelijke attributen, tot de controller in kwestie weer naar behoren reageert op het elektrische signaal (De Eerste-Hageman-methode behelst het gebruik van Hageman-tape ook wel bekend als ductape: "It ain't broken, it just lacks Hageman-tape"). Voor het oplossen van de overige problemen (of als Pauls methoden per ongeluk niet toepasbaar waren), kon ik gelukkig altijd nog bij John binnenlopen. John, bedankt daarvoor. Ik vond het erg jammer dat je drukke tijdsschema het niet toeliet om betrokken te blijven bij het diamant-project (en dat zegt meer iets over het succes van zonnecellen), maar gelukkig wilde je wel altijd tijd vrij maken voor een kort vraagje. Voor mijn experimenten kon ik rekenen op Wil, Erik en Harry: Bedankt voor alle hulp bij het solderen, repareren en in elkaar knutselen van van-alles-en-nog-wat dat ik een keer gesloopt of nodig had Speciaal voor Wil, bedankt voor het meehelpen met het opruimen van de glazen ruiten in het scrubberhok, en Erik bedankt dat je de hamer niet terug gooide. In de cleanroom had ik vaak gezelschap van Gerard en Peter (ook wel eens getypeerd als Statler en Waldorf), Tim, Hina en Mariusz. Gerard, bedankt voor de MOCVD tips, de reserve-onderdelen voor de Eva, de discussies over het afgelopen/aankomende competitieprogramma, wielrennen, en het geklaag op de processing van Peter. Peter, bedankt voor de hulp met alle chemicalin, de schaterlach, en het geklaag op de gegroeide lagen van Gerard. Beiden (en Paul, Arjan en sergeant-majoor Mulder) bedankt voor de gezellige fietsweken in Frankrijk. Tim: Met jou heb ik ook vele GaN-conferenties bezocht (van Veldhoven, via Scheveningen, Ameland, Montreux en Korea naar Lunteren), goede, originele en minder volwassen discussies kunnen voeren over alles-en-nog-wat dat (zijdelings) met het dagelijks werk te maken had. Hina, Mariusz, thanks for your helpful discussions and contributions to my work, the cultural insights and the Polish beer.. Ward, Antonie (iooa), bedankt voor jullie bijdragen. Ik hoop dat ik jullie net zo veel heb kunnen leren als jullie mij. Veel succes in de toekomst! Het is wel duidelijk denk ik: er was een goede sfeer op de afdeling, ook dankzij de andere personen (niet direct betrokken bij het werk maar wel bij de ontspanning van een kop koffie, etentjes, afdelingsuitjes of een praatje tussendoor) die er waren tijdens mijn promotie: Gunther, Jan, Jim, Ton, Ine (iooa,iav), Aryan, Boukje, Jan-Willem, Jasper, Joep, Koen, Merel, Mireille, Roel, Salar en Sjoerd (iav).

Vanuit Applied Molecular Physics heb ik het meest te maken gehad met Hans en Ivan. Hans, bedankt voor het bij elkaar houden van het hechte diamant-team waardoor we vele nieuwe ideen hebben bedacht en uitgevoerd en voor je strakke begeleiding. Ivan, met jou heb ik de beste samenwerking gehad. We hebben heel veel goede en inspirerende discussies gehad (maar waren het uiteindelijk altijd eens), gezellige groeiruns gedaan en een paar leuke conferenties bezocht. Bovendien heb je me nog veel geleerd over het schrijven van wetenschappelijke publicaties en het transporteren van opstellingen. Samen hebben we onder andere de Raman setup verhuisd, twee diamant reactoren gebouwd/verplaatst en een scratch tester naar Leuven gebracht. Ervaring die elke verhuizing van pas komt!

Ik hoop dat je in Leuven een mooie vaste plek kan krijgen, want daar heb je wel ongeveer recht op (vind ik dan, en dan hebben we meteen weer een reden om wat te vieren!). Verder ben ik dank verschuldigd aan Arjan v.V., Cor, Gowri, Ine, Leander en Peter voor hun (technische) ondersteuning en hulp bij experimenten. En voor de AMP groepsactiviteiten wil ik graag Afric, Arjan D., Dennis, Elena, Frans, Gautam, James, Liesbeth, Marius, Mernoosh, Nico, Robert en Tanja bedanken.

Om de vergelijking met een film maar even vast te houden en door te trekken, nog speciale aandacht voor de ondersteuning op locatie. Renata, you introduced me in my first year of my Ph.D. to the complexity of measuring and interpretation of Raman Spectroscopy during a three days personal workshop in Montpellier. Eventhough there was a little mixup of Polish, France and English, it was very clear and you teached me a lot, which was helpful during my whole Ph.D. Thanks for that (and Jan too!). Jos en Peter (van glas natuurlijk), bedankt voor alle snelle hulp wanneer er wat glas of kwarts gesneuveld was, bijvoorbeeld toen tijdens een technisch mankement de buitenbuis van de reactor opengescheurd was en alles in het honderd (en onder water) liep. En bijzondere dank nog aan Martin Wientjes van Wiediam in Wanrooij, omdat je voor mij aan die ieniemienie-kleine diamanten substraten moeilijk slijpbare schuine zijden hebt aangebracht (wat stiekem gewoon de redding van het laatste artikel en daarmee mijn onderzoek was). En dat dan ook nog in de zomervakantie, terwijl het bedrijf stil lag, voor mij hebt willen doen. Hartstikke bedankt!

En dan "last but absolutely not least", wil ik nog speciaal bedanken, mijn lieve Stefanie (Speciaal geval, dus niet-iooa). Tien jaar lang al zijn we samen, en wat zul jij afgezien moeten hebben. Ik weet zeker dat ik het zonder jou niet had gered en heb er eigenlijk nog 4 extra bladzijden voor nodig om alles op te noemen waar je me bij hebt geholpen of in hebt gesteund en dan nog denk ik dat ik wat vergeet! Daarom verdien je voor de film van mijn promotie de Oscar voor Best Actress in Supporting Role. Gefeliciteerd en het meest bedankt van allemaal! Ik hoop dat ik jou net zo kan helpen en dat we uiteindelijk samen nog vele jaren kunnen genieten van deze inspanning...

14

Curriculum Vitae

Gerbe van Dreumel was born on the 14^{th} of february 1981 in Wijchen. After finishing his secondary school (Atheneum) at the Pax Christi College in Druten, he started in 1999 with a Chemistry studies at the former Katholieke Universiteit Nijmegen, now the Radboud University. In 2004, Gerbe did a internship guided by dr. P.W.G. Poodt at the Solid State Chemistry departement of prof. dr. E. Vlieg, which was an interferometric study of concentration profiles around growing crystals. This was followed by an externship at the Dutch Forensic Institute (NFI) on the forensic application of pyrolysis gas chromatography mass spectrometry on rubber and paint fragments. From september 2006 till september 2010, the author was appointed a position as Ph.D. student in a collaboration project between the Applied Materials Science departement and the Applied Molecular Physics department of the Radboud University in Nijmegen. The research was carried out under supervision of prof. dr. J.J. ter Meulen and prof. dr. E. Vlieg with daily guidance of dr. J.G. Buijnsters, dr. W.J.P. van Enckevort, and dr. P.R. Hageman. The results are presented in this thesis. Since the 29^{th} of november 2010, Gerbe is working as optical engineer at the LightLabs department of Royal Philips Electronics Inc.

References

[1] A. P. Grzegorczyk, *GaN grown on sapphire by MOCVD. Material for HEMT structures*, PhD thesis, Radboud University Nijmegen, 2006.

[2] J. Edgar, *Properties of Group III Nitrides*, volume 11, INSPEC, London, 1st edition, 1994.

[3] P. Ruterana, M. Albrecht, and J. Neugebauer, *Nitride Semiconductors, Handbook on Materials and Devices*, Wiley-VCH, Weinheim, 1st edition, 2003.

[4] V. Kirilyuk, *Optical Characterization of Gallium Nitride*, PhD thesis, Radboud University Nijmegen, 2002.

[5] H. P. Maruska and J. J. Tietjen, Appl. Phys. Lett. **15**, 327 (1969).

[6] S. N. Mohammad and H. Morkoç, Prog. Quant. Electr. **20**, 361 (1996).

[7] A. R. A. Zauner, *Homo- and Hetero-epitaxial Growth of Gallium Nitride by Metalorganic Chemical Vapour Deposition*, PhD thesis, Radboud University Nijmegen, 2001.

[8] O. Ambacher, J. Phys. D: Appl. Phys. **31**, 2653 (1998).

[9] M. C. J. C. M. Krämer, *Gallium Nitride-based Microwave High-Power Heterostructure Field-Effect Transistors*, PhD thesis, Eindhoven University of Technology, 2006.

[10] F. Bernardini, V. Fiorentini, and D. Vanderbilt, Phys. Rev. B **56**, R10024 (1997).

[11] F. A. Ponce and D. P. Bour, Nature **386**, 351 (1997).

[12] E. F. Schubert, *Light-Emitting Diodes*, Cambridge University Press, New York, 2nd edition, 2006.

[13] M. S. Shur, Solid State Electron. **42**, 2131 (1998).

[14] S. J. Pearton and C. Kuo, MRS Bulletin **22**, 17 (1997).

[15] O. Ambacher, J. Smart, J. R. Shealy, N. G. Weimann, K. Chu, M. Murphy, W. J. Schaff, L. F. Eastman, R. Dimitrov, L. Witmerr, M. Stutzmann, W. Rieger, and J. Hilsenbeck, J. Appl. Phys. **85**, 3222 (1999).

[16] O. Ambacher, R. Dimitrov, M. Stutzmann, B. Foutz, M. Murphy, J. Smart, J. R. Shealy, N. G. Weimann, and L. F. Eastmann, Inst. Phys. Conf. Ser. **166**, 493 (2000).

[17] S. Nakamura, S. J. Pearton, and G. Fasol, *The blue laser diode: the complete story*, Wiley, Weinheim, 2nd edition, 2000.

[18] D. A. B. Miller, D. S. Chemla, T. C. Damen, A. C. Gossard, W. Wiegmann, T. H. Wood, and C. A. Burrus, Phys. Rev. Lett. **53**, 2173 (1984).

[19] S. F. Chichibu, A. C. Abare, M. S. Minsky, S. Keller, S. B. Fleischer, J. E. Bowers, E. Hu, U. K. Mishra, L. A. Coldren, S. P. DenBaars, and T. Sota, Appl. Phys. Lett. **73**, 2006 (1998).

[20] J. R. Shealy, V. Kaper, V. Tilak, T. Prunty, J. A. Smart, B. Green, and L. F. Eastman, J. Phys.: Condens. Matter **14**, 3499 (2002).

[21] M. A. Khan, J. N. Kuznia, A. R. Bhatarai, and D. T. Olsen, Appl. Phys. Lett. **62**, 1786 (1993).

[22] J. I. Pankove, S. S. Chang, H. C. Lee, R. Molnar, T. D. Moustakas, and B. van Zeghbroeck, Tech. Dig. Int. Electron Devices Meet. **94**, 389 (1994).

[23] R. Gaska, J. W. Yang, A. Osinsky, Q. Chen, M. A. Khan, A. O. Orlov, G. L. Snider, and M. S. Shur, Appl. Phys. Lett. **72**, 707 (1998).

[24] Y. F. Wu, A. Saxler, M. Moore, R. P. Smith, S. Sheppard, P. M. Chavarkar, T. Wisleder, U. K. Mishra, and P. Parikh, IEEE Electr. Dev. Lett. **25**, 117 (2004).

[25] Y. Okamoto, Y. Ando, T. Nakayama, K. Hataya, H. Miyamoto, T. Inoue, M. Senda, K. Hirata, M. Kosaki, N. Shibata, and M. Kuzuhara, IEEE Trans. Electr. Dev. **51**, 2217 (2004).

[26] *Nitronex Corporation, Application Note AN-012, 2008.*

[27] E. Wörner, C. Wild, W. Müller-Sebert, R. Locher, and P. Koidl, Diamond Relat. Mater. **5**, 688 (1996).

[28] J. G. Buijnsters, *Hot-filament chemical vapour deposition of diamond onto steel*, PhD thesis, Radboud University Nijmegen, 2003.

[29] J. Isberg, J. Hammersberg, E. Johansson, T. Wikström, D. J. Twitchen, A. J. Whitehead, S. E. Coe, and G. A. Scarsbrook, Science **297**, 1670 (2002).

[30] M. J. Uren, T. Martin, B. T. Hughes, K. P. Hilton, A. Wells, R. S. Balmer, D. C. Herbert, A. M. Keir, D. J. Wallis, A. J. Pidduck, and M. Missous, Phys. Stat. Sol. A **194**, 468 (2002).

[31] A. Denisenko and E. Kohn, Diamond Relat. Mater. **14**, 491 (2005).

[32] M. H. Nazaré and A. J. Neves, *Properties, Growth and Applications of Diamond*, volume 26, INSPEC, London, 1st edition, 2001.

[33] J. J. Schermer, *Flame deposition of diamond. A brilliant growth technique*, PhD thesis, Radboud University Nijmegen, 2003.

[34] G. J. H. M. Janssen, *Homoepitaxial diamond: Synthesized by CVD processes*, PhD thesis, Radboud University Nijmegen, 1994.

[35] H. J. McSkimin, P. Andreatch, and P. Glynn, J. Appl. Phys. **43**, 985 (1973).

[36] H. Liu and D. S. Dandy, Diamond Relat. Mater. **4**, 1173 (1995).

[37] P. W. May, Endeavour **19**, 101 (1995).

[38] G. Davies, Chem. Phys. Carbon **13**, 1 (1977).

[39] H. B. Dyer, F. A. Raal, L. du Preez, and J. H. N. Loubser, Phil. Mag. **11**, 763 (1965).

[40] T. M. Tritt, *Thermal Conductivity: Theory, Properties and Applications*, Kluwer, New York, 1st edition, 2004.

[41] J. Che, T. Çagin, W. Deng, and W. Goddard, J. Chem. Phys. **113**, 6888 (2000).

[42] R. L. Sproull, Sci. Am. **december**, 92 (1962).

[43] J. E. Graebner, S. Jin, G. W. Kammlott, J. A. Herb, and C. F. Gardinier, Nature **359**, 401 (1992).

[44] L. Wei, P. K. Kuo, R. L. Thomas, T. R. Anthony, and W. F. Banholzer, Phys. Rev. Lett **70**, 3764 (1993).

[45] R. S. Sussmann, *CVD Diamond for Electronic Devices and Sensors*, Wiley, 1st edition, 2009.

[46] A. C. Ferrari and J. Robertson, Phys. Rev. B **63**, 121405(R) (2001).

[47] J. Hartmann, M. Costello, and M. Reichling, Phys. Rev. Lett. **80**, 117 (1998).

[48] J. Hartmann, P. Voigt, and M. Reichling, J. Appl. Phys. **81**, 2966 (1997).

[49] M. Reichling, T. Klotzbücher, and J. Hartmann, Appl. Phys. Lett. **73**, 756 (1998).

[50] P. W. May, H. Y. Tsai, W. N. Wang, and J. A. Smith, Diamond Relat. Mater. **15**, 526 (2006).

[51] M. Oba and T. Sugino, Jpn. J. Appl. Phys. **39**, L1213 (2000).

[52] M. Oba and T. Sugino, Diamond Relat. Mater. **10**, 1343 (2001).

[53] S. Yugo, T. Kanai, T. Kimura, and T. Muto, Appl. Phys. Let. **58**, 1036 (1991).

[54] B. R. Stoner, G. H. M. Ma, S. D. Wolter, and J. T. Glass, Phys. Rev. B **45**, 11067 (1992).

[55] M. Seelmann-Eggebert, P. Meisen, F. Schaudel, P. Koidl, A. Vescan, and H. Leier, Diamond Relat. Mater. **10**, 744 (2001).

[56] Y. S. Zou, Y. Yang, Y. M. Chong, Q. Ye, B. He, Z. Q. Yao, W. J. Zhang, S. T. Lee, Y. Cai, and H. S. Chu, Cryst. Growth Des. **8**, 1770 (2008).

[57] M. Dipalo, Z. Gao, J. Scharpf, C. Pietzka, M. Alomari, F. Medjdoub, J.-F. Carlin, N. Grandjean, S. Delage, and E. Kohn, Diamond Relat. Mater. **18**, 884 (2009).

[58] P. R. Hageman, J. J. Schermer, and P. K. Larsen, Thin Solid Films **443**, 9 (2003).

[59] D. Zhang, Y.-Z. Bai, F.-W. Qin, J.-M. Bian, F.-C. Jia, Z.-L. Wu, J.-J. Zhao, and X. Jiang, Chin. Phys. Lett. **27**, 018102 (2010).

[60] M. Imura, K. Nakajima, M. Liao, Y. Koide, and H. Amano, J. Cryst. Growth **312**, 1325 (2010).

[61] A. Dussaigne, M. Malinverni, D. Martin, A. Castiglia, and N. Grandjean, J. Cryst. Growth **311**, 4539 (2009).

[62] M. Alomari, A. Dussaigne, D. Martin, N. Grandjean, C. Gaquiere, and E. Kohn, Electr. Lett. **46**, 299 (2010).

[63] J. W. Zimmer, Mater. Res. Soc. Symp. Proc. **956** (2007).

[64] G. K. Celler and S. Cristoloveanu, J. Appl. Phys. **93**, 4955 (2003).

[65] M. Rudziński, *GaN grown on SiC by MOCVD*, PhD thesis, Radboud University Nijmegen, 2008.

[66] A. Aleksov, X. Li, N. Govindaraju, J. M. Gobien, S. D. Wolter, J. T. Prater, and Z. Sitar, Diamond Relat. Mater. **14**, 308 (2005).

[67] N. K. Annamalai, P. Fechner, and J. Sawyer, SOI Conf. 1992, IEEE Int. , 64 (1992).

[68] A. Aleksov, J. M. Gobien, X. Li, J. T. Prater, and Z. Sitar, Diamond Relat. Mater. **15**, 248 (2006).

[69] J. W. Zimmer and G. Chandler, Proc. CS Mantech **Austin, Texas** (2007).

[70] J. W. Zimmer and G. Chandler, Proc. CS Mantech **Chicago** (2008).

[71] K. D. Chabak, J. K. Gillespie, V. Miller, A. Crespo, J. Roussos, M. Trejo, D. E. Walker, G. D. Via, G. H. Jessen, J. Wasserbauer, F. Faili, D. I. Babić, D. Francis, and F. Ejeckam, IEEE Electr. Dev. Lett. **31**, 99 (2010).

[72] J. G. Felbinger, M. V. S. Chandra, Y. Sun, L. F. Eastman, J. Wasserbauer, F. Faili, D. I. Babić, D. Francis, and F. Ejeckam, IEEE Electr. Dev. Lett. **28**, 948 (2007).

[73] D. Francis, F. Faili, D. Babić, F. Ejeckam, A. Nurmikko, and H. Maris, Diam. Relat. Mater. **19**, 229 (2010).

[74] D. Francis, J. Wasserbauer, F. Faili, D. Babić, F. Ejeckam, W. Hong, P. Specht, and E. Weber, Proc. CS MANTECH **Austin, Texas**, 133 (2007).

[75] Q. Diduck, J. Felbinger, L. F. Eastman, D. Francis, J. Wasserbauer, F. Faili, D. I. Babić, and F. Ejeckam, IEEE Electr. Lett. **45**, 758 (2009).

[76] J. R. Petherbridge, P. W. May, S. R. J. Pearce, K. N. Rosser, and M. N. R. Ashfold, J. Appl. Phys. **89**, 1484 (2001).

[77] F. C.-N. Hong, G.-T. Liang, J. J. Wu, D. Chang, and J.-C. Hsieh, Appl. Phys. Let. **63**, 3149 (1993).

[78] C. Pan, C. J. Chu, J. L. Margrave, and R. H. Hague, J. Electrochem. Soc. **141**, 3246 (1994).

[79] Y. H. Lee, H. S. Kim, G. Y. Yeom, J. W. Lee, M. C. Yoo, and T. I. Kim, J. Vac. Sci. Technol. A **16**, 1478 (1998).

[80] L. Liu and J. H. Edgar, Mat. Sci. Eng. **R37**, 61 (2002).

[81] W. A. Melton and J. I. Pankove, J. Cryst. Growth **178**, 168 (1997).

[82] E. V. Etzkorn and D. R. Clarke, J. Appl. Phys. **89**, 1025 (2001).

[83] D. A. Stocker, E. F. Schubert, W. Grieshaber, K. S. Boutros, and J. M. Redwing, Appl. Phys. Lett. **73**, 1925 (1998).

[84] G. B. Springfellow, *Organometallic Vapor-Phase Epitaxy, Theory and Practice*, Academic Press, Boston, 1989.

[85] P. R. Hageman, *MOCVD growth and doping studies of III/V semiconductors*, PhD thesis, Radboud University Nijmegen, 1993.

[86] H. M. Manasevit, F. M. Erdmann, and W. I. Simpson, J. Electrochem. Soc. **118**, 1864 (1971).

[87] H. Amano, M. Iwaya, T. Kashima, M. Katsuragawa, I. Akasaki, J. Han, S. Hearne, J. A. Floro, E. Chason, and J. Fighiel, Jpn. J. Appl. Phys. **37**, L1540 (1998).

[88] T. Hashimoto, M. Yuri, M. Ishida, Y. Terakoshi, O. Imafuji, T. Sugino, and K. Itoh, Jpn. J. Appl. Phys. **38**, 6605 (1999).

[89] H. Kawakami, K. Sakurai, K. Tsubouchi, and N. Mikoshiba, Jpn. J. Appl. Phys. **27**, L161 (1988).

[90] S. Keller, B. P. Keller, Y.-F. Wu, B. Heying, D. Kapolnek, J. S. Speck, U. K. Mishra, and S. P. DenBaars, Appl. Phys. Lett. **68**, 1525 (1996).

[91] A. Yamamoto, M. Tsujino, M. Ohkubo, and A. Hashimoto, J. Cryst. Growth **137**, 415 (1994).

[92] K. Uchida, A. Watanabe, F. Yano, M. Kouguchi, T. Tanaka, and S. Minigawa, J. Appl. Phys. **79**, 3487 (1996).

[93] K. Uchida, A. Watanabe, F. Yano, M. Kouguchi, T. Tanaka, and S. Minigawa, Sol. Stat. Elec. **41**, 135 (1997).

[94] T. Hashimoto, Y. Terakoshi, M. Ishida, M. Yuri, O. Imafuji, T. Sugino, A. Yoshikawa, and K. Itoh, J. Cryst. Growth **189/190**, 254 (1998).

[95] X. L. Sun, H. Yang, J. J. Zhu, Y. T. Wang, Y. Chen, G. H. Li, and Z. G. Wang, Phys. Stat. Sol. A **188**, 653 (2001).

[96] M. Yeadon, M. T. Michael, F. Hamdani, S. Pekin, H. Morkoç, and J. M. Gibson, J. Appl. Phys. **83**, 2847 (1998).

[97] N. Grandjean, J. Massies, and M. Leroux, Appl. Phys. Lett. **69**, 2071 (1996).

[98] F. Dwikusuma and T. F. Kuech, J. Appl. Phys. **94**, 5656 (2003).

[99] H. Amano, N. Sawaki, I. Akasaki, and Y. Toyoda, Appl. Phys. Lett. **48**, 353 (1986).

[100] T. Ito, M. Sumiya, Y. Takano, K. Ohtsuka, and S. Fuke, Jpn. J. Appl. Phys. **38**, 649 (1999).

[101] S. Nakamura, Jpn. J. Appl. Phys. **30**, L1705 (1991).

[102] X. H. Wu, D. Kapolnek, E. J. Tarsa, B. Heying, S. Keller, B. P. Keller, U. K. Mishra, S. P. DenBaars, and J. S. Speck, Appl. Phys. Lett. **68**, 1371 (1996).

[103] J. N. Kuznia, M. A. Khan, D. T. Olsen, R. Kaplan, and J. Freitas, J. Appl. Phys. **73**, 4700 (1993).

[104] A. E. Wickenden, D. K. Wickenden, and T. J. Kistenmacher, J. Appl. Phys. **75**, 5367 (1994).

[105] D. D. Koleske, M. E. Coltrin, K. C. Cross, C. C. Mitchell, and A. A. Allerman, J. Cryst. Growth **273**, 86 (2004).

[106] L. Sugiura, K. Itaya, J. Nishio, H. Fujimoto, and Y. Kokubun, J. Appl. Phys. **82**, 4877 (1997).

[107] D. Kapolnek, X. H. Wu, B. Heying, S. Keller, B. P. Keller, U. K. Mishra, S. P. DenBaars, and J. S. Speck, Appl. Phys. Lett. **67**, 1541 (1995).

[108] S. Kim, J. Oh, J. Kang, D. Kim, J. Won, J. W. Kim, and H.-K. Cho, J. Cryst. Growth **262**, 7 (2004).

[109] L. Macht, *Extended defects in GaN: Selective etching and optical properties*, PhD thesis, Radboud University Nijmegen, 2005.

[110] R. Dwiliński, R. Doradziński, J. Garczyński, L. P. Sierzputowski, A. Puchalski, Y. Kanbara, K. Yagi, H. Minakuchi, and H. Hayashi, J. Cryst. Growth **311**, 3015 (2009).

[111] R. Dwiliński, R. Doradziński, J. Garczyński, L. P. Sierzputowski, A. Puchalski, Y. Kanbara, K. Yagi, H. Minakuchi, and H. Hayashi, J. Cryst. Growth **310**, 3911 (2008).

[112] D. Ehrentraut, Y. Kagamitani, T. Fukuda, F. Orito, S. Kawabata, K. Katano, and S. Terada, J. Cryst. Growth **310**, 3902 (2008).

[113] F. P. Bundy, H. T. Hall, H. M. Strong, and R. H. Wentorf, Nature **176**, 51 (1955).

[114] H. Liander, A.S.E.A. Journal **28**, 97 (1955).

[115] J. C. Angus, H. C. Will, and W. S. Stanko, J. Appl. Phys. **39**, 2915 (1968).

[116] B. V. Spitsyn, L. L. Builov, and B. V. Deryagin, J. Cryst. Growth **52**, 219 (1981).

[117] P. W. May, Phil. Trans. R. Soc. Lond. A **358**, 473 (2000).

[118] P. K. Bachmann and W. J. P. van Enckevort, Diamond Relat. Mater. **1**, 1021 (1992).

[119] P. K. Bachmann and D. U. Wiechert, Diamond Relat. Mater. **1**, 422 (1992).

[120] P. K. Bachmann, H.-J. Hagemann, H. Lade, D. Leers, F. Picht, D. U. Weichert, and H. Wilson, Mater. Res. Soc. Symp. Proc. **339**, 267 (1994).

[121] N. A. Prijaya, J. C. Angus, and P. K. Bachmann, Diamond Relat. Mater. **3**, 129 (1994).

[122] M. N. R. Ashfold, P. W. May, C. A. Rego, and N. M. Everitt, Chem. Soc. Rev. **23**, 21 (1994).

[123] S. Matsumoto, Y. Sato, M. Tsutsumi, and N. Setaka, J. Mater. Sci. **17**, 3106 (1982).

[124] B. V. Spitsyn, L. L. Builov, and A. E. Alexenko, Braz. J. Phys. **30**, 471 (2000).

[125] M. Kamo, Y. Sato, S. Matsumoto, and N. Setaka, J. Cryst. Growth **62**, 642 (1983).

[126] P. K. Bachmann, H.-J. Hagemann, H. Lade, D. Leers, D. U. Weichert, H. Wilson, D. Fournier, and K. Plamann, Diamond Relat. Mater. **4**, 820 (1995).

[127] M. Werner and R. Locher, Rep. Prog. Phys. **61**, 1665 (1998).

[128] L. M. Hanssen, W. A. Carrington, J. E. Butler, and K. A. Snail, Mater. Lett. **7**, 289 (1988).

[129] J. G. Buijnsters, L. Vázquez, and J. J. ter Meulen, Diam. Relat. Mater. **18**, 1239 (2009).

[130] E. M. Galimov, Nature **243**, 389 (1973).

[131] R. N. Greiner, D. S. Phillips, J. D. Johnson, and F. Volk, Nature **333**, 440 (1988).

[132] A. K. Khachatryan, S. G. Aloyan, P. W. May, R. Sargsyan, V. A. Khachatryan, and V. S. Baghdasaryan, Diamond Relat. Mater. **17**, 931 (2008).

[133] V. Y. Dolmatov, Russ. J. Appl. Chem. **79**, 1913 (2006).

[134] T. Bohnen, *Hydride vapor phase epitaxy growth of GaN, InGaN, ScN, and ScAlN*, PhD thesis, Radboud University Nijmegen, 2010.

[135] H. M. Mansour and A. J. Hickey, Pharm. Sci. Tech. **8**, 99 E1 (2007).

[136] J. L. Weyher, P. D. Brown, A. R. A. Zauner, S. Müller, C. B. Boothroyd, D. T. Foord, P. R. Hageman, C. J. Humphreys, P. K. L. I. Grzegory, and S. Porowski, J. Cryst. Growth **204**, 419 (1999).

[137] W. Qian, M. Skowronski, and G. S. Rohrer, Mat. Res. Soc. Symp. Proc. **423**, 475 (1996).

[138] G. A. Slack and S. F. Bartram, J. Appl. Phys. **46**, 89 (1975).

[139] M. Leszczynski, H. Teisseyre, T. Suski, I. Grzegory, M. Bockowski, J. Jun, S. Porowski, K. Pakula, J. M. Baranowski, C. T. Foxon, and T. S. Cheng, Appl. Phys. Lett. **69**, 73 (1996).

[140] M. S. Kumar and J. Kumar, Mater. Chem. Phys. **77**, 341 (2002).

[141] *ICSD Card for GaN hexagonal: 74-0243.*

[142] D. D. Manchon, A. S. Barker, P. J. Dean, and R. B. Zetterstrom, Solid State Commun. **8**, 1227 (1970).

[143] T. Kozawa, T. Kachi, H. Kano, M. Hashimoto, N. Koide, and K. Manabe, J. Appl. Phys. **75**, 1098 (1994).

[144] H. Harima, J. Phys.: Condens. Matter. **14**, R967 (2002).

[145] T. Azuhata, T. Sota, K. Suzuki, and S. Nakamura, J. Phys.: Condens. Matter. **7**, L129 (1995).

[146] S. Murugkar, R. Merlin, A. Botchkarev, A. Salvador, and H. Morkoç, J. Appl. Phys. **77**, 6042 (1995).

[147] M. A. Reshchikov and H. Morkoç, J. Appl. Phys. **97**, 06130101 (2005).

[148] U. Birkle, M. Fehrer, V. Kirchner, S. Einfeldt, D. Hommel, S. Strauf, P. Michler, and J. Gutowski, MRS Internet J. Nitride Semicond. Res. **4S1**, G5.6 (1999).

[149] B. Monemar, Phys. Rev. B **10**, 676 (1974).

[150] O. Lopatiuk, L. Chernyak, Y. Feldman, and K. Gatrsman, Thin Solid Films **515**, 4365 (2007).

[151] G. W. G. van Dreumel, J. G. Buijnsters, T. Bohnen, J. J. ter Meulen, P. R. Hageman, W. J. P. van Enckevort, and E. Vlieg, Diamond Relat. Mater. **18**, 1043 (2009).

[152] R. Koda, T. Oki, T. Miyajima, H. Watanabe, M. Kuramoto, M. Ikeda, and H. Yokoyama, Appl. Phys. Lett. **97**, 021101 (2010).

[153] M. Rabarot, J. Widiez, S. Saada, J.-P. Mazellier, C. Lecouvey, J.-C. Roussin, J. Dechamp, P. Bergonzo, F. Andrieu, O. Faynot, S. Deleonibus, L. Clavelier, and J. P. Roger, Diamond Relat. Mater. **19**, 796 (2010).

[154] G. W. G. van Dreumel, T. Bohnen, J. G. Buijnsters, W. J. P. van Enckevort, J. J. ter Meulen, P. R. Hageman, and E. Vlieg, Diamond Relat. Mater. **19**, 437 (2010).

[155] A. Y. Polyakov, A. V. Markov, M. P. D. M. V. Mezhennyi, A. A. Donskov, S. S. Malakhov, A. V. Govorkov, Y. P. Kozlova, V. F. Pavlov, N. B. Smirnov, T. G. Yugova, A. I. Belogorokhov, I. A. Belogorokhov, A. K. Ratnikova, Y. Y. Fyodorov, O. Y. Kudryashov, I. A. Leontyev, V. I. Ratushnyi, and S. J. Pearton, J. Vac. Sci. Technol. B **28**, 1011 (2010).

[156] B. V. Spitsyn, W. L. Hsu, A. E. Gorodetsky, R. K. Zalavutdinov, A. P. Zakharov, L. L. Bouilov, V. P. Stoyan, V. F. Dvoryankin, and G. V. Chaplygin, Diamond Relat. Mater. **7**, 356 (1998).

[157] X. Zhang, S. J. Chua, Z. C. Feng, J. Chen, and J. Lin, Phys. Stat. Sol. A **176**, 605 (1999).

[158] J.-H. Boo, S.-B. Lee, Y.-S. Kim, J. T. Park, K.-S. Yu, and Y. Kim, Phys. Stat. Sol. A **176**, 711 (1999).

[159] F. K. de Theije, A. R. A. Zauner, P. R. Hageman, W. J. P. Enckevort, and P. K. Larsen, J. Cryst. Growth **197**, 37 (1999).

[160] A. Koukito, M. Mayumi, and Y. Kumagai, J. Cryst. Growth **246**, 230 (2002).

[161] T. Yang, K. Uchida, T. Mishima, J. Kasai, and J. Gotoh, Phys. Stat. Sol. A **180**, 45 (2000).

[162] D. G. Zhao, D. S. Jiang, J. J. Zhu, Z. S. Liu, S. M. Zhang, H. Yang, and J. W. Liang, J. Cryst. Growth **303**, 414 (2007).

[163] X. Zhang, P. D. Dapkus, and D. H. Rich, Appl. Phys. Lett. **77**, 1496 (2000).

[164] S. Figge, T. Böttcher, S. Einfeldt, and D. Hommel, J. Cryst. Growth **221**, 262 (2000).

[165] O. Briot, S. Clur, and R. L. Aulombard, Appl. Phys. Lett. **71**, 1990 (1997).

[166] T. Bohnen, A. E. F. de Jong, W. J. P. van Enckevort, J. L. Weyher, G. W. G. van Dreumel, H. Ashraf, P. R. Hageman, and E. Vlieg, J. Cryst. Growth **311**, 4685 (2009).

[167] V. Lebedev, K. Tonisch, F. Niebelschütz, V. Cimalla, D. Cengher, I. Cimalla, C. Mauder, S. Hauguth, O. Ambacher, F. M. Morales, J. G. Lozano, and D. González, J. Appl. Phys. **101**, 054906 (2007).

[168] J. L. Weyher, S. Lazar, L. Macht, Z. Liliental-Weber, R. J. Molnar, S. Müller, V. G. M. Sivel, G. Nowak, and I. Grzegory, J. Cryst. Growth **305**, 384 (2007).

[169] D. W. Shaw, J. Cryst. Growth **31**, 130 (1975).

[170] L. G. Schulz, J. Appl. Phys. **20**, 1030 (1949).

[171] F. Schulze, A. Dadgar, J. Bläsing, T. Hempel, A. Diez, J. Christen, and A. Krost, J. Cryst. Growth **289**, 485 (2006).

[172] V. Lebedev, J. Jinschek, U. Kaiser, B. Schröter, W. Richter, and J. Kräusslich, Appl. Phys. Lett. **76**, 2029 (2000).

[173] G. Vogg, C. R. Miskys, J. A. Garrido, M. Hermann, M. Eickhoff, and M. Stutzmann, J. Appl. Phys. **96**, 895 (2004).

[174] M. Imura, K. Nakajima, M. Liao, Y. Koide, and H. Amano, Diam. Relat. Mater. **19**, 131 (2010).

[175] T. Kozawa, T. Kachi, H. Kano, H. Nagase, N. Koide, and K. Manabe, J. Appl. Phys. **77**, 4389 (1995).

[176] B. Gil, O. Briot, and R.-L. Aulombard, Phys. Rev. B **52**, R17028 (1995).

[177] M. Albrecht, S. Christiansen, G. Salvati, C. Zanotti-Fregonara, Y. T. Rebane, Y. G. Shreter, M. Mayer, A. Pelzmann, M. Kamp, K. Ebeling, and M. Bremser, Mat. Res. Soc. Symp. Proc. **468**, 293 (1997).

[178] T. F. Huang, A. Marshall, S. Spruytte, and J. S. H. Jr., J. Cryst. Growth **200**, 362 (1999).

[179] V. Kirilyuk, M. Zielinski, P. C. M. Christianen, A. R. A. Zauner, J. L. Weyher, P. R. Hageman, and P. K. Larsen, Mat. Res. Soc. Proc. **639**, G6.23.1 (2001).

[180] A. Dadgar, F. Schulze, M. Wienecke, A. Gadanecz, J. Bläsing, P. Veit, T. Hempel, A. Diez, J. Christen, and A. Krost, New J. Phys. **9**, 389 (2007).

[181] J. Furthmüller, J. Hafner, and G. Kresse, Phys. Rev. B **53**, 7334 (1996).

[182] M. D. Winn, M. Rassinger, and J. Hafner, Phys. Rev. B **55**, 5364 (1997).

[183] T. Frauenheim, U. Stephan, P. Blaudeck, D. Porezag, and H.-G. Busmann, Diam. Relat. Mater. **3**, 966 (1994).

[184] Y. Kuang, Y. Wang, N. Lee, A. Badzian, T. Badzian, and T. T. Tsong, Appl. Phys. Lett. **67**, 3721 (1995).

[185] B. S. Swartzentruber, N. Kitamura, M. G. Lagally, and M. B. Webb, Phys. Rev. B **47**, 13432 (1993).

[186] B. S. Swartzentruber, Y. W. Mo, M. B. Webb, and M. G. Lagally, J. Vac. Sci. Technol. A **9**, 210 (1990).

[187] M. S. Couto, W. J. P. van Enckevort, B. Wichman, and M. Seal, Appl. Surf. Sci. **62**, 263 (1992).

[188] I. V. Markov, *Crystal Growth for Beginners, Fundamentals of Nucleation, Crystal Growth and Epitaxy*, World Scientific, Singapore, 2nd edition, 2008.

[189] E. I. Givargizov, M. O. Kliya, V. Melik-Adamyan, A. I. Grebenko, R. C. DeMattei, and R. S. Feigelson, J. Cryst. Growth **112**, 758 (1991).